INTEGRAL THEORY FOR TURBULENT BASE FLOWS AT SUBSONIC AND SUPERSONIC SPEEDS

Thesis by

Irwin E. Alber

In Partial Fulfillment of the Requirements

For the Degree of

Doctor of Philosophy

California Institute of Technology

Pasadena, California

1967

(Submitted May 24, 1967)

ACKNOWLEDGMENTS

I would very much like to express my sincere gratitude and appreciation to Professor Lester Lees for both his technical and personal guidance during the course of this study. Professors Anatol Roshko and Toshi Kubota are to be thanked for their many helpful contributions and suggestions. An expression of appreciation is also due Mrs. Virginia Conner for her excellent assistance in the preparation of this manuscript.

I wish to acknowledge the receipt of an Institute Research and Teaching Assistantship for the years 1963-1965. Thanks is also due North American Aviation for a Graduate Fellowship during the academic years 1966-1967. Additional financial aid was made possible through the support of the U. S. Air Force Office of Scientific Research under Contract No. AF 49(638)-1298.

This thesis is dedicated to my wife Lana and my daughters Deborah and Barbara, for their untiring perseverance and devotion throughout my studies.

ABSTRACT

The integral near wake analysis of Reeves and Lees developed for supersonic laminar base flows is extended to the case of fully turbulent separated adiabatic flow behind a rearward facing step at both subsonic and supersonic speeds. A turbulent eddy viscosity model is formulated for the shear stress scaling of the dissipation integral in the mechanical energy equation. It is shown that the eddy viscosity can be described simply by one incompressible constant (valid for both shear layers and wakes) and one reference density ρ_r. Using a compressibility transformation, theoretical solutions for the spreading rates of free shear layers are found to agree with experiment when the reference density is chosen to be the centerline density for the wake flow.

Two alternate methods are presented for joining the wake flow solution to the body: first, through a turbulent free shear layer mixing solution, and then through the use of a two parameter family of velocity profiles valid near the body. A simple conservation model is presented to relate the viscous sublayer after expansion to the initial boundary layer ahead of the step.

For free stream Mach numbers $M_1 \leq 2.3$, the integral theory is found to give good estimates for the length scales and centerline pressure variations measured experimentally for both wake flows and step flows (where reattachment is to a solid surface).

ABSTRACT (Cont'd)

An iterative method of solution for the incompressible wake flow problem is presented as an extension of the work of Green. The calculation proposes the proper criteria for obtaining a convergent solution. The base pressure coefficient is found to be equal to the difference between the momentum thicknesses in the far wake and at the base.

TABLE OF CONTENTS

TABLE OF CONTENTS (Cont'd)

LIST OF FIGURES

LIST OF FIGURES (Cont'd)

LIST OF SYMBOLS

a	speed of sound; also velocity profile parameter; $U_{\mathcal{L}}/U_e$ for wake
b	measure of wake width
c	defined by equation (4.34)
c_p	specific heat at constant pressure
C_p	$(P-P_\infty)/\frac{1}{2}\rho U_\infty^2$
C_D	$D/\frac{1}{2}\rho U_\infty^2 h$
D	determinant of integral system of equations [see eqn. (5.19)] also drag of body
f	see equation (5.10)
$f'(\eta)$	$\frac{U}{U_e}$ similar velocity profile
$F(Z)$	analytic complex function
g	defined in equations (4.31)
h	base height
$\mathcal{H}$	θ_i/δ_i^*
I_d	energy dissipation integral [see eqn. (4.21)]
J	θ_i^*/δ_i^*
K	eddy viscosity constant = $\epsilon/\Delta u.b$
ℓ_{mix}	mixing length (along d.s. ℓ) of isobaric region
$\overline{m}$	entrained mass flow
M	Mach number
m	$[\gamma-\frac{1}{2}]M^2$
N	$(P_{tot}-P_b)/(P_\infty-P_b)$ Nash's reattachment factor, also d.s 2 parameter shape factor
N_i	Numerator of system of integral equations [see eqn. (5.19)]

LIST OF SYMBOLS (Cont'd)

P, p	pressure
Pr	Prandtl number
Q	source strength [see eqn. (9.23)]
R	dissipation function $(2\delta_i^*/U_e^2 \int_0^{\delta_i} (\frac{\partial U}{\partial Y})^2 \, dY)$
Re_L	freestream Reynolds number based on body length
R_T	Townsend's turbulent wake Reynolds number $= \frac{(\Delta u)b}{\epsilon}$
T	Temperature
u, v	velocity components parallel and normal to the centerline, respectively
u^*	normalized velocity on dividing streamline $(U/U_e)_{\psi=0}$
U	transformed or incompressible velocity
x, y	coordinates parallel and normal to centerline or dividing streamline
X, Y	Transformed coordinates
Z	velocity integral $1/\delta_i^* \int_0^{\delta_i} (U/U_e)dY$
β	Falkner-Skan pressure gradient parameter, also pressure gradient parameter for equilibrium b.l. $\beta = \frac{\delta^* dP/dx}{\tau_w}$
γ	ratio of specific heats
Δu	velocity difference across wake
Δ	sublayer thickness
ϵ	eddy viscosity
$\tilde{\epsilon}$	transformed eddy viscosity $= (\rho_r/\rho_e)^2 K_\theta U_e \bar{\theta}$
δ	wake or boundary layer thickness
δ^*	displacement thickness
η	similarity variable

LIST OF SYMBOLS (Cont'd)

ξ	transformed axial distance
θ	momentum thickness
$\overline{\theta}$	transformed momentum thickness
θ^*	mechanical energy thickness
Θ	local angle between "external" streamline at $y = \delta$ and x-axis, $\tan^{-1}(v_e/u_e)$
ν	Prandtl-Meyer angle; also kinematic viscosity
ρ	density
σ^*	turbulent spreading parameter (incompressible)
σ_θ	momentum thickness spreading parameter, eqn. (4.38)
τ	shear stress
Ψ	transformed stream function
ψ	physical stream function

Subscripts

$\mathfrak{C}$	center line
e	local "external" inviscid
1	ahead of the step
2	after expansion
i	transformed
w	wall
r	reference conditions for compressible turbulent transformation
o	rear stagnation point, also shear layer quiescent region
∞	wake downstream conditions

LIST OF SYMBOLS (cont'd)

Superscripts

$'$	denotes velocity fluctuation
$\bar{}$	time average
$\sim$	transformed quantity

I. INTRODUCTION

Numerous experimental and theoretical studies (1,2,3) in recent years have been directed toward obtaining a better understanding of the mechanism of flow separation and reattachment behind blunt and slender bodies at both subsonic and supersonic speeds (see figure 1). Initial interest centered on the prediction of base pressure. Design of hypersonic re-entry vehicles has led to the consideration of the base heating problem and the correlation of wake observables with the flow field in the near wake.

For freestream Reynolds numbers (Re_L) greater than 1 to 5×10^6 a boundary layer approaching a cavity or base is in most cases fully turbulent. These conditions apply to almost all separated flows in the subsonic and low to moderate supersonic flight regimes.

As well as their direct engineering importance, turbulent separated flows provide a basic flow situation against which many theories for free turbulent flow may be tested and evaluated.

The initial theoretical work of Korst (1), Nash (2), McDonald (3) and others on the supersonic turbulent base flow problem was concerned mainly with the prediction of base pressure, through the use of various reattachment criteria.

While pointing out the important role of the separated shear layer, Chapman (4) and Korst (1) essentially disregarded the mechanics of the reattachment process in order to calculate the base pressure. They assumed that the total pressure along the dividing streamline (separating the recirculating flow from the external flow) is completely converted to the static pressure downstream of

reattachment, $P_{tot}_{d.s.} = P_\infty$. Nash (2) points out the rather fortuitous cancellation of errors in the Chapman-Korst analysis, i.e., the incorrect assumption of isentropic recompression coupled with the neglect of the initial boundary layer. However, he, too, treats the recompression process as a "black box", by using an empirical factor, $N = (P_{tot}_{d.s.} - P_b)/(P_\infty - P_b) \approx .35$, to relate the total pressure on the dividing streamline, $P_{tot}_{d.s.}$, to the freestream static pressure, P_∞. McDonald (3) obtained a unique solution for the base pressure by requiring that the "shape parameter of the reattached boundary layer should be of the flat plate type" ($\mathcal{H} \approx 1.2\text{-}1.6$).

Starting with an initial mixing profile, McDonald employed a stream tube approach (assuming isentropic flow along streamlines) to determine the integral thicknesses θ and δ^* at the rear stagnation point. He totally disregards the effect of the viscous mixing and the interaction with the outer flow and uses an empirical equation to relate the development of the reattaching shape factor $\mathcal{H}$ to the velocity U_e at the edge of the boundary layer. He iterates on the base pressure until $\mathcal{H}_\infty = \mathcal{H}_{\text{flat plate}}$.

All of the above theories are incapable of predicting such important wake characteristics as the length of the recompression region (of the order of 4-8 step heights), the location of the rear stagnation point, the growth rate of the wake boundary layer and the longitudinal pressure variations in the reattachment region. These theories cannot determine the above mentioned quantities because they disregard the essential viscid-inviscid interaction which determines the reattachment process and thus the whole turbulent base flow field. In 1952,

Crocco and Lees (5) developed a theory for the supersonic near wake. The effect of viscous-inviscid interaction was included through the use of the integral continuity equation, which equates the angle Θ induced at the edge of the inner viscous flow to the angle of the inviscid outer flow $\tan^{-1} \frac{v_e}{u_e}$. While a crude semi-empirical model was used for the viscous mixing, it was established that a unique value of the base pressure (in the supersonic case) could be obtained through the requirement that the integral conservation equations produce a solution curve which passes smoothly through a saddle point singularity downstream of the rear stagnation point, referred to as the "critical point". This singularity is analogous to the "throat" at Mach 1 in a converging-diverging nozzle, since the subcritical boundary layer (subsonic in the mean) becomes supercritical (supersonic in the mean) after passing through the critical point. Experimental evidence of the existence of such a point for base flows was presented by Carriere in reference (6).

The theoretical model of Reeves and Lees (7) and Webb, Golik and Lees (8), developed for the laminar near wake, has improved on the Crocco-Lees solution through the use of multi-moment integral equations† with suitable wake profiles for the hypersonic laminar near wake behind blunt bodies. It was shown that solutions at low wake Mach numbers ($M \leq 3$) and at high Reynolds numbers employing single parameter Stewartson wake profiles gave results which were in good agreement with experiment.

† The semi-empirical "mixing rate" law of the Crocco-Lees theory is replaced by the use of the integral mechanical energy equation for the wake.

Recently Green (9) attacked the incompressible turbulent reattachment and base flow problem using integral methods and thin airfoil theory for the viscous-inviscid interaction. Unfortunately a complete solution was not obtained in the reverse flow region upstream of the rear stagnation point or in the far wake. It appears, though, that the incompressible problem can be properly handled by coupling the viscous integral equations developed for supersonic flow to the proper incompressible inviscid outer flow field.

With the above theoretical studies as a foundation, the purposes of this present investigation are:

(1) to extend the integral inviscid-viscid solutions developed for the laminar supersonic wake of a blunt body to the analysis of turbulent base flows at moderate supersonic speeds behind a rearward facing step.

(2) to improve on the work of Green and obtain a more rigorous method of solution for the incompressible turbulent near and far wake.

It has also been suggested that reattachment to a solid surface can be treated by a wake type solution, since the reattaching boundary layer has a large steadily decreasing wake component downstream of the rear stagnation point. It is thus possible as an extra feature of interest to determine by comparison of the wake theory with experimental data whether or not the axis shear stress in the reattachment region can be neglected in the calculation of separated flows which reattach to solid surfaces. It would then, it is hoped, be possible to treat both wake and solid surface base flows by the same theory.

The adiabatic supersonic turbulent base flow field is examined in sections II-VIII. Some of the methods developed in these sections are then used in section IX in order to formulate the method of solution for the incompressible case.

II. DESCRIPTION OF THE SUPERSONIC FLOW FIELD

The principal objective of this study is to try to understand the gross effect of the turbulence and dynamics on the important length scales and pressure levels in the near wake. Thus, in order to formulate a simple model for the two-dimensional turbulent base flow field, it is most necessary to make use of the available experimental measurements so as to delineate, if possible, the most important features of a highly complex flow pattern.

II. 1. The Two-Dimensional Turbulent Base Flow Field

Several important regions in the supersonic turbulent base flow field behind a rearward facing step have been clearly established by the investigations of Larson et al. (10), Hama (11), Hastings (12), Roshko and Thomke (13), Badrinarayan (14), and many others. Using the Schlieren photograph of figure (2), the schematic flow field sketch of figure (3), and the experimental results of the authors above, it is possible to discern certain distinct features of the base flow in the vicinity of the step.

Along the upper surface of the step an undisturbed fully developed boundary layer with adjacent inviscid supersonic flow approaches the corner; with edge Mach number M_1 and static pressure P_1. In a small region near the corner, of the order of a boundary layer thickness, pressure signals from the separated flow downstream of the corner are propagated upstream through the subsonic portion of the boundary layer. The resulting effect is a rapid expansion of the boundary layer. This produces a drop in pressure just upstream of the step and a "diving in" of the sonic line in the boundary layer toward

the wall.

The boundary layer and adjacent outer inviscid flow initially undergo an expansion to a pressure somewhat lower than the base pressure. Since a pressure rise is required in order to separate an attached boundary layer, a compression is generated near the end of the expansion fan. This compression gives rise to the characteristic lip shock seen in figure 2 which separates the outer (almost inviscid) part of the expanding boundary layer from a new viscous sublayer which is formed just below the edge of the step. This sublayer (10-20% of the thickness of the initial boundary layer) then develops as a free shear layer into a region of recirculating flow at nearly constant pressure. Actually there exists a slight pressure rise toward the base, along the centerline, due to the stagnation of the inner reversed flow on the base. In the initial mixing region the velocity on the shear layer dividing streamline increases rapidly as mass is entrained from the dead air region.

As the mixing layer approaches the axis, the outer flow is turned back toward a direction parallel to the centerline and the pressure rises because of the interaction of the shear layer with the external flow. The velocity on the dividing streamline drops to zero at the rear stagnation point as the dividing streamline dives in to the axis at an angle of 90°, thus closing off the region of recirculating flow from the developing downstream wake.

The centerline pressure continues to increase downstream of the rear stagnation point as the pressure recovers to approximately the pressure ahead of the step. The compression waves generated by

the reattaching viscous flow coalesce to form the familiar wake shock. The shock acts to turn the nearly inviscid (but rotational) outer portion of the expanded boundary layer and adjacent inviscid flow back parallel to the axis.

All of the features noted above have been found in experiments for both turbulent and laminar approaching boundary layers. The basic difference in the two types of flow is largely due to the fact that the turbulent mixing rate ($\sim \frac{d\bar{m}}{dx}$) is of the order of ten times the laminar value. This results in higher velocities on the dividing streamline for the turbulent shear layers as opposed to the laminar layers, with the consequence of a lower base pressure for turbulent flow. A further result of the difference in mixing rates is that the length scales involved in the laminar interaction are somewhat greater than for the turbulent interaction. The wake profiles measured by Badrinarayan (14) show that there is little difference in the basic shapes of the laminar and turbulent wake profiles. Thus one might conclude that an integral analysis of the turbulent near-wake can be carried out by using any suitable set of wake profiles, provided that an appropriate length scale is adopted through the turbulent shear stress model.

II. 2. The Lip Shock

The presence of a lip shock near the end of the corner expansion fan emanating from within the viscous portion of the flow has been the object of several recent papers (11, 15). Both the experimental studies of Hama (11) and Scherberg and Smith (15) have indicated that the flow in the vicinity of the corner undergoes an overexpansion and then a pressure recovery through an oblique shock of varying strength. Hama

has shown that the lip shock strength ($P_2/P_{o.e.}$) can be correlated with the overexpansion ratio ($P_{o.e.}/P_1$) and that this ratio varies with the Reynolds number of the flow approaching the step.

Two basic reasons have been set forth to explain the lip shock phenomena. In the first instance the lip shock is considered to be a separation shock, the jump across which is just sufficient to separate the attached boundary layer approaching the base. The separation shock is generated from disturbances fed upstream from the base through the subsonic portion of the boundary layer.

A second cause of the lip shock can be traced to the reflection of the boundary layer rotational expansion waves from the free jet boundary formed in the base region. In actuality the lip shock may result from a combination of these two effects, with a small separation compression emanating from within the viscous layer being reinforced by a coalescence of the rotational expansion waves.

The experiments of Hama show that the lip shock can intersect the wake shock, thus producing a reflected expansion fan which can seriously change the shape of the static pressure rise profile along the centerline of the wake. However, for Mach numbers $M_\infty \leq 2$, the pressure profiles of Roshko and Thomke, Hastings, and others tend to show no appreciable evidence of this shock-shock interaction.

The measurements of Hastings on the lip shock strength of base flows near Mach 2 with moderate to thick initial boundary layers ($\delta_1/h = .2\text{-}5.0$), indicate a negligible (less than 10%) pressure jump across the shock. The overexpansion ratio for this range of initial

conditions also indicates a low shock strength if the correlation plot of Hama is used.

Thus it appears that the effect of the lip shock, as it influences the development of the wake flow field, may be neglected at Mach numbers of approximately 2 or less provided that the overexpansion ratio $\frac{P_{o.e.}}{P_1} \approx \frac{P_{base}}{P_1}$ is not too small ($\frac{P_{o.e.}}{P_1} \geq 0.4\text{-}0.5$).

Since complicated characteristics calculations would be required to simulate the lip shock and its attendant interactions and because a simple base flow model is sought in order to bring out the essential features of the turbulent viscous-inviscid interaction, the validity of a model which assumes an isentropic inviscid flow field is necessarily limited to those regions listed above where the lip shock strength is small.

III. FORMULATION OF THE SUPERSONIC PROBLEM

A statement of the theoretical wake problem [that one would like to solve] is as follows: Given an initial turbulent boundary layer with thickness δ_1, edge Mach number M_1, and static pressure P_1 approaching the corner of a rearward facing step of height h; determine the development of the overall wake flow features (e.g., u^*, δ, M_e, $\frac{P_e}{P_1}$, Θ, $u_{\mathcal{L}}$) as a function of the normalized axial distance from the base, x/h (see figure 3).

In practice, the inverse problem provides the most direct means of obtaining a solution, since there is no Reynolds number scaling to consider for the turbulent wake flow problem.† For a given downstream edge Mach number M_∞, a normalized wake solution downstream of the rear stagnation point is determined which passes smoothly through the Crocco-Lees critical point. This solution is made independent of the initial boundary layer thickness by normalization of all length scales (x, δ^*, etc.) by the displacement thickness at the rear stagnation point $\delta_i^*(0)$. The wake solution is then directed upstream into the reversed flow region (see section V). For any given free shear layer, the velocity on the dividing streamline u^* is initially zero at the base, and increases rapidly in the initial region of constant pressure mixing. u^* continues to increase until it reaches a maximum value ($0 \le u^* \le .587$) at the point where the wake flow field begins to interact. It then begins to decrease until it goes to zero at the rear

† No Reynolds number scaling appears in the solution provided that a turbulent eddy viscosity is employed which is proportional to a characteristic thickness of the wake, e.g., $\epsilon \sim \theta$.

stagnation point. By considering any value of u^* along the wake solution curve $u^* = u^*(x/\delta_i^*(0), M_\infty)$ in the reversed flow region as the maximum u^* possible, for a given set of initial upstream conditions, then it is possible, by a suitable matching with a mixing solution $u^*_{max} = u^*(\frac{\ell_{mix}}{h}, \frac{\delta_2}{h}, M_e)$ near the base, to determine the initial sublayer thickness δ_2/h necessary to produce that maximum value of u^*. By matching the distance to the upper edge of the sublayer mixing solution with the height of the wake boundary (see figure 4) and requiring continuity of M_e, u^*, and mass flow at the joining point† one can then not only determine δ_2/h at the corner, but the mixing length $\frac{\ell_{mix}}{h}$ and the wake scaling parameter $\delta_i^*(0)/h$ as well. Thus the wake solution is joined in this inverse manner to a step of height h.

By using a simple integral conservation model (see section VII) to determine the relation between the thickness (δ_1) of the undisturbed boundary layer approaching the step and the viscous sublayer thickness (δ_2) after expansion about the corner, the wake solution is then identified with a properly determined set of initial conditions (δ_1/h, M_1, P_1).

---

† A similar matching technique was employed by Grange, Klineberg and Lees (16) for the laminar near wake behind a blunt body, however a double iteration procedure was required in order to obtain a solution due to the Reynolds number scaling and the fact that the separation point was not known á priori.

IV. TURBULENT SHEAR STRESS MODEL

If a set of integral conservation equations are employed in order to analyze the near and far wake flow fields, the only major difference between the laminar and turbulent flow solutions will be in the length scale introduced into the problem through the viscous dissipation integral $\int_o^\delta \tau \frac{\partial u}{\partial y} dy$. Thus, if one is able to obtain an expression for the magnitude and approximate variation of the turbulent shear stress throughout the viscous layer, by use of an appropriate semi-empirical hypothesis, it should then be possible to obtain a good estimation of the important length scales and pressure levels for the turbulent base flow problem.

In the absence of any other acceptable theoretical model, the important assumption is made that the turbulent Reynolds stress $\tau = -\rho \overline{u'v'}$ is of the Boussinesq form, i.e.,

$$\tau = \rho \epsilon \frac{\partial u}{\partial y} \tag{4.1}$$

where ϵ is the well-known eddy viscosity coefficient.

IV.1. Incompressible Wake Eddy Viscosity

Townsend, (17) in his experiments on the low-speed wake behind a cylindrical rod, found that near the wake axis, the shear stress could be expressed by an equation of the form of (4.1). This behavior is evident when one notes that near the centerline

$$\overline{u'v'} \sim y$$

because of symmetry. In addition, since $\partial u/\partial y$ is zero on the wake axis

$$\frac{\partial u}{\partial y} \sim y$$

Therefore $\tau_{Reynolds} \equiv -\rho \overline{u'v'} \sim \rho \frac{\partial u}{\partial y}$ and if $\epsilon = \epsilon(x)$ is chosen as the constant of proportionality, then

$$\tau_R = \rho\epsilon \frac{\partial u}{\partial y}$$

Furthermore, if the mean flow and the correlation coefficient of velocity fluctuations are self-preserving, as found experimentally by Townsend far from the body ($x/d > 500$) then one may write

$$\frac{u_e - u}{\Delta u} = f(y/b) \tag{4.2}$$

$$\frac{\overline{u'v'}}{\overline{u'^2}} = g(y/b) \tag{4.3}$$

where b is a measure of the wake width and Δu is the maximum velocity difference across the wake = $(u_e - u_{\mathcal{C}})$.

Near the wake axis $g(y/b) \sim y/b$ because of symmetry. Townsend's measurements also indicated that near the centerline the intensity of turbulence $\sqrt{\overline{u'^2}}$ is proportional to the wake velocity defect (Δu), i.e.,

$$\overline{u'^2} \sim \Delta u^2 \tag{4.4}$$

Therefore, from equations (4.3) and (4.4) one obtains the following expression for the Reynolds stress based on the fluctuation measurements

$$\tau_R = -\rho \overline{u'v'} \sim -\rho(\Delta u)^2 (y/b) \tag{4.5}$$

In addition, the velocity gradient of the self-preserving mean flow from equation (4.2) is

$$\frac{\partial u}{\partial y} = -\frac{1}{b}(\Delta f)f'$$

Using the Boussinesq form for the shear stress

$$\tau_B = \rho\epsilon\frac{\partial u}{\partial y} = -\rho\epsilon\frac{(\Delta u)}{b}f'$$

and near the axis of symmetry $f' \sim y/b$. Thus τ_B assumes the form

$$\tau_B \sim -\rho\epsilon\frac{(\Delta u)}{b}\left(\frac{y}{b}\right) \tag{4.6}$$

Equating expressions (4.5) and (4.6), one finds that the eddy viscosity has the following form for self-preserving flow

$$\epsilon \sim \Delta u \cdot b$$

or
$$\epsilon = K_b(\Delta u)b \tag{4.7}$$

where K is a "universal" constant for 2-d incompressible self-preserving turbulent wakes, which must be found experimentally.

The constant of proportionality K is simply the reciprocal of Townsend's experimentally determined "universal" Reynolds number

$$R_T = \frac{(\Delta u)b}{\epsilon} \approx 12.5 \tag{4.8}$$

where b is the width of the mean velocity distribution

$$\frac{u_e - u}{\Delta u} = \exp\left[-\tfrac{1}{2}\, y^2/b^2\right] \tag{4.9}$$

defined by the condition

$$\frac{u_e - u(b)}{\Delta u} = e^{-\frac{1}{2}} = 0.605$$

This constant was determined by matching Townsend's experimental mean velocity profile to his theoretical solution

$$1 - \frac{u}{u_e} = \frac{R_T^{\frac{1}{2}} C_d^{\frac{1}{2}}}{2(2\pi)^{\frac{1}{4}}} \left(\frac{d}{x-x_o}\right) \exp\left[-\sqrt{\frac{\pi}{2}} \frac{R_T}{C_d} \frac{y^2}{(x-x_o)d}\right]$$

Lees and Hromas (18), in their study of turbulent diffusion in the wake of a blunt-nosed body, pointed out that the characteristic length for their study is not the body diameter but the momentum thickness, θ, which is essentially the drag coefficient of the inner wake.

It is possible, then, to redefine a new "universal" Reynolds number $R_{\theta T}$ which has as its characteristic length, the momentum thickness θ defined by the relation

$$\theta \approx \int_0^\infty \frac{\rho}{\rho_e} \frac{u}{u_e} \left(1 - \frac{u}{u_e}\right) dy \qquad (4.10)$$

which for the case of an incompressible wake with a Gaussian profile, (equation 4.9), becomes

$$\theta \approx \int_0^\infty \left(1 - \frac{u}{u_e}\right) dy = \frac{\Delta u}{u_e} b \int_0^\infty e^{-\frac{1}{2}\xi^2} d\xi$$

Evaluating the Gaussian integral one finds

$$\theta u_e = \sqrt{\frac{\pi}{2}}\, \Delta u\, b \qquad (4.11)$$

Thus the turbulent momentum thickness Reynolds number is given as

$$R_{\theta_T} = \frac{u_e \theta}{\epsilon} = \sqrt{\frac{\pi}{2}}\, R_T = 15.7$$

and the proportionality constant $K_\theta = (R_{\theta_T})^{-1}$ is

$$K_{\theta_{wake}} = .064 \text{ and } \epsilon_{wake} = K_\theta u_e \theta \tag{4.12}$$

IV.2. Incompressible Turbulent Boundary Layer Eddy Viscosity

Clauser (19), in his experimental study on the turbulent equilibrium boundary layer with pressure gradient, determined that the outer portion ($\sim 80\%$) of the boundary layer could be calculated from a Falkner-Skan like family of solutions, provided that an eddy viscosity model of the form

$$\epsilon_{b.\ell.} = K_{b.\ell.}\ u_e\ \delta^* \tag{4.13}$$

was chosen.

For the case of reattachment to a solid surface this result implies that a large portion of the boundary layer can be considered wake-like and thus amenable to a wake-type analysis.

IV.3. Incompressible Free Shear Layer Eddy Viscosity

Göertler(20) also employed the eddy viscosity model given by equation (4.7),† in order to calculate the similar solution for the velocity profile of a constant pressure free mixing layer (see figure 5). He assumed the width b of the layer to be proportional to the mixing distance x, thus

$$\epsilon_{\substack{free \\ shear}} = K_x(\Delta u)x \tag{4.14}$$

The first approximation to his solution

$$\frac{u}{u_e} = \tfrac{1}{2}\left[1 + \text{erf}\left(\frac{\sigma y}{x}\right)\right] \tag{4.15}$$

† Equation (4.7) is generally referred to as Prandtl's free mixing eddy viscosity hypothesis.

has been used extensively by many researchers to determine the spreading parameter σ $(= \frac{1}{2\sqrt{K_x}})$, for both incompressible and compressible free shear layers. Reported experimental values of σ range between 10 and 12 for incompressible flow, with a value $\sigma \approx 11.0$, usually used in most incompressible numerical computations.

Both the free shear layer spreading rate near the body and the growth rate of the far wake downstream of the body are, perhaps, the most important elements for determining the length scales in the turbulent base flow problem. One is then led to ask whether or not it is possible to prescribe a single eddy viscosity model which (based on the experimental data) can be used to determine the growth rates in both the free shear layer and far wake regions.

If one uses the Prandtl eddy viscosity model (equation 4.7) and selects as the representative thickness the physical wake or shear layer thickness $\left[\delta = (y_{u=0.99} - y_{u=0.01})\right]$ then one finds a considerable difference in the values of the proportionality constant K required to match the experimental viscous layer growth in each region. If the eddy viscosity has the form

$$\epsilon_\delta = K \Delta u \delta \tag{4.16}$$

then one finds that $K_{\delta_{wake}} = .043$ and $K_{\delta_{\substack{shear \\ layer}}} = .007$. The constants differ by a factor of 6. Thus if (4.16) were used for ϵ, it would then be necessary to adopt some arbitrary sliding scale for K in order to determine the eddy viscosity in some area of the flow in between the shear layer and far wake regions. The displacement thickness

$$\delta^* = \int_0^\infty (1 - \frac{\rho}{\rho_e} \frac{u}{u_e}) \, dy$$

would be a poor choice for ϵ since its value goes to infinity for a free mixing layer.

Perhaps the most appropriate width, which is finite for the free shear layer (for finite x), is the shear layer momentum thickness θ. The eddy viscosity thus assumes the form previously considered for the far wake,

$$\epsilon_\theta = K_\theta u_e \theta \tag{4.17}$$

Using the error function profile (equation 4.15) to determine θ

$$\frac{\sigma\theta}{x} = \int_0^\infty \frac{u}{u_e} (1 - \frac{u}{u_e}) \, d(\frac{\sigma y}{x}) = C_1 = .39844$$

and equating expressions (4.14) and (4.17) for ϵ, we find†

$$K_{\theta_{\substack{\text{shear} \\ \text{layer}}}} = \frac{1}{4\sigma C_1} = \underline{\underline{.057}} \text{ for } \sigma = 11.0 \tag{4.18}$$

In comparison, the value for the far wake was found to be

$$K_{\theta_{\text{wake}}} = \underline{\underline{.064}}$$

Thus, within the range of experimental error, the eddy viscosity coefficient K_θ for the similar free shear layer and far wake can be considered identical ($K_\theta = .06 \pm .004$) provided that the characteristic thickness for ϵ is chosen to be the momentum thickness θ of the viscous layer.

---

† Note $K_x = 1/4\sigma^2$

Even though similarity is never fully achieved, for the free shear layer with finite initial boundary layer, and likewise is obtained only in the wake flow far downstream of the base, the important assumption is made that the eddy viscosity assumes the form

$$\epsilon_{incomp} = .06\, u_e \theta \tag{4.19}$$

throughout the entire incompressible base flow field.† This formulation implies that ϵ instantaneously takes on the value corresponding to the eddy viscosity of a locally similar flow.

IV.4. Comparison of Incompressible Eddy Viscosity Shear Stress Experimental Base Flow Data

Experimental measurements have been made by Tani, et al. (21) and Mueller (22) of the turbulent fluctuations and shear stress variations in the low-speed flow field behind a rearward-facing step. Their data make possible a comparison of the measured maximum turbulent shear stress $\left.\frac{-2\overline{u'v'}}{U_\infty^2}\right|_{max}$ and dissipation integral $\frac{1}{\rho U_\infty^3}\int_o^\delta \tau \frac{\partial u}{\partial y}\, dy$ at some point in between the free shear layer and far wake regions. The data at the measured rear stagnation point is best suited for a comparison with the theory, since all that is required in addition to the eddy viscosity model of equation (4.19) is some appropriate r.s.p. velocity profile, such as the $\beta = -.1988$ Stewartson profile (to be used later in the integral analysis of section V).

The non-dimensional maximum turbulent shear stress $\tau/\frac{1}{2}\rho U_\infty^2$ as deduced from the eddy viscosity model is simply

† In sections IV.5 and IV.6 the effects of compressibility on the eddy viscosity formulation 4.19 are considered.

$$\left.\frac{-\overline{2u'v'}}{U_\infty^2}\right|_{max} = \frac{\tau_{max}}{\frac{1}{2}\rho U_\infty^2} = \frac{2\epsilon}{U_\infty}\left(\frac{\partial u/U_\infty}{\partial y}\right)_{max}$$

$$= 2K_\theta\left(\frac{\theta}{\delta^*}\right)\left(\frac{\partial u/U_\infty}{\partial y}\right)_{max} = 2K_\theta \mathcal{K} F''_{max} \qquad (4.20)$$

$$= \underline{\underline{.0255}} \text{ (Theory)}$$

where $\mathcal{K} = .248$ and $F'' = .860$ for the $\beta = -.1988$ Stewartson r.s.p. velocity profile. The experimental values of Mueller and Tani are as follows

$$\left.\frac{-2u'v'}{U_\infty^2}\right|_{\text{Mueller expt.}} = \underline{\underline{.024 - .034}}$$

Step height
h = .25-.75 inches
r.s.p. @ $x/h \approx 7.0$

$$\left.\frac{-2u'v'}{U_\infty^2}\right|_{\text{Tani expt.}} = \underline{\underline{.020-.030}}$$

h = .5-6.0 cm
r.s.p. @ x/n = 6.0

The mechanical energy dissipation integral, I_d, as mentioned previously, is the only term through which the turbulent scaling is introduced into the integral flow conservation equations. This quantity is given simply by the theory as

$$I_d = \int_0^\delta \frac{\tau}{\rho U_\infty^2}\,\frac{\partial}{\partial y}\left(\frac{U}{U_\infty}\right)dy$$

$$= \frac{1}{2} K_\theta \mathcal{K} R = \underline{\underline{9.55 \times 10^{-3}}} \text{ (Theory)} \qquad (4.21)$$

where

$$R = \frac{2\delta^*}{U_\infty^2}\int_0^\delta \left(\frac{\partial u}{\partial y}\right)^2 dy = 1.260 \text{ from the Stewartson profile}$$

The experimental values found by Mueller are

$$I_{d\,|\,\substack{\text{Mueller}\\ \text{expt.}}} = \underline{\underline{5.5 \times 10^{-3} - 11.0 \times 10^{-3}}} \quad h = .25\text{-}.75 \text{ inches}$$

As one notes from a comparison of the values above, the eddy viscosity model provides a good prediction of the magnitude of the shear stress and dissipation integrals obtained from the incompressible flow measurements made at the rear stagnation point.

Thus we may proceed with some conviction that the scaling in the non-similar regions of the flow will be adequately predicted by our choice of the eddy viscosity model (4.19).

In the next section we will attempt to extend this model for ϵ to compressible flows using the available compressible free shear layer measurements as a guide.

IV.5. Transformation of the Free Turbulent Compressible Boundary Layer Equations

The equations of mean motion of the free steady two-dimensional turbulent compressible boundary layer of a perfect gas with variable density $\rho(x, y)$ are given in the form:

Continuity:

$$\frac{\partial}{\partial x}(\rho u) + \frac{\partial}{\partial y}(\rho v) = 0 \tag{4.22}$$

Momentum:

$$\rho u \frac{\partial u}{\partial x} + \rho v \frac{\partial u}{\partial y} = -\frac{\partial p}{\partial x} + \frac{\partial \tau}{\partial y}$$

$$0 = -\frac{\partial p}{\partial y} \tag{4.23}$$

By considering the turbulent Prandtl number equal to unity ($P_{R_t} = 1$) and assuming no heat transfer at the boundaries, the flow is adiabatic,† in which case

Energy:

$$C_p T + \frac{1}{2} u^2 \; T \text{ constant} = C_p T_e + \frac{1}{2} u_e^2 \tag{4.24}$$

The external flow at the edge of the boundary layer is assumed isentropic. The external conditions far downstream of the body ($v_e = 0$, $u_e = u_\infty$) are characterized by the subscript ∞. If it is required that the compressible free turbulent boundary layer equations (4.22-4.24) transform into an equivalent incompressible form and that the shear stress obey the Boussinesq law (4.1), then one finds in analogy with laminar flow that such a transformation can be obtained by employing a modified†† Stewartson transformation

$$dY = \frac{a_e}{a_\infty} \frac{\rho}{\rho_\infty} dy \qquad dX = \frac{a_e}{a_\infty} \frac{\rho_e}{\rho_\infty} dx$$

$$\Psi = \psi \qquad U = \frac{a_\infty}{a_e} u \tag{4.25}$$

and by assuming that the compressible transformation of the eddy viscosity is of the form

$$\rho^2 \epsilon = f(x) = \rho_r^2 \epsilon_o$$

The quantity ρ_r is a reference density in the real flow which will be determined by comparison of the theoretical spreading rates of the

† This study is limited to the simple case of adiabatic wake flows. The much more difficult case of non-adiabatic wake flows will be dealt with in a future study.

†† The transformation of the x variable is changed from the laminar form $dX = a_e/a_\infty \; P_e/P_\infty \; dx$, in order to scale the eddy viscosity term properly.

compressible free shear layer with experiment (see section IV. 6). Using the incompressible correlation of ϵ (equation 4. 17) as a guide, the compressible eddy viscosity is thus assumed to have the form

$$\epsilon = \frac{\rho_r^2}{\rho^2} K_\theta u_e \theta \tag{4.26}$$

Using the modified Stewartson transformation (4. 25) and the eddy viscosity model (4. 26), the transformed boundary layer equations then become

$$\frac{\partial U}{\partial X} + \frac{\partial V}{\partial Y} = 0 \tag{4.27}$$

$$\frac{U\partial U}{\partial X} + V \frac{\partial U}{\partial Y} = U_e \frac{dU_e}{dX} + \tilde{\epsilon} \frac{\partial^2 U}{\partial Y^2} \tag{4.28}$$

where $$\tilde{\epsilon} = \left(\frac{\rho_r}{\rho_e}\right)^2 K_\theta U_e \overline{\theta} \tag{4.29}$$

$\overline{\theta}$ is the transformed momentum thickness defined as

$$\overline{\theta} = \int_0^{\delta_i} \frac{U}{U_e}\left(1 - \frac{U}{U_e}\right) dY = \frac{a_\infty \rho_\infty}{a_e \rho_e} \theta \tag{4.30}$$

With the constant K_θ essentially determined by the incompressible flow correlation, the effect of compressibility on the turbulent scaling is relegated to determining the ratio of the reference density to the density at the edge of the free boundary layer. For an adiabatic wake flow, one may write this ratio in the form

$$\frac{\rho_r}{\rho_e} = \left[1 + g\left(\frac{\gamma-1}{2}\right) M_e^2 \left(1 - \frac{u_\ell}{u_e}\right)^2\right] \tag{4.31}$$

where g is a constant to be determined experimentally. One notes that for $g = 0$ $\quad \rho_r = \rho_e$

and for $g = 1$ $\quad \rho_r = \rho_\ell$

Thus the reference density can be determined in a manner similar to the Eckert reference enthalpy for turbulent wall boundary layers.

IV.6. Similar Solution of the Compressible Constant Pressure Free Shear Layer

In this section we seek to determine the reference density by comparing a theoretical solution for the constant pressure compressible free shear layer spreading rates with those obtained by experiment. We will first investigate a mixing solution far enough away from the point of separation for a similarity solution to apply, i.e. $x/\theta_o \to \infty$. Starting with the transformed equations (4.27-4.29), we employ the stream function ψ which satisfies the continuity equation, where

$$\psi = U_e \, \xi(X) f(\eta)$$

The similarity variable η is simply

$$\eta = Y/\xi(X)$$

Substituting in the momentum equation (4.28), with $dU_e/dx = 0$, we find

$$f''' + ff'' \frac{\xi(X)}{\tilde{\varepsilon}} U_e \frac{d\xi(X)}{dX} = 0$$

For similarity, i.e., $f' = \frac{U}{U_e} = f'(\eta)$ only, we require

$$\frac{\xi}{\tilde{\varepsilon}} U_e \frac{d\xi}{dX} = \text{constant} = a$$

Without loss of generality we set $a = 1$ thus obtaining the familiar Blasius equation of laminar flow

$$f''' + ff'' = 0 \qquad (4.32)$$

with the following boundary conditions

$f'(-\infty) = 0$ $\qquad$ $f(0) = 0$ implies $\eta = 0$

$f'(+\infty) = 1$ $\qquad$ corresponds to the dividing streamline $\psi = 0$

Solutions of the equation above have been provided both by Göertler (20) and Chapman (23). Thus it is noted that the shape of the similar velocity profiles in both laminar and turbulent flow are identical, provided that an eddy viscosity model of the Prandtl form is used. The only difference in the two cases is the length scale $\xi(X)$. For the transformed eddy viscosity as given by equation (4.29) we obtain

$$\xi d\xi = \left(\frac{\rho_r}{\rho_e}\right)^2 K_\theta \bar{\theta} dX \tag{4.33}$$

For similarity the following relationship between $\bar{\theta}$ and ξ exists

$$\bar{\theta} = \xi \int_{-\infty}^{\infty} f'(1-f')\, d\eta = \xi C$$

where

$$C = \int_{-\infty}^{\infty} f'(1-f')\, d\eta = .8756$$

Thus upon integration of (4.33) we find

$$\xi = \left(\frac{\rho_r}{\rho_e}\right)^2 K_\theta C X \tag{4.34}$$

and therefore

$$\theta = \bar{\theta} = \left(\frac{\rho_r}{\rho_e}\right)^2 K_\theta C^2 X \quad \dagger$$

---

† $\theta = \bar{\theta}$ and $x = X$ for a constant pressure shear layer provided the flow conditions at ∞ are taken to be the same as those at the edge of the mixing layer, i.e. $\rho_\infty a_\infty = \rho_e a_e$.

While dimensional analysis can independently show that similar turbulent shear layers spread linearly with X, equation (4.34) in addition implies that if the reference density is less than the edge density in compressible flow, then the magnitude of the linear spread will be smaller in compressible than in incompressible flow. Such a trend has been noted by many experimentalists.

This points to the selection of the density in the quiescent zone (g = 1) as a likely candidate for the reference dentity. In addition if it is required that the transformation reduces to itself in a region of the real flow where the density is incompressible, i.e., in the quiescent region, then in order that the local shear stress in the vicinity of this region correspond to that of an incompressible flow, we must place

$$\rho^2 \epsilon \Big|_{u \to 0} = \rho_r^2 \epsilon_o$$

or $$\rho_r = \rho_{u=o} \equiv \rho_o$$

While Coles (33) correctly points out that such a requirement is not at all necessary for a compressibility transformation of the equations, we will assume the reference density to be ρ_o(g = 1) and then check this assumption with the experimental results.

For the case g = 1 and $u_{\mathcal{L}} \approx u_o \approx 0$, equation (4.31) yields

$$\left(\frac{\rho_r}{\rho_e}\right)_{\substack{\text{const} \\ \text{press}}} = \frac{\rho_o}{\rho_e} = \frac{1}{1+\frac{\gamma-1}{2} M_e^2} \qquad (4.34)$$

Comparison with Experimental Data

The evaluation of the spreading rate for the turbulent half jet has been the object of numerous experimental investigations over the past 40 years. The early experimental work of Tollmien (24), Reichardt (25) and Liepmann and Laufer (26), helped to establish an approximately constant value of the mixing coefficient σ ($\sim 1/K$) for the incompressible flow of a half jet ($\sigma \approx 11.0$). The usual method for determining the spreading rate was to compare measured velocity distributions in the nondimensional form of $\sigma y/x$ vs. U/U_e with some known theoretical velocity distribution, such as that derived by Tollmien (based on Prandtl's mixing length hypothesis) or Göertler's velocity profile, or the previously mentioned error function profile (Göertler's first approximation). The incompressible jet spreading parameter ($\sigma^* \equiv \sigma_{M=0}$) is related to our mixing coefficient K_θ by the relation

$$\sigma^* = \frac{1}{2K_\theta C} \tag{4.35}$$

While the incompressible value of σ appears to be well established (within a range of 10 to 20%), the attempt to extend the measurement of the mixing coefficient to cases where compressibility effects are important ($M_e \geq 1.0$) has resulted in a great discrepancy between the reported values. For example, experimental values at Mach 2 as reported by McDonald (3) differ by almost a factor of 2. The most common experimental method (27, 28, 29) for obtaining a quasi-two dimensional-turbulent mixing zone is the investigation of the velocity profiles in the potential core regime of an axisymmetric jet exhausting

from a nozzle into a quiescent atmosphere (see figure 5). Since the shear layer width is small in comparison to the nozzle radius, axisymmetric effects are generally neglected. Other experiments, such as those of Charwat and Yakura, Sirieix (30) and Bailey and Kuethe (31), have used two dimensional step configurations and made probes of the constant pressure free shear layer regime.

Outside of common experimental errors (such as those caused by probe calibrations, etc.) there appear to be two major causes for the discrepancies in the reported values of σ. The first cause may be attributed to the fact that, in many of the cases, the flow had not reached a similarity state, (i.e., where $x/\theta_o \to \infty$ and $u/u_e = f'(\eta)$) because of the presence of a sizable initial boundary layer prior to separation. This problem is particularly true in the cases of pure base flow setups such as in the experiments of Charwat and Yakura at Mach 2 and those of Larson, et al. (10) at Mach 3 where recompression began before similarity could be achieved. Since the rate of growth in the initial non-similar region is greater than that of the asymptotic ($x/\theta_o \to \infty$) linear growth, low values of σ are reported. As will be shown later, a good criteria for judging if similarity has been reached is that

$$\frac{x/\theta_o}{\sigma^*\left(1+\frac{\gamma-1}{2}M_e^2\right)^2} \geq 10 \qquad (4.36)$$

We note from equation (4.36) that as the Mach number of the external flow increases, the longitudinal distance along the mixing layer (x) at which a similar profile may be expected must also increase. Thus,

for example, if experiments at $M_e = 1$ just satisfy the criteria above, then at $M_e = 3$ the distance at which similarity may be expected is increased by more than a factor 5, for the same initial value of θ_o.

The second cause of experimental discrepancy may be attributed to the various techniques adopted by the many experimentalists in order to determine the parameter σ. The most common technique employed, even at Mach numbers of 2 or more, is to find the value of σ which allows the best fit of the measured velocity profile with some well-known incompressible profile. Different authors have used different profiles, resulting in additional confusion. In several of the cases reported, how a best fit is obtained is not always clear. While some authors place emphasis on the upper portion of the profile, where $u/u_e \to 1$, others treat the middle portion of the profile as the important region of interest. One technique which has recently received attention, is to match the slope of the measured velocity profile, at a point where $u/u_e = .5$, with the slope of the error function profile, $u/u_e = \frac{1}{2}(1+\text{erf}\,\frac{\sigma y}{x})$. Using the compressibility transformation in a manner similar to that used by King and Denison (32) we can theoretically determine the effect of compressibility on a σ defined by this matching technique. The following relation results.

$$\frac{\sigma_{slope}}{\sigma^*} = \frac{\sigma_s}{\frac{1}{2}(KC)^{-1}} = \frac{(\rho_e/\rho_o)^2}{\left\{1 + (\frac{\rho_e}{\rho_o} - 1)\left[1 - (\frac{u}{u_e})^2\right]\right\}}\Bigg|_{\frac{u}{u_e} = .5} \qquad (4.37)$$

where $\rho_e/\rho_o = 1 + \frac{\gamma-1}{2} M_e^2$ for adiabatic flow

While equation (4.37) could be used as a means of comparison between the compressibility transformation and the data on σ, such a comparison still suffers from the fact that an arbitrary point in the velocity profile is selected to provide a value of σ supposedly valid as a scale factor for the entire profile. It is clear from equation (4.37) that different values of σ could be obtained by matching slopes at different points in the profile, i.e., at points other than $u/u_e = 5$.

A test of the compressibility transformation which would be more meaningful, particularly for an integral method of solution, would be one based on the spreading rate of an integral parameter of the velocity profile, namely the momentum thickness θ. This test would eliminate the confusion arising from the use of various curve-fitting methods. Based on the compressibility transformation the expression for the momentum thickness is:

$$\frac{\theta}{x} = (\rho_e/\rho_o)^2 K_\theta C^2$$

If we define the momentum thickness spreading parameter σ_θ as

$$\sigma_\theta \equiv \frac{(d\theta/dx)_{\text{incompressible}}}{(d\theta/dx)_{\text{compressible}}} \sigma^* = \frac{C/2}{(d\theta/dx)_{\text{compressible}}} \tag{4.38}$$

then we note that the rate of spread of the momentum thickness decreases as the square of the density ratio, or that

$$\frac{\sigma_\theta}{\sigma^*} = \left(\frac{\rho_e}{\rho_o}\right)^2 = \left(1 + \frac{\gamma-1}{2} M_e^2\right)^2 \tag{4.39}$$

Values of the momentum thickness were calculated from all available shear layer velocity profiles by simple numerical integration. A typical result of this technique is shown in figure 6 where a plot of

θ vs. x from the data of Maydew and Reed (28) is presented. The constant slope of the curve ($d\theta/dx$) is easily determined and a value of σ_θ readily calculated from equation (4.38). A plot of the values of σ_θ against ρ_e/ρ_o for the data of Maydew and Reed (M_e = 0.70, 0.85, 0.95, 1.49, 1.96) shows excellent agreement between theory (equation 4.39) and experiment, thus confirming the á-priori choice of g = 1 and ρ_o as the reference density. King and Denison previously found the same result based on a least squares fit of experimental and theoretical profiles. Extrapolating the theoretical curve to $\rho_e/\rho_o = 1$ along a line of slope 2 (in a log-log plot) results in a value of $\sigma^* = 9.42$. This value of σ^* corresponds to a value of $K_\theta = .0606$ which is in good agreement with the average magnitude of K_θ ($\approx .06$) determined solely from incompressible shear layer and wake experiments.

A final plot of the data and theory for σ_θ/σ^* vs. ρ_e/ρ_o is presented in figure (7) along with a comparison of the experimental values of the spreading parameter σ_{slope} with the theory of equation (4.37). One notes that both sets of curves show good agreement between experiment and theory up to Mach 3, with the data of Sirieix at Mach 4 falling somewhat below the theory. It is possible that similarity may not have been reached, based on the criteria of equation (11a), in the measurements at Mach 4; accounting for the lower value of σ. The somewhat lower value of σ^* (9.42 as opposed to a nominal value of 11 for incompressible flow) is not considered to be a serious discrepancy since its use is essentially as a scale factor ($K_\theta = .06$) in the compressibility transformation, valid for both free shear layer

and wake flows. The important point to be established here is the prediction by the transformation of the correct effect of compressibility on integral quantities. This objective is believed to have been met, at least insofar as the low Mach number compressible similar free shear is concerned.

V. INTEGRAL WAKE FLOW SOLUTION METHOD

The turbulent wake flow solution, for the region of near wake interaction not too close to the base, follows the same integral technique adopted by Lees and Reeves (7) for the laminar near wake; the only difference being that the kinematic viscosity ν_∞ in the transformed dissipation integral $\int_o^\delta \tau \frac{\partial u}{\partial y} dy$ is replaced by a transformed eddy viscosity of the form

$$\tilde{\epsilon} = \frac{\rho_r^2}{\rho_e^2} K_\theta U_e \overline{\theta} \qquad (5.1)$$

V.1. The Wake Reference Density

In order to make use of the eddy viscosity model, it is necessary to specify a reference density for the wake. For the free shear layer portion of the flow, it was determined (section IV) that the density ρ_o in the recirculating region was the appropriate reference density for scaling the overall spreading rate of the adjacent shear layer. Far behind the body, where the density throughout the wake approaches the free stream density ρ_∞, it is clear that conditions in the recirculating region cannot be of importance in determining the local far wake growth rates. It appears therefore that an appropriate reference density might be one that varies with the local flow conditions. The density along the centerline of the wake satisfies both the condition that it equal the density in the quiescent region near the body, and that it approach the free stream density far from the body. Thus the important assumption is made that

$$\rho_r = \rho_{\mathfrak{L}} \qquad (5.2)$$

For adiabatic flow we therefore have the relation

$$\frac{\rho_r}{\rho_e} = \left[1 + \frac{\gamma+1}{2} M_e^2 \left(1 - u_{\mathfrak{C}}^2/u_e^2\right)\right]^{-1} \qquad (5.3)$$

It would be difficult to ascertain experimentally if this choice of ρ_r indeed scales conditions in the far wake: as $u_{\mathfrak{C}}/u_e \to 1$ there is little to distinguish the centerline density from any other local density. At the rear stagnation point the axial pressure gradient is just balanced by the tangential shear stress gradient, i.e.,

$$\frac{dp}{dx} = \frac{\partial \tau}{\partial y} \approx \varepsilon \frac{\partial^2 u}{\partial y^2} \qquad u_{\mathfrak{C}} = 0 \qquad (5.4)$$

Using this fact, one can determine the suitability of the selected reference density as a scaling parameter for the compressible reattaching wake flow by comparing the theoretical solution for the axial pressure gradient at the r.s.p. $\left[\frac{dp}{dx} \sim \left(\frac{\rho_r}{\rho_e}\right)^2\right]$ with the appropriate experimental data. Such a comparison is carried out in section VIII.

V.2. Integral Equations for Wake Viscous-Inviscid Interaction

The interaction of the viscous or dissipative flow in the near wake with the external inviscid flow is but one example taken from a family of viscous fluid-mechanics problems in which the outer flow field is not known á-priori (in contrast to usual boundary layer theory), but must be determined by the interplay between the dissipative and inviscid flow fields.

Because of the complexities of the interaction phenomena, integral or moment conservation equations have been developed in order to bring out the essential gross features of the flow, such as

length scales and pressure levels. The integral approach of Reeves and Lees (7) as applied to the problems of shock-wave boundary layer interaction and the laminar near wake, has demonstrated that the overall features of the interaction can be adequately described, provided that the velocity profiles, from which the integral quantities are derived, exhibit the correct qualitative behavior. For the particular case of wake flows, not too close to the base, we follow Reeves and Lees in adopting for the velocity profiles in the integral equations the Stewartson wake solutions $[U/U_e = f'(\eta)]$ of the Falkner-Skan equations

$$f''' + ff'' + \beta [1 - (f')^2] = 0 \qquad (5.5)$$

with the boundary conditions

$$f(0) = f''(0) = 0 \qquad f'(\infty) = 1$$

These profiles display the correct qualitative behavior noted of base flows (see figure 8), i.e., a series of reversed flow profiles with zero shear on the axis for use upstream of the rear stagnation point ($-.1988 \leq \beta \leq 0$) and a series of zero shear profiles downstream of the rear stagnation point with positive axis velocities ($-.50 \leq \beta \leq -.1988$).† They also exhibit the exact behavior near the r.s.p., of the full Navier-Stokes equations as found by Reeves (7) in a series expansion about that point.

Even in those turbulent base flow cases where reattachment occurs on a solid surface, the profiles of the reattaching turbulent

† Note that as $\beta \to -.5$ the velocity profile approaches the far wake Gaussian solution

boundary layer exhibit a strong wake-like quality which, except in a region very close to the wall, makes the boundary layer appear to have a finite slip. This wake-like character, which is particularly dominant near points of separation and reattachment, was effectively demonstrated by Coles (33) when he proposed the "law of the wake" for the turbulent boundary layer.

The Falkner-Skan profiles are again "unhooked" from the pressure gradient parameter β, by making the normalized integral quantities (e.g., $\mathcal{H} = \theta/\delta^*$) functions of a single independent parameter a(X). For flow downstream of the rear stagnation point the independent parameter a(X) is the normalized centerline velocity

$$a(X) = \frac{U_{\mathcal{C}}}{U_e} \quad \text{for} \quad \frac{U_{\mathcal{C}}}{U_e} > 0 \tag{5.6}$$

In the reversed flow field just upstream of the rear stagnation point, a(X) is the velocity on the dividing streamline

$$a(X) = (U/U_e)_{\psi=0} = u^* \quad \frac{U_{\mathcal{C}}}{U_e} < 0 \tag{5.7}$$

The work of Webb, Golik, and Lees (8) has shown that single parameter Stewartson profiles appear to work quite well downstream of the rear stagnation point, and provide considerable improvement over polynomial profiles in the region immediately upstream of the r. s. p.

Single parameter reversed flow profiles, while adequate in the region near the r. s. p. cannot properly describe the flow in the region near the base where <u>two</u> independent length scales are important, the thickness of the separated shear layer and the height of the

reversed flow region, which must be equal to the base height (h) at the body ($u_{\mathcal{L}} = u^* = 0$).

In this section, we consider only that portion of the flow which is adequately described by single parameter profiles.†

To describe the wake flow properly we require, in addition to the parameter a(X), at least two additional independent quantities (for adiabatic flow); the Mach number at the edge of the boundary layer M_e, and a suitable thickness variable such as δ_i^* (the transformed displacement thickness).

The three integral equations necessary for a solution of the three unknowns a(X), $M_e(X)$, and $\delta_i^*(X)$ are chosen to be the integral forms of the conservation equations of (1) x-momentum, (2) mechanical energy, and (3) continuity.

Using the transformed continuity equation (4.27), the transformed momentum equation (4.28) is integrated across the boundary layer to obtain the integral momentum equation with zero shear on the axis.

MOMENTUM

$$\mathcal{H} \frac{d\delta_i^*}{dX} + \delta_i^* \frac{d\mathcal{H}}{da} \frac{da}{dX} + [2\mathcal{H}+1] \frac{\delta_i^*}{M_e} \frac{dM_e}{dX} = 0 \qquad (5.8)$$

where

$$\mathcal{H}(a) = \frac{\theta^*}{\delta_i} \text{ and } \delta_i^* = \int_0^\delta (1 - \frac{U}{U_e}) \, dY$$

Integrating the continuity equation (4.22) across the layer in modified

† In section VII various schemes for joining the reattaching wake flow to the body are set forth and evaluated.

Stewartson coordinates,† yields the following equation relating the local outer inviscid streamline angle, $\Theta = \tan^{-1}\frac{v_e}{u_e}$, to the normal velocity induced by the inner flow.

CONTINUITY

$$\left[\mathcal{K} + \frac{1+m_e}{m_e}\right]\frac{d\delta_i^*}{dX} + \delta_i^*\frac{d\mathcal{K}}{dz}\frac{da}{dX} + f\frac{\delta_i^*}{M_e}\frac{dM_e}{dX} = \frac{\tan\Theta}{m_e} \qquad (5.9)$$

where

$$f = 2\mathcal{K} + \frac{3\gamma-1}{\gamma-1} + \frac{\gamma+1}{\gamma-1}\frac{m_e}{1+m_e}\mathcal{K} + \frac{M_e^2-1}{m_e(1+m_e)}Z$$

and $$Z = \frac{1}{\delta_i^*}\int_0^{\delta}\frac{U}{U_e}\,dY \qquad (5.10)$$

Since the flow at the outer edge of the wake is assumed isentropic, the Prandtl-Meyer relation can be used to link the inner and outer flow. Thus,

$$\Theta = \nu(M_\infty) - \nu(M_e) \qquad (5.11)$$

where

$$\nu(M_e) = \sqrt{\frac{\gamma+1}{\gamma-1}}\tan^{-1}\left[\sqrt{\frac{\gamma-1}{\gamma+1}}\sqrt{M_e^2-1}\right] - \tan^{-1}\sqrt{M_e^2-1} \qquad (5.12)$$

Multiplying the transformed momentum equation (4.28) by U and integrating provides us with the third equation needed for solution of the three unknowns δ_i^*, M_e, and a. This equation is the only one containing the eddy viscosity term, which can be considered as the scaling function for the wake dissipation integral $\int_0^{\delta_i}\tau\frac{\partial u}{\partial y}\,dy$. The mechanical energy equation thus may be written as:

† The outer flow field is assumed isentropic.

MECHANICAL ENERGY

$$J\frac{d\delta_i^*}{dX} + \delta_i^*\frac{dJ}{da}\frac{da}{dX} + 3J\frac{\delta_i^*}{M_e}\frac{dM_e}{dX} = \left(\frac{\tilde{\epsilon}}{U_e\delta_i^*}\right)\frac{2\delta_i^*}{U_e^2}\int_0^{\delta_i}\left(\frac{\partial U}{\partial Y}\right)^2 dY$$

$$= K_\theta\left(\frac{\rho_{\mathbb{C}}}{\rho_e}\right)^2 \mathcal{H}/R \qquad (5.13)$$

where

$$J = \frac{\theta_i^*}{\delta_i^*} \quad \theta_i^* = \int_0^{\delta_i}\frac{U}{U_e}\left(1 - \frac{U^2}{U_e^2}\right)dY \text{ and } R = \frac{2\delta_i^*}{U_e^2}\int_0^{\delta_i}\left(\frac{\partial U}{\partial Y}\right)^2 dY$$

For a given value of the profile parameter "a" the non-dimensional quantities $\mathcal{H}$, J, R and Z are numerically evaluated by integrating the Stewartson similar wake flow solution (figure 8) corresponding to a particular value of "a" $\left[\frac{U}{U_e} = f'(\eta, a)\right]$. These quantities are then curve-fitted as a function of "a" to facilitate differentiation and numerical integration. The functions (as previously listed by Lees and Reeves) are the following

Upstream of Rear Stagnation Point

$$\begin{aligned} a(X) &= u^* = (U/U_e)_{\psi=0} \qquad 0.54 < a < 0 \\ \mathcal{H} &= .2482 - .4351a - .0366a^2 \\ J &= .376 - .582a \\ R &= 1.260 + 2.280 + 30.4a^5 \\ Z &= 1.034 - 1.38a \end{aligned} \qquad (5.14)$$

Downstream of Rear Stagnation Point

$$\begin{aligned} a(x) &= U_{\mathbb{C}}/U_e \qquad 0 < a < .75 \\ \mathcal{H} &= .2492 + .880a - .1585a^2 \\ J &= .376 + 1.177a + .427a^2 \\ R &= .020 + 2.39\,(a-.72)^2 \\ Z &= 1.034 + 2.932a + 12.65a^4 \end{aligned} \qquad (5.15)$$

V.3. Numerical Integration of the Differential Equations

Equations (5.8), (5.9) and (5.13) represent a system of three first order differential equations, linear in the derivatives $\frac{dM_e}{dx}$, $\frac{d\delta_i^*}{dx}$, $\frac{da}{dx}$.

By employing Cramer's rule, a simultaneous solution of this system may be written as

$$\frac{\tilde{\delta}_i^*}{M_e}\frac{dM_e}{d\tilde{x}} = \frac{N_1(M_e, a)}{D(M_e, a)} \tag{5.16}$$

$$\tilde{\delta}_i^* \frac{d\mathscr{V}}{da}\frac{da}{d\tilde{x}} = \frac{N_2(M_e, a)}{D(M_e, a)} \tag{5.17}$$

$$\frac{d\tilde{\delta}_i^*}{d\tilde{x}} = \frac{N_3(M_e, a)}{D(M_e, a)} \tag{5.18}$$

provided that the determinant of coefficients D does not vanish.

We note that by normalizing X and δ_i^* by the value of δ_i^* at the rear stagnation point

$$\tilde{x} = X/\delta_i^*(0) \qquad \tilde{\delta}_i^* = \delta_i^*/\delta_i^*(0)$$

we can determine a solution which is independent of the size of the wake boundary layer. Thus we see that the initial boundary layer on the body determines only the stretching of the interaction length scales but does not affect the pressure levels at and downstream of the rear stagnation point.

Noting the coefficients of the derivatives in the conservation equations, the numerators and denominators in equations (5.16-5.18) are found to be the following

$$N_1(M_e, a) = \frac{\tan\Theta}{m_e}\left[\mathscr{V}\frac{dJ}{d\mathscr{V}} - J\right] + \left(\frac{1+m_e}{m_e}\right)K'\mathscr{V}R$$

$$N_2(M_e, a) = \frac{\tan\Theta \cdot J}{m_e}\left[1-\mathscr{V}\right] + K'\mathscr{V}R\left[\mathscr{V}f-(2\mathscr{V}+1)\left(\mathscr{V}+\frac{1+m_e}{m_e}\right)\right] \qquad (5.19)$$

$$N_3(M_e, a) = \frac{\tan\Theta}{m_e}\left[3J - \frac{dJ}{d\mathscr{V}}(2\mathscr{V}+1)\right] + K'\mathscr{V}R\left[(2\mathscr{V}+1)-f\right]$$

$$D(M_e, a) = \left(\mathscr{V}\frac{dJ}{d\mathscr{V}} - J\right)f + (\mathscr{V}-1)J + \left[\mathscr{V}+\frac{1+m_e}{m_e}\right]\left[3J - (2\mathscr{V}+1)\frac{dJ}{d\mathscr{V}}\right]$$

where $K' = K_\theta(\rho_{\mathfrak{L}}/\rho_e)^2$

Webb, Golik and Lees (8) have shown numerically (using polynomial profiles) that the denominator D possesses four real roots in the region $-1 \le \frac{u_{\mathfrak{L}}}{u_e} \le 1$. The two upstream singularities are not of practical interest because of the fact that the centerline velocities required at these points are much greater than the maximum value $\frac{u_{\mathfrak{L}}}{u_e} = -.18435$ obtained for the Stewartson family of solutions. The singular point at $u_{\mathfrak{L}}/u_e = 1.0$ is approached only infinitely far downstream of the rear stagnation point and is thus unimportant to the solution. The singularity immediately downstream of the stagnation point is shown to possess a saddle point behavior with the solution curve corresponding to that asymptote through the point which has the appropriate wake behavior. At the saddle point we require that $N_1=N_2=N_3=D=0$,† in order to provide a continuous transition from "subcritical" to "supercritical" flow. D. Ai (34) performed a rigorous mathematical investigation of all the singular points of the laminar flow integral equations

† Note that if N_i and D are both = 0, this implies that $N_j = N_k = D$

by studying the phase space solution trajectories in the vicinity of these points. His analysis confirmed the existence and behavior of the singularities found previously only by numerical integration.

The location of the critical point, which is unknown á-priori, is found in the following manner: starting at the rear stagnation point ($\tilde{\delta}_i^* = 1.0$ a = 0), a trial value of the edge Mach number $M_e(0)$ is selected for a given M_∞. Equations (5.16-5.18) are then integrated numerically on an IBM 7090 computer using a Runge-Kutta technique. The resulting integral curves are evaluated until either $N_1 \to 0$, corresponding to $\frac{dM_e}{dx} > 0$, or until $D \to 0$, corresponding to $du_\ell/dx < 0$. Since neither of these two conditions is physically acceptable for a recompressing wake flow, it is concluded that the solution curve lies between these sets of integral curves, i.e., along the solution asymptote of the saddle-point singularity. D. Ai showed that, while numerical integration toward a saddle point is inherently unstable, the solution trajectories found by using large high-speed computers can be made to essentially coincide with those found in a Taylor series expansion about the critical point provided that the margin of error for the initial eigenvalue is kept small $\left[\text{e.g. } (M_{e_{n+1}} - M_{e_n})/M_{e_n} = O(10^{-8})\right]$.

Since the solution curves only depend on the initial choice of the parameter $M_e(0)$, for a fixed value of "a", it is clear then that $M_e(0)$ represents the proper initial eigenvalue for the problem. A plot of a typical set of solution curves in the D vs. "a" plane is seen in Fig. 9. Differences in values of $M_e(0)$ as small as 10^{-8} are seen to be sufficient to distinguish between the two types of integral curves

($dM_e/dx > 0$ and $da/dx < 0$). Since the critical point could not in practice be approached arbitrarily closely, the solution downstream of the critical point ($N_i = D = 0$) was obtained by extrapolating across the critical point and resuming the integration with the new set of starting conditions. There is little error involved in this technique, since the critical point is quite close to free stream conditions; p_e/p_∞ at the critical point was found to be near unity ($.75 \leq p_e/p_{\infty_{crit}} \leq 1$ for $M_\infty \leq 4$).

The wake solution in the reversed flow region is easily obtained once the value of $M_e(0)$ is known. Equations (5.16-5.18) are integrated upstream from the rear stagnation point ($\delta_i^* = 1$, $a = 0$, $M_e = M_e(0)$) with the appropriate reverse-flow curve fits used for the integral quantities (equations 5.15).

The results of a typical numerical calculation ($M_\infty = 2.0$) are shown in figure (10), where the edge Mach number M_e, normalized wake thickness $\delta/\delta_i^*(0)$†, and dividing streamline velocity u^* are plotted as a function of the normalized axial distance from the rear stagnation point $x/\delta_i^*(0)$.

Far upstream of the r.s.p. the edge Mach number distribution is nearly flat, indicating that a region of constant pressure is being approached. As the wake flow proceeds toward the r.s.p., M_e begins to decrease rapidly as the effect of the interaction becomes more pronounced, dM_e/dx reaching a maximum at the r.s.p. Downstream of

---

† From the compressibility transformation

$$\frac{\delta}{\delta_i^*(0)} = \frac{\rho_\infty a_\infty}{\rho_e a_e} \cdot \left[\frac{\delta_i^*}{\delta_i^*(0)}\right] \cdot \left[m_e(1+\mathcal{K}) + 1 + Z\right]$$

the r. s. p., dM_e/dx again decreases as the edge Mach number approaches the constant downstream flow conditions ($M_e \rightarrow M_\infty$).

The wake thickness $\delta/\delta_i^*(0)$ decreases rapidly from its large value in the reversed flow region, reaches a minimum near the critical point and then increases slowly. In the far wake region $\delta \sim x^{\frac{1}{2}}$ as given by simple scaling arguments.

The velocity on the dividing streamline u^* in the reversed flow region increases rapidly from zero at the r. s. p. and approaches a limiting value of .58 infinitely far upstream. Any u^* along this curve ($x/\delta_i^*(0) < 0$) can be considered the maximum u^* possible for a given initial boundary layer at the base. In the following section we will discuss two possible methods for connecting these wake flow solutions to a base with a particular initial boundary layer thickness δ_2 after the turn.

VI. FLOW FIELD MODEL NEAR THE BODY

In the region near the base, from the separation point to the start of the interaction pressure rise, the base height h and the shear layer thickness δ are independent length scales. The Stewartson single parameter reversed flow profiles are inadequate in this region not only because δ and h' (the height of the reversed flow region) are directly related, but because the limiting profile shape $u_{\mathfrak{C}} \to 0$ $\beta \to 0$ corresponds to the Chapman constant pressure solution for a free mixing layer, $u^* = .587$. Since $u^* = 0$ at the separation point, for a finite initial thickness δ_2, it is clear that the flow near the body cannot be represented by the $\beta \to 0$ solution.

One means of representing the flow field near the base, in which the shear layer thickness is independent of the geometry, is to assume that the flow can be represented by the development of a constant pressure mixing layer, with finite initial thickness, downstream of a semi-infinite step [see figure (11)]. As noted in section II. 1, numerous experimental investigations of the base flow region have shown that the static pressure is nearly constant in the initial mixing region $\left[\frac{\ell_{mix}}{h} = 0(1)\right]$. Theoretical solutions for the mixing of a free shear layer with finite initial thickness at separation have been developed by Kubota and Dewey (47) and Denison and Baum (48) for laminar flows. The application of the integral theory of Kubota and Dewey for the case of a turbulent free shear layer is considered below in section VI.1. This solution is then connected up with the wake solution developed in section V, by a suitable set of joining conditions, which are presented in section VI. 2.

An alternate method for joining the single parameter wake flow solution to the base is to construct a family of two parameter wake profiles, where δ and h' are independent, and employ them in an appropriate set of moment equations to find wake solutions near the body. This solution scheme is presented in section VI. 3 and the results compared with the more simple free mixing layer solution.

VI. 1. Non-Similar Turbulent Free Shear Layer

In order to join the wake flow solution with the body flow field, and thus provide a length scale for the problem, it is necessary to determine the development of the velocity on the dividing streamline and the rate of growth of the separated shear layer. After expansion of the wall boundary layer about the corner, the initial sublayer separates from the wall and begins to entrain mass from the "dead water region" in the base (see figure 11). In the initial mixing region the rate of growth follows that of a wall turbulent boundary layer and the initial momentum thickness θ_2 is the dominant length scale in this regime. Momentum from the outer flow increases the velocity on the dividing streamline as the shear layer profiles are transformed from boundary layer like profiles to those of the Göertler-Chapman type far downstream (the similar mixing region). Since in a real base flow problem the flow begins to reattach before the asymptotic profiles can be attained, it is most important to properly determine the effect of the initial layer on the mixing process.

Using polynomial profiles in the momentum integral method developed by Kubota and Dewey (47) for the constant pressure laminar

free mixing layer, allows us to determine a simple closed form solution for the corresponding turbulent mixing layer. Assuming that the continuity and momentum equations (4.27) and (4.28) are valid for the constant pressure mixing process in the non-similar region, we integrate the momentum equation first from the dividing streamline to the outer edge of the shear layer and then from the dividing streamline to the inner edge of the shear layer (see figure 11) to obtain the following two integral equations:

$$\frac{d}{dX}\left[\bar{\delta}_1 \int_0^1 f(1-f)\, d\eta\right] = \frac{\tilde{\varepsilon}}{U_e \bar{\delta}_1} \left(\frac{\partial f}{\partial \eta}\right)_{\eta=0} \qquad \eta > 0 \qquad (6.1)$$

$$\frac{d}{dX}\left[\bar{\delta}_2 \int_{-1}^0 g^2\, d\xi\right] = \frac{\tilde{\varepsilon}}{U_e \bar{\delta}_1} \left(\frac{\partial g}{\partial \xi}\right)_{\xi=0} \qquad \xi < 0 \qquad (6.2)$$

where

$$f(\eta) = \frac{U}{U_e} \qquad \eta = \frac{Y}{\bar{\delta}_2} \qquad Y > 0$$

$$g(\eta) = \frac{U}{U_e} \qquad \xi = \frac{Y}{\bar{\delta}_2} \qquad Y < 0$$

The solution for an initial quadratic profile is as follows:

The velocity profile is broken into two layers, joined at the dividing streamline by the requirement of continuity of velocity and shear, and fitted to the boundary conditions at the shear layer edges

$$\left.\begin{aligned} f &= 1 \\ f' &= 0 \end{aligned}\right\} \eta = 1 \qquad \left.\begin{aligned} g &= 0 \\ g' &= 0 \end{aligned}\right\} \xi = -1$$

Thus the velocity profiles may be written as

$$f = 1 - (1-u^*)(1-\eta)^2 \qquad (6.3)$$

$$g = u^* (\xi+1)^2 \qquad (6.4)$$

where u^* is the normalized velocity on the dividing streamline. The matching conditions for the two profiles require that

$$\frac{\bar{\delta}_2}{\bar{\delta}_1} = \frac{u^*}{1-u^*}$$

or

$$\frac{\bar{\delta}_1}{\bar{\delta}_1+\bar{\delta}_2} = \frac{\bar{\delta}_1}{\bar{\delta}} = 1-u^* \tag{6.5}$$

Substituting (6.3), (6.4) and (6.5) into (6.1) and (6.2) yields two first order ordinary differential equations for the unknown $u^*(X)$ and $\bar{\delta}(X)$

$$\begin{aligned} \frac{d}{dX}\left\{\frac{(1-u^*)^2}{2}\bar{\delta}\left[\frac{1}{3}-\frac{(1-u^*)}{5}\right]\right\} &= \left(\frac{\rho_o}{\rho_e}\right)^2 K\frac{\bar{\theta}}{\bar{\delta}} \\ \frac{d}{dX}\left\{\frac{(u^*)^3}{10}\bar{\delta}\right\} &= \left(\frac{\rho_o}{\rho_e}\right)^2 K\frac{\bar{\theta}}{\bar{\delta}} \end{aligned} \tag{6.6}$$

$$\boxed{\begin{aligned} u^* &= 0 \\ \bar{\delta} &= \bar{\delta}_o \end{aligned} \qquad \text{at } X = 0}$$

Since the form factor $\frac{\bar{\theta}}{\bar{\delta}}$ varies little over the entire mixing process

$$.12 < \frac{\bar{\theta}}{\bar{\delta}} < .13$$

we will assume that the right hand sides of equations (6.6) are constant, $(\frac{\bar{\theta}}{\bar{\delta}}) \simeq .125$. After integrating and combining the equations we obtain the rather simple solution for the velocity on the dividing streamline

$$S = \frac{x}{\sigma_\theta \theta_o} = \frac{19.7\ u^{*3}}{2 - u^* - 4u^{*2}} \tag{6.7}$$

and the growth of the momentum thickness

$$\frac{\theta}{x} = \frac{.090}{\sigma_\theta (u^*)^3} \tag{6.8}$$

note: $\sigma_\theta = \dfrac{(\rho_e/\rho_o)^2}{2KC} = \left(1 + \dfrac{\gamma-1}{2} M_e^2\right)^2 \sigma^*$

θ_o is the initial momentum thickness at the beginning of the mixing region ($\sim \delta_2$ in figure 4).

Equation (6.8) demonstrates that the rate of growth of the shear layer will be greater than linear if the velocity on the dividing streamline is less than the asymptotic value, since the growth θ/x is inversely proportional to the curve of u^*. Thus, measurements of σ_θ (or some equivalent σ) for a high Mach number base flow, such as reported by Larson (10) at M = 3, will usually be much lower than the actual value because $u^* < .587$ for a finite θ_o.

Equation (6.7) is plotted in figure (12). This relation gives us the important length scale for this isobaric compressible turbulent shear layer $S = x/\sigma_\theta \theta_o$, i.e. the mixing distance x divided by the product of the initial momentum thickness θ_o and the momentum thickness spreading parameter σ_θ. We note that as $x/\sigma_\theta \theta_o \to \infty$, $u^* \to .593$ a quantity quite close to the theoretical value of $u^* = .587$ for the Chapman-Göertler solution. Figure (12) also indicates the previously mentioned criteria for similarity [equation (4.36)], namely that the velocity on the dividing streamline does not approach its asymptotic value until $x/\sigma_\theta \theta_o \gtrsim 10$. By a suitable conversion of the variables, the solution of King and Denison (32) for an initial Blasius profile is also shown in figure (12). The turbulent solutions for the two initial profiles are quite similar, as was to be expected from the good agreement noted by Kubota and Dewey (47) for the equivalent laminar solutions. Also included in figure (12) is an integral solution using a

simple sine wave profile and the results of a linearized calculation by Nash (49) using a 1/7 power profile. The basic similarity of all the solutions indicates that the shape of the initial profile does not effect the fundamental character of the solution but only shifts it slightly depending upon the initial profile chosen. The solution for the quadratic profile was used in all subsequent calculations for the constant pressure free shear layer.

VI. 2. Joining Conditions

Instead of trying to determine the value of u^*_{match} for some initial sublayer momentum thickness to step height ratio (θ_2/h), which would require the use of an iteration procedure, the inverse problem is solved; namely given a value of u^*_{match} find the value of θ_2/h which satisfies the proper matching conditions. The latter technique requires no iteration. The four conditions required for matching are: continuity of M_e, of u^*, and of mass flow above the dividing streamline, and in addition an important geometric constraint which requires that the height of the free shear layer at the joining point be equal to the height of the wake boundary layer. This last condition, illustrated in figure (4), in essence ties down the shear layer solution (in an infinite domain) to a physical reversed flow wake profile with a reference axis, i.e. the centerline. From the four matching conditions we can thus determine not only the length of the mixing region (ℓ) which determines θ_2/h ($\frac{\theta_2}{h} = \frac{1}{S(u^*)} \cdot \frac{1}{\sigma_\theta} : \frac{\ell_{mix}}{h}$)†, but also the length scale for the wake flow, $\delta_i^*(0)$.

---

† $S(u^*) = \ell/\sigma_\theta \theta_o$

The geometric matching relation is as follows [see figure (4)]:

$$\sin(-\Theta) = \frac{h - \delta_{wake}}{\ell_{mix}} \tag{6.9}$$

where Θ is the streamline inclination at the outer edge of the wake determined by the wake integral solution at $u^* = u^*_{join}$, the mixing distance ℓ_{mix} is given by the expression

$$\frac{\ell_{mix}}{h} = \frac{1 - \delta/\delta_i^*(0)\ \frac{\delta_i^*(0)}{h}}{\sin(-\Theta)} \tag{6.10}$$

in terms of the wake functions $\Theta(u^*_{join})$ and $\frac{\delta}{\delta_i^*(0)}(u^*_{join})$. The transformed rear stagnation displacement thickness δ_i^* is determined from the requirement of continuity of mass above the dividing streamline at the joining point.

The mass flow above the dividing streamline for the wake is simply

$$\frac{\dot{m}}{\rho_e u_e h} = \frac{a_\infty}{a_e}\frac{\rho_\infty}{\rho_e}\gamma_i^* Z \frac{\delta_i^*(0)}{h} \tag{6.11}$$

The mass flow for the shear layer may be written as [see equations (6.3)-(6.8)]

$$\begin{aligned}\frac{\dot{m}}{\rho_e u_e h} &= \frac{\overline{\delta}_i}{h}\int_0^1 f\,d\eta = \frac{\overline{\delta}}{h}\frac{(1-u^*)(2+u^*)}{3} \\ &= \frac{.672}{\sigma_\theta (u^*)^3}\frac{\ell_{mix}}{h}\frac{(1-u^*)(2+u^*)}{3}\end{aligned} \tag{6.12}$$

Equating the mass flows of equations (6.11) and (6.12) and substituting the geometric relation (6.10) determines the length scale $\delta_i^*(0)/h$. Substituting this value in equation (6.10) gives the length of the mixing

region. The distance x_o/h from the step to the beginning of the interaction is

$$\frac{x_o}{h} = \frac{\ell_{mix}}{h} \cos(-\Theta) \qquad (6.13)$$

The usual expression for ℓ_{mix}/h used by many authors (McDonald, Korst, etc.) is $\ell_{mix}/h = 1/\sin\theta$. They assume that the constant pressure region extends to the axis. This assumption can lead to overestimating x_o/h by almost 100%. Thus we see that it is necessary to consider both shear layer and wake flow solutions to obtain even such a fundamental quantity as the length of the constant pressure region.

Figure (13) shows the effect of the upstream boundary layer thickness δ_1/h† on the length of the constant pressure region for the case, $M_\infty = 2.0$. One notes that x_o/h is nearly constant ($x_o/h \approx 1.6$) for initial thicknesses less than the step height ($\delta_1/h < 1.0$). As δ_1/h is increased beyond a value of 1.0, x_o/h is seen to fall off rapidly, so that for boundary layer thicknesses greater than twice the step height h, the length of the constant pressure region is nearly zero.

In the following section x_o/h will be calculated using the results of a two-parameter integral solution near the base.

VI. 3. Two Parameter Reversed Flow Wake Solutions

Golik, Webb and Lees (8) attempted to find a set of two parameter reversed flow profiles for use in a multi-moment integral method which would allow a continuous integration of the integral wake equations from the rear stagnation point to the base. By disconnecting the

† The relation between δ_2 and δ_1 is developed in section VII.

axis velocity from the Stewartson reversed flow velocity profiles, an extra degree of freedom was produced. These normalized Stewartson profiles were then represented by two independent parameters, $U_o = u_{\mathcal{L}}/u_e$ and a shape factor $N(= \delta^*/\delta|_{U_o=0})$. Starting at the rear stagnation point with a prescribed value of N, the moment equations were integrated upstream. The absolute value of the centerline velocity $|U_o|$ first increases and then decreases back to zero. At the point where $U_o = 0$ again, this may be considered the location of the base. While this solution has qualitatively the correct behavior noted of base flows, the present author noted two distinct limitations associated with this calculation procedure. First, it was found that solutions could only be found for a narrow range of initial sublayer thicknesses $.37 < \delta_2/h < .66$, corresponding to a boundary thickness ahead of the step $2 < \delta_1/h < 4$. For most practical cases we are interested in initial thickness one order of magnitude smaller. The second problem associated with this 2 parameter solution is that while the base pressure becomes constant near the base (without any prior assumptions) the length of the constant pressure region is almost 5 times longer than the value of x_o/h found using the free shear layer matching analysis of the previous section. This slow approach to the base is believed due to the use of the Stewartson profiles, which although normalized, still retain the behavior of the Chapman constant pressure solution. While the flow in the recirculating region is quite complicated, it may basically be thought of as resulting from the interplay between two distinct stagnation flow fields; (1) a reattaching

wake-like flow at the rear stagnation point; and (2) a stagnating low shear low velocity reversed flow at the base bounded above by a small region of high shear. It appears that it would be difficult indeed to find one set of profiles which would possess these two widely diverse features. Therefore, a set of profiles was sought which has the correct two parameter behavior near the base, but not necessarily the appropriate behavior near the rear stagnation point (where the single parameter Stewartson profiles can be employed). Such a set of profiles was suggested by J. E. Green (9) in his study of the incompressible turbulent base flow problem† [see figure (14)]. This family of profiles is characterized by the two independent parameters, P (a measure of the axis velocity), and h/ℓ (the ratio of the height of the region of constant reversed flow to the thickness of the shear layer). The profile has the characteristics of a free shear layer (given by a simple cosine shape) bounding a region of constant reversed flow velocity. The equation of the profile is as follows:

$$\frac{u}{u_e} = 1 - 2P \qquad 0 \le Y \le h \qquad (6.14)$$

$$\frac{u}{u_e} = 1 - P\left[1 + \cos \pi \left(\frac{y-h}{\ell}\right)\right] \qquad h \le Y \le h + \ell \qquad (6.15)$$

From figure (14), one notes that when $P = 1/2$ $u_{\mathcal{L}} = 0$ and the profile has the character noted of a shear layer initially separating from the edge of the base.

---

† Green was unable to obtain a solution upstream of the rear stagnation point with these profiles because they do not exhibit the proper single parameter behavior needed at the r. s. p.

As in the case of the matching of the constant pressure mixing layer with the single parameter Stewartson wake flow solution, the joining point is unknown á-priori, but is determined by a suitable set of joining conditions. No geometrical relation is required in joining the single and double parameter solutions, since the integration proceeds along the same axis coordinate system. We require at the joining point continuity of M_e (or Θ), δ_i^*, u^*, and mass flow above the dividing streamline. The last two joining conditions are sufficient to establish initial values for the two profile parameters P and $h' = h/\ell$. The initial values of P and h' are determined by simultaneously solving the following two equations

$$\psi = 0 \quad \text{on d.s.} \qquad h'(1-2P)+\frac{1}{\pi}(1-P)\cos^{-1}\left[\frac{1-u^*}{P}-1\right]-\frac{1}{\pi}\left[(1-u^*)^2+2(1-u^*)P\right]^{\frac{1}{2}} = 0$$

$$Z_{2P} = Z_{St.} \qquad \frac{(1-P)+h'(1-2P)}{P(1+2h')} = Z(u^*)_{\text{Stewartson}} \tag{6.16}$$

In order to solve for the four unknowns M_e, δ^*, P, and h' we require a fourth equation in addition to the integral equations of continuity, x-momentum, and mechanical energy (first moment of momentum). Rather than adopt an additional second moment of momentum to describe the flow, which heavily weights the outer portions of the wake, the momentum equation along the centerline was selected as the fourth governing equation

$$U_{\mathbb{C}} \frac{dU_{\mathbb{C}}}{dX} = U_e \frac{dU_e}{dX} + \tilde{\varepsilon}\left(\frac{\partial^2 U}{\partial Y^2}\right)_{Y=0} \tag{6.17}$$

In the region close to the base the shear gradient near the wake axis is quite small. The term $\frac{\partial^2 U}{\partial Y^2}$ is identically zero at the wake axis

for the Green two parameter profiles. We therefore neglect the viscous term on the far right hand side of equation (6.17). This equation then implies that the velocity gradient on the axis is determined solely by the static pressure gradient along the axis and vice-versa. Thus upstream of the joining point were $U_{\mathbb{C}} \frac{dU_{\mathbb{C}}}{dX}$ must be positive for the flow to stagnate at the base, $U_e \frac{dU_e}{dX}$ must also be positive indicating that the pressure must rise toward the base (a phenomenon noted in many experiments). Thus we can expect a slight discontinuity in the pressure gradient at the joining point, indicating the change over from one type of stagnation flow to another. In an actual experiment this change in pressure gradient is continuous but takes place in a very short distance, of the order of 1/10 h. Equation (6.17) also implies that at the base, $U_{\mathbb{C}} = 0$, the pressure gradient vanishes. Thus the shape of the pressure profile in the reverse flow region will have the form indicated in the sketch below

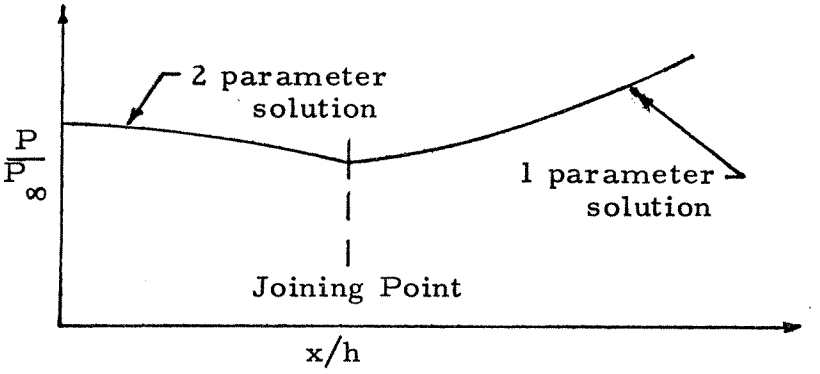

The complete set of differential equations employed in the two parameter region are as follows:

$$\delta^*(2-4P)\frac{dP}{dX} + \frac{\delta^*}{M_e}\frac{dM_e}{dX}4P(1-P) = 0$$

$$\mathcal{H}\frac{d\delta^*}{dX} + \delta^*\left[\frac{d\mathcal{H}}{dP}\right]\frac{dP}{dX} + \delta^*\left[\frac{d\mathcal{H}}{dh'}\right]\frac{dh'}{dX} + \frac{\delta^*}{M_e}\frac{dM_e}{dX}[2\mathcal{H}+1] = 0$$

$$J\frac{d\delta^*}{dX} + \delta^*\left[\frac{dJ}{dP}\right]\frac{dP}{dX} + \delta^*\left[\frac{dJ}{dh'}\right]\frac{dh'}{dX} + \frac{\delta^*}{M_e}\frac{dM_e}{dX}[3J] = K\left(\frac{\rho_{\mathcal{L}}}{\rho_e}\right)^2\mathcal{H}R$$

$$\left[\mathcal{H}+\frac{1+m_e}{m_e}\right]\frac{d\delta^*}{dX} + \delta^*\left[\frac{d\mathcal{H}}{dP}\right]\frac{dP}{dX} + \delta^*\left[\frac{d\mathcal{H}}{dh'}\right]\frac{dh'}{dX} + \frac{\delta^*}{M_e}\frac{dM_e}{dX}[f] = \frac{1}{m_e}\tan\Theta$$

where

$$\mathcal{H} = \frac{(1-\frac{3P}{2}) + 2h'(1-2P)}{1+2h'} \qquad J = \frac{(1-P)(2-\frac{5P}{2}) + 4h'(1-2P)(1-P)}{1+2h'}$$

$$Z = \frac{(1-P+h'(1-2P)}{P(1+2h')} \qquad R = \pi^2 P^3 (1+2h')$$

These equations are numerically integrated as in section V, until $P = \frac{1}{2}$, $u_{\mathcal{L}} = 0$ which corresponds to the base. The pressure rise from the joining point to the base is found to be of the order of 1%, which agrees well with the assumption of a negligible pressure variation in this regime. Figure (14) presents a comparison of the length of the constant pressure region determined by the two parameter integration with the results found using the constant pressure mixing solution. Both solutions agree quite closely up to $\delta_1/h \approx 1.0$ and are seen to diverge somewhat at the higher values of δ_1/h, while maintaining the same qualitative dropoff in x_o/h with increasing δ_1/h. Thus, for most cases, the simpler mixing solution appears to give approximately the same length scales as the more complex 2 parameter solution. However, the two parameter solution can be used to obtain estimates of the effects of base heat transfer and base bleed

which the shear layer calculation does not make possible. For example, the heat transfer coefficient at the base $h = q_w/(T_w - T_r)$ could be predicted from laminar stagnation point theory (in the region near the axis) as suggested by Larson et al. (10), by using the gradient of the centerline velocity $C = d\, u_{\mathcal{L}}/dX$ in the equation

$$h = \frac{k_w}{\sqrt{\nu_w}} \left(\frac{Nu}{\sqrt{Re}_w}\right) \sqrt{C} \qquad (6.18)$$

One notes that if the 2 parameter solution is continued upstream of the point where $u_{\mathcal{L}} = 0$ the velocities of the inner flow region become positive. Stopping the solution at any positive $u_{\mathcal{L}}$ would correspond to the case of mass injection at the base, the mass flow being simply

$$\dot{m}_{base} = \rho_b\, u_{\mathcal{L}_{base}}\, h \qquad (6.19)$$

Preliminary calculations indicate the correct trend of increasing base pressure with increasing bleed rate, but the relative increase of P_b seems to be a good deal smaller than experiments suggest. Non-isentropic effects coupled with the simplicity of the cosine profiles may account for the discrepancy between theory and experiment.

In the following section, a model is presented which will link the sublayer flow after the turn with the initial boundary upstream of the step.

VII. CORNER EXPANSION OF THE UPSTREAM BOUNDARY LAYER

The expansion about a sharp corner of a viscous-rotational boundary layer is an extremely difficult fluid mechanical problem (as yet unsolved in full detail) due to the fact that both longitudinal and transverse, pressure and shear gradients, are equally present in the process. In order to obtain the salient length scales involved in the wake flow problem (e.g. wake width and recompression length), the most important feature required of our analysis of the boundary layer expansion process is not the detailed velocity and shear variations, but the thickness of the viscous layer, after the turn, which serves as an initial condition for the free shear layer. After a short region of constant pressure mixing, it is this inner layer which is joined to the wake solution. Thus it is the initial thickness of the viscous sublayer Δ_2 after expansion which will be an important feature in determining the length scale of the problem.

The turbulent base flow schlierens of Hastings [figure (15)] over a wide range of initial boundary layer thicknesses ($.1 < \frac{\delta_1}{h} < 10$) indicate that as the upstream boundary layer undergoes the expansion process, a new viscous sublayer is formed immediately after the turn, approximately 10-20% of the thickness of the original layer. This sublayer then grows downstream of the corner as the free mixing layer. While the thickness of the total initial layer may have increased 50% due to the corner expansion (i.e. $\delta_2 \approx 1.5\ \delta_1$), it is asserted that the length scale of the problem is determined only by the inner layer or sublayer ($\Delta_2 \approx .15\ \delta_1$) and that the outer portion of the expanded boundary layer merely acts as a weak inviscid field of external vorticity.

VII. 1. Viscous Sublayer Model

The flow model for the corner expansion process is shown in figure (16). The total boundary layer upstream of the corner (station 1) is characterized by the quantities δ_1 and M_{e_1}. For an initial turbulent boundary layer we assume the well known 1/7th power profile for the velocity distribution

$$\frac{u}{u_{e_1}} = \left(\frac{y}{\delta_1}\right)^{1/7} \tag{7.1}$$

Let us consider a small inner region, of the initial layer, of thickness Δ_1. The Mach number at the upper edge of Δ_1 is denoted as M_{Δ_1}. We assume that as the pressure at the wall drops from P_1 to $P_2(=P_b)$ during the corner expansion process, that shear stresses will only be important inside a stream tube (ψ_Δ) which expands from an initial thickness Δ_1 to a final thickness Δ_2. The flow along the bounding streamline ψ_Δ is assumed isentropic. Therefore, we can easily determine the sublayer edge Mach number M_{Δ_2} from the isentropic relation

$$\frac{\left[1 + \frac{\gamma-1}{2} M_{\Delta_2}^2\right]}{\left[1 + \frac{\gamma-1}{2} M_{\Delta_1}^2\right]} = \left(\frac{P_1}{P_2}\right)^{\frac{\gamma-1}{\gamma}} \tag{7.2}$$

At station 2 we assume that the velocity profile of the sublayer is the same quadratic profile chosen for the constant pressure free shear layer analysis†

$$\text{Station 2} \qquad \frac{U}{U_{\Delta_2}} = 2\eta - \eta^2 \qquad \eta = \frac{Y}{\Delta} \tag{7.3}$$

† The flow is considered adiabatic and the Howarth-Dorodnitsyn transformation is assumed valid at station 2.

Since the sublayer thicknesses Δ_1 and Δ_2 at the beginning and end of the streamtube are unknowns, we require two equations to relate these quantities. These relations are supplied by a stream tube balance of the mass and momentum entering and leaving a "black box" situated near the corner. The conservation of mass for the streamtube is

MASS

$$\int_0^{\Delta_2} \rho_2 u_2 \, dy - \int_0^{\Delta_1} \rho_1 u_1 \, dy = 0 \qquad (7.4)$$

Applying the momentum theorem to the control volume gives us the following approximate expression

MOMENTUM

$$\int_0^{\Delta_2} \rho_2 u_2^2 \, dy - \int_0^{\Delta_1} \rho_1 u_1^2 \, dy + \Delta_2(p_2 - p_1) - \bar{\tau}_w \Delta x = 0 \qquad (7.5)$$

Equation (7.5) introduces into the problem, through the shear force term $\bar{\tau}_w \Delta x$, the unknown average shear stress $\bar{\tau}_w$ and the unknown length Δx of the corner interaction. In order to estimate the magnitude of the quantity $\bar{\tau}_w \Delta x$ in terms of the known parameters of the problem (e.g. $\Delta_2, P_2/P_1$, etc.), we use the differential form of the momentum equation to note that at the wall the viscous and pressure terms just balance, i.e.

at the wall $\qquad \frac{\partial \tau}{\partial y} = \frac{dp}{dx}$

For an accelerating boundary layer, the shear stress gradient decreases away from the wall

$$\left(\frac{\partial \tau}{\partial y}\right)_{y>0} < \left(\frac{\partial \tau}{\partial y}\right)_{y=0} \qquad (7.6)$$

Mellor and Gibson (50) have obtained solutions of the equations of motion for the velocity profiles and shear stress distributions of equilibrium turbulent boundary layers where the pressure gradient parameter, $\beta = \delta^* \left(\frac{dp}{dx}\right)/\tau_o$ is held constant. Using Prandtl's mixing length theory in the overlap layer ($\epsilon = K^2 y^2 \left|\frac{\partial u}{\partial y}\right|$) and joining this with an eddy viscosity in the outer layer which is considered constant with respect to y ($\epsilon = KU\delta^*$), defect solutions of the form $(U-u)/u_\tau = f'(\eta)$ were found[+] for various values of the parameter β. Solutions were found for β in the range $-0.5 \leq \beta \leq \infty$. The $\beta = -0.5$ solution corresponds to the development of a turbulent equilibrium boundary layer undergoing the maximum acceleration possible. The distribution of shear stress for the $\beta = -0.5$ case is shown in figure (17). One notes that $\partial\tau/\partial y$ decreases away from the wall, as noted in equation (7.6). The assumption is now made that we can employ the $\beta = -0.5$ solution in order to estimate the relative magnitude of shear and pressure forces throughout a highly accelerated turbulent boundary layer.

We define an average shear stress gradient as follows

$$\left(\frac{\partial \tau}{\partial y}\right)_{\substack{\text{ave} \\ @\ \eta}} \equiv r_\Delta \left(\frac{\partial \tau}{\partial y}\right)_{\substack{\text{wall} \\ @\ \eta=0}}$$

where

$$r_\Delta \equiv \frac{1}{2}\left[\left(\frac{\partial \tau}{\partial y}\right)_\eta + \left(\frac{\partial \tau}{\partial y}\right)_{\eta=0}\right]\Bigg|_{\substack{\text{using} \\ \beta = -0.5 \text{ solution}}}$$

[+] $\eta = \sqrt{\frac{C_f}{2}}\left(\frac{y}{\delta^*}\right)$ A typical value of $\gamma = \sqrt{\frac{C_f}{2}} = .04$ $\eta \approx \frac{1}{3}\frac{y}{\delta}$

Since $\left(\frac{\partial \tau}{\partial y}\right)_{\eta=0} = \frac{dp}{dx}$, then we estimate the difference of the pressure and shear forces in equation 7.5 as follows

$$\Delta_2(P_2-P_1) - \bar{\tau}_w \Delta x = \Delta_2(P_2-P_1) - r_\Delta [\Delta_2(P_2-P_1)]$$

$$= \Delta_2(P_2-P_1)[1-r_\Delta] \qquad (7.6)$$

Substituting equation (7.6) into the momentum equation (7.5) yields

$$\int_0^{\Delta_2} \rho_2 u_2^2 \, dy - \int_0^{\Delta_1} \rho_1 u_1^2 \, dy + \Delta_2(P_2-P_1)[1-r_{\Delta_2}] = 0 \qquad (7.7)$$

Equations (7.4) and (7.7) represent two equations for the two unknown quantities Δ_2/δ_1 and Δ_1/δ_1.

VII.2. Sublayer Solution Method and Results

Solving equations (7.4) and (7.7) for the initial mixing sublayer thickness Δ_2/δ_1 yields the following two equations

MASS

$$\frac{\Delta_2}{\delta_1} = \frac{(A_2/A^*)_{\Delta_2}}{(A_1/A^*)_{\Delta_1}} \frac{(\rho_{e_1}/\rho_{\Delta_1})}{(u_{\Delta_1}/u_{e_1})} \frac{Q_1(\Delta/\delta_1)}{[1-(\delta^*/\Delta)_2]} \qquad (7.8)$$

MOMENTUM

$$\frac{\Delta_2}{\delta_1} = P_1(\Delta/\delta_1)\left\{\frac{M_{\Delta_1}^2}{M_{\Delta_2}^2}\frac{P_1}{P_2}\frac{(\rho_{e_1}/\rho_{\Delta_1})}{(u_{\Delta_1}/u_{e_1})^2}\frac{1}{\left[1-\left(\frac{\delta^*}{\Delta}\right)_2-\left(\frac{\theta}{\Delta}\right)_2\right]} - (1-r_{\Delta_2})\,\mathcal{C}_p\right\}^{-1} \qquad (7.9)$$

where

$$Q_1\left(\frac{\Delta}{\delta_1}\right) = \int_0^{\Delta/\delta_1} \frac{\rho}{\rho_{e_1}} \frac{u}{u_{e_1}}\, d\left(\frac{y}{\delta_1}\right) \qquad \mathcal{C}_p = \frac{1-p_2/p_1}{\gamma M_e^2}$$

$$P_1\left(\frac{\Delta}{\delta_1}\right) = \int_0^{\Delta/\delta_1} \frac{\rho}{\rho_{e_1}} \frac{u^2}{u_{e_1}^2}\, d\left(\frac{y}{\delta_1}\right)$$

and for adiabatic flow

$$\frac{\rho_{e_1}}{\rho} = 1 + \frac{\gamma-1}{2} M_{e_1}^2 \left[1 - \left(\frac{u}{u_{e_1}}\right)^2\right]$$

For a given M_{e_1} and base pressure ratio p_2/p_1, a trial value of M_{Δ_1} is assumed and a value of Δ_2/δ_1 is calculated from each of equations (7.8) and (7.9). In general, these two values will not be equal, and a new value of M_{Δ_1} is then selected. We iterate on M_{Δ_1} (using a high speed computer) until $\Delta_{2_{mass}} = \Delta_{2_{momentum}}$ within a given degree of accuracy.

Typical results for a pressure ratio $p_2/p_1 = .4$ are given in the table below

M_∞	M_{Δ_1}	Δ_1/δ_1	Δ_2/δ_1
1.5	1.01	.12	.25
2.0	1.18	.08	.18
3.0	1.36	.05	.12
6.0	1.55	.03	.08

These results indicate that the thickness of the sublayer after the turn Δ_2 is approximately 10-20% of δ_1 as suggested by the Schlieren photographs of Hastings.

Also one notes that the effective edge Mach number before the turn M_{Δ_1} is close to unity, even for an outer edge Mach number M_{e_1}

as high as 6.0. Recently some investigators of the turning problem have made the assumption that the inner viscous layer is formed by the expansion of the flow below the same line ($M_{\Delta_1} = 1.0$). These results indicate that such an assumption may not be grossly in error.

This low effective edge Mach number ($M_{\Delta_1} \approx 1.0\text{-}1.5$) indicates that if the initial boundary layer is relatively large compared to the step height [$\theta_1/h \approx 0(1)$], then no matter how high the freestream Mach number M_{e_1}, the viscous interaction in the near wake will be influenced only by the low Mach number portion of the flow. The base pressure data of Hastings (12) shown in figure (18) illustrates this effect most clearly. For initial values of $\theta_1/h \ll 1$, the base pressure shows the familiar trend of a decreasing base pressure with increasing step Mach number ($M_1 = 1.56 - 3.10$ in Hastings' experiments). But as the initial thickness is increased above the point where $\theta_1/h > 1$, the measured base pressures of all the Mach numbers tested increase and tend to merge with one another, and appear to be approaching some upper limit. This limit is easily obtained from the integral theory of section V.

The maximum value of the base pressure corresponds to the pressure at the rear stagnation point (zero constant pressure mixing) of a wake flow with a free stream edge Mach number near unity (the inner edge Mach number limit). This limiting base pressure was found to be

$$\left(\frac{P_b}{P_\infty}\right)_{\substack{MAX \\ M \to 1}} = .78$$

The base pressures for Mach numbers as high as 3.10 are seen to approach this limit, as one notes in figure (18).

Of course it should be pointed out that when the step size becomes so small that no definable inner boundary layer exists, as is required in the model, then this limiting value ceases to be of significance.

On the other end of the boundary layer spectrum, that is for $\theta_1/h \ll 1$, we are led to ask: what is the effective edge Mach number for the wake? In this case the initial Mach number at the edge of the sublayer after the turn is relatively low. But due to the entrainment of mass by the shear layer at its outer edge, it engulfs more and more of the high Mach number portion of the initial boundary layer. Therefore, if θ_1/h is small enough, then a short distance downstream of the corner, the Mach number at the edge of the shear layer will correspond to that Mach number produced by an inviscid expansion of the flow from the upstream outer edge Mach number M_{e_1}. Thus, for the wake calculation we would set $M_\infty = M_{e_1}$.

Figure (19) presents a plot of the fraction of the mass flow in the initial boundary layer that is entrained by the shear layer and wake flow up to the end of the constant pressure mixing, and up to the critical point, as a function of the boundary layer thickness ahead of the step. The plot indicates that for initial values of δ_1/h less than $\approx .2$, that almost all of the mass of the initial boundary layer is entrained by mixing in the near wake, and thus the effective value of $M_\infty \approx M_{e_1}$. For values of $\delta_1/h > 5.0$, less than 10% of the initial boundary layer

is entrained, and thus we may set $M_\infty \approx M_{\Delta_1}$. In the intermediate region $.2 < \delta_1/h < 5$, the effective edge Mach number is continually changing as mixing proceeds downstream of the base. As an outer characteristics program is not embodied in this study to account for the crossing of the various rotational outer flow streamlines by the viscous inner flow, the present analysis used the criteria that for $\delta_1/h \leq .5$ $M_\infty \approx M_{e_1}$ and for $\delta_1/h > 2.0$ $M_\infty \approx M_{\Delta_1}$.

The major point to be gleaned from this section as far as the overall wake flow analysis is concerned is that the viscous sublayer which serves as the initial condition for the free shear layer mixing is only a small portion of the initial boundary layer. It is this thickness Δ_2 and not the large thickness δ_1, which determines the maximum value of u^* and thus the base pressure, and it is Δ_2 alone which will determine by geometrical matching the length scale for the wake interaction.

The combined results of sections V-VII are presented in the following section (VIII) in which the theoretical base flow solution is compared with the existing experimental data.

VIII. NUMERICAL SOLUTIONS FOR THE SUPERSONIC TURBULENT WAKE AND COMPARISONS WITH EXPERIMENT

VIII. 1. Pressure and Wake Thickness Distributions

An example of the complete base flow solution from the sublayer constant pressure mixing region to the reattached wake flow downstream of the rear stagnation point, where $p_e/p_\infty \to 1$, is shown in figure (20). The case considered is for $M_\infty = 2.0$ and $\theta_1/h = .038$. The general trends of the results are evident in this figure. We note, from the graph at the top of figure (20), that the mixing region is confined to a thin layer which extends over an axial distance of some $1\frac{1}{2}$ step heights. For this case, which is typical of the experimental values of θ_1/h, the initial boundary layer height is approximately 50% of the step height. The size of the sublayer at the start of mixing, after undergoing expansion, appears to be quite a bit smaller, of the order of 20% of the step height, growing to about 40% at the joining point. The height of the wake boundary layer δ is seen to decrease, after the joining point, to about 30% of the step height at the critical point.

Turning to the second curve of figure (20) for the distribution of static pressure along the centerline, we find that the pressure is constant initially at about 45% of the free stream value for the first $1\frac{1}{2}$ step heights, followed by the reversed flow region of recompression where the pressure rises to about 65% of p_∞ at the rear stagnation point, at a distance of about $3\frac{1}{2}$ step height from the base. Downstream of the rear stagnation point, the static pressure continues to rise and recovers to over 90% of the free stream pressure in less than 6 step heights. This region $(\frac{x}{h}) < 6)$ thus constitutes what we may call

the turbulent near wake.

The bottom curve of figure (20) demonstrates how the velocity on the dividing streamline u^* varies throughout the near wake. As noted earlier, u^* increases rapidly from zero to a maximum at the joining point, and then decreases to zero again at the rear stagnation point. Downstream of the r. s. p., u^* increases once again as the velocity along the centerline of the wake approaches unity far downstream. An additional quantity of interest, the total pressure variation along the dividing streamline, is easily deduced from the static pressure and u^* distributions of figure (20). In the constant static pressure region, p_o^* increases due to the initial rapid increase of u^*. In the reversed flow interaction region the total pressure at first decreases a little due to the drop in u^*, but passes through a minimum and increases again due to the increasing static pressure in the reattachment region. Thus, the total pressure at the rear stagnation point ($= P_{\substack{\text{static} \\ \text{r.s.p.}}}$) is not much different than the total pressure at the beginning of the interaction, verifying an assumption used by Nash (2) in his base pressure theory. Unfortunately, Nash chose to relate the incremental increase of static pressure from the base to the rear stagnation point, $(P_{rsp}-P_b)$, to the overall pressure rise, $(P_\infty-P_b)$, by the factor

$$N = \frac{P_{rsp}-P_b}{P_\infty-P_b} \simeq \frac{P^*_{o\,join}-P_b}{P_\infty-P_b} = \frac{P^*_{o_j}/P_\infty - P_b/P_\infty}{1 - P_b/P_\infty} \qquad (8.1)$$

He assumed that this factor was a constant for all wake flows ($\approx .35$). While $P^*_{o\,join}/P_\infty$ is nearly constant, for a given Mach number M_∞, one notes that P_b/P_∞ varies with the upstream value of θ_1/h. A better

correlating parameter might have been

$$\tilde{N} = P_{o_j}^{*}/P_{\infty} \approx P_{r.s.p.}/P_{\infty} \qquad (8.2)$$

which is a function only of Mach number M_{∞}. Needless to say, it is felt that while such parameters may be used to correlate the base pressure, they do not reflect the essential interaction mechanism involved in the near wake base flow. The principal means for establishing the validity of the integral interaction solution and eddy viscosity model rests not so much on determining a better correlation for the base pressure, although this is an important parameter, but upon the comparison of the theoretical length scales and pressure distributions with experiment.

Figures (22, 23 and 24) present a comparison of the theoretical centerline pressure distributions with the data of several experimentalists [Hastings (12), Roshko-Thomke (13), Thomann (51), Fuller-Reid (52), Badrinarayan (14), Rom (53)] for a range of Mach numbers $M_{\infty} = 1.5\text{-}2.30$ and initial momentum thicknesses $\theta_1/h = .008\text{-}.075$.

The data shown in figures (22) and (23) were based on experiments where reattachment was to a solid surface.† Estimations of the location of the rear stagnation point by floor oil flow patterns and (in Thomann's work) by surface shear measurements show good agreement

† A question may arise as to the validity of the comparison of a wake theory with data obtained from reattachment to a solid surface. The measurements of Hama (11), in the vicinity of the rear stagnation point, showed that the axial pressures in flows reattaching with and without splitter plates differed by only a few percent. Thus, we feel that insofar as pressure distributions and other overall wake quantities are concerned, the wake analysis may be applied to splitter and non-splitter flows with equal confidence. We are in essence assuming that surface shear forces are negligible in the reattachment zone when compared with inertia forces.

between theory and experiment. For the wake study of Badrinarayan, figure (24), the location of the rear stagnation point was determined by finding the axial location where static and Pitot pressure readings were identical. The experimental location of the rear stagnation point found using this technique is about one-half base height upstream of the location determined by the theory.

For Mach numbers up to 2.3, there appears to be excellent agreement between the theoretical and experimental pressure profiles. The theoretical values of base pressure, while generally higher than the experimental values of P_b, differ by less than 15%. In addition, the lengths of the constant pressure region x_o/h are quite closely predicted by the theory.

For Mach numbers of 3 and above, the theory was found not to give the steep pressure rise noted in the experiments of Larson (10) and the measured base pressures were almost 50% smaller than the corresponding theoretical values.

In the experiments of Rom, et. al. (53) at $M_\infty = 2.25$, as noted in figure (24), the strength of the lip shock was found not to be of negligible strength, $(P_2/P_1)_{\substack{L.P. \\ shock}} = 1.48$. Thus, it is felt that the presence of a noticeable lip shock and the accompanying non-isentropic phenomenon in the vicinity of the corner, at the higher Mach numbers $M_\infty \geq 3$, are responsible in large measure for the differences between the experimental data and the theory (which is based on the assumption of an isentropic outer flow). But for approach Mach numbers of 2 or less it appears that the theory predicts the turbulent near wake pressure distribution and length scales quite well.

As to the effect of the initial momentum thickness θ_1/h on the base pressure, a comparison between theory and the base pressure data of numerous experimentalists is shown in figures (25) [$M_\infty = 1.50$] and (26) [$M_\infty = 2.00$]. The trend of the theory is in excellent agreement with the data (although 10-20% higher) even when the value of θ_1/h varies over an order of magnitude. For the case of $M_\infty = 1.50$, one notes that the base pressure varies only from about .45 to .7 over a large range of initial thicknesses.† For the case of very large initial boundary layers ($\theta_1/h \gg 1$), the base pressure approaches a maximum value as noted in section VII. In the limit as $\theta_1/h \to \infty$, the maximum value of the velocity on the dividing streamline goes to zero, $u^*_{max} \to 0$. $\theta_1/h \to \infty$ In addition the effective freestream Mach number M_∞ tends toward unity, due to the fact that only the inner sublayer participates in the near wake interaction. Thus the base pressure corresponding to the case $\theta_1/h \to \infty$ is the pressure at the rear stagnation point for a sonic base flow

$$\frac{P_b}{P_\infty}\Big|_{\theta/h \to \infty} \to \frac{P_{rsp}}{P_\infty}\Big|_{M \approx 1.0} \approx .78$$

As shown in figure (18), this appears to be the maximum base pressure for all base flows, no matter what the value of the freestream Mach number is.

---

† It should be noted that contrary to the practice of many authors the θ/h axis in figures (25) and (26) is plotted on a logarithmic basis rather than a linear basis to: (1) avoid the temptation to extrapolate the results to the completely fictitious value of $\theta/h = 0$; and (2) to emphasize the region of small θ/h where a gradual drop in the base pressure takes place over a large range of θ/h, rather than, as in the linear plots, showing a rapid drop in p_b/p_∞ as $\theta/h \to 0$.

Conclusions about the supersonic wake flow solution, based on the comparisons made herein between the integral theory and the experimental data are discussed in section X.

IX. FORMULATION OF THE INCOMPRESSIBLE PROBLEM

Nearly all of the recent studies on the problem of the viscous-inviscid interaction of separating and reattaching flows have been confined to the supersonic or hypersonic flow regimes. Studies of the low-speed separation problem have generally been divorced from the more fashionable high-speed investigations. However, Roshko and Lau (35) and Tani, Iuchi and Komoda (21) in their studies of low-speed separation have pointed out that many of the ideas developed for supersonic separation problems can be adopted for use in studying some of the outstanding unsolved problems in the incompressible flow domain. In addition, experiments which are more easily performed in large low-speed wind tunnel facilities, can give added insight into the basic phenomena of viscous-inviscid interaction, no matter what the external flow speed may be.

Recently Green (9) formulated an integral wake method of solution for the incompressible turbulent reattachment problem. The great similarity of Green's method to the moment method developed herein for supersonic turbulent flow, makes it clear that the moment equations developed in Section V can be applied almost directly to the incompressible flow problem, provided that an appropriate incompressible inviscid solution of the external flow field is employed. Green suggested the use of the solution derived for thin airfoil theory, namely

$$\frac{U_e}{U_\infty}(x) = 1 + \frac{1}{\pi}\int_{-\infty}^{\infty} \frac{\tan \Theta(\xi)}{x - \xi}\, d\xi \qquad (9.1)$$

An integral equation of this form can be used to link the viscous and inviscid flow of the incompressible wake problem, just as the isentropic Prandtl-Meyer relation

$$\Theta(x) = \nu_e[M_e(x)] - \nu(M_\infty) \qquad (9.2)$$

was used to link the viscous and inviscid flow, through the continuity equation (5.9), in the supersonic wake problem.

The basic difference between the subsonic and supersonic viscous-inviscid interaction phenomena can be clearly seen if one examines the form of equations (9.1) and (9.2).

For the case of supersonic interaction (equation 9.2) one notes that the edge Mach number M_e is determined solely by the local streamline inclination Θ. In contrast, the edge velocity U_e, in the low-speed problem (equation 9.1), is determined by the distribution of Θ, throughout the entire flow field. The full elliptic nature of the incompressible wake problem, requires that all "source" contributions to the integral in equation (9.1) from the front of the body, to the base, to the rear stagnation point, to the far wake must be properly included in order to obtain a valid solution.

While Green's study of the incompressible problem produced many helpful suggestions (e.g. his selection of the two-parameter cosine profiles, and his use of thin airfoil theory for the external flow) he (1) did not properly employ the viscous integral equations to obtain a stable solution; (2) was unable to integrate the full set of equations into the reversed flow region; and (3) did not match his near wake to the proper far wake asymptotic solution.

In this section an attempt is made to correct the difficulties noted above, by making use of some of the techniques developed earlier for the supersonic base flow problem, and by properly formulating a stable iteration scheme for the solution of the resulting integro-differential equations.

IX. 1. The Two-Dimensional Incompressible Turbulent Base Flow Field

The general features of the turbulent incompressible flow field behind a rearward facing step are readily seen if one examines the measurements of the mean longitudinal velocity field and plate pressure distribution obtained by Tani, et. al., shown in figure (27). Even though reattachment is to a solid surface, the mean velocity profiles downstream of the rear stagnation point appear to have an increasing finite slip, such as would be the case for a reattaching wake flow. The low speed separation behind a body without a splitter plate along the centerline does not have the steady behavior of the flow noted above, due to periodic vortex shedding from the body. However, if a splitter plate with a length of about 10 step heights were employed, then the vortex shedding could be suppressed and the flow downstream of the splitter plate would then develop as a "steady" (in the mean) wake flow. Thus a theoretical wake model might be related to an actual wake flow field provided that a splitter plate was used to stabilize the flow near the body.

The pressure distribution (figure 27b) obtained by Tani indicates several important features of the flow, some of which are quite

similar to those of the supersonic case. The pressure in the region immediately behind the base is approximately constant, with a slight rise toward the base due to the stagnation of the reverse flow. The length of the constant pressure region is approximately twice that of the supersonic quiescent region. At about 3 step heights, the pressure begins to rise as the shear layers begin to interact with the outer flow. C_p continues to increase until about one step height downstream of the reattachment point ($x/h \approx 6.8$) where it reaches a maximum and then begins to decrease toward the pressure level far downstream of the step.

Roshko and Lau (35) studied the reattachment pressure distribution at low speeds behind bodies of various shapes. Figure 28 reproduces their results for the ordinary pressure coefficient†

$$C_p = \frac{p - p_\infty}{\frac{1}{2}\rho u_\infty^2}$$

as a function of the normalized distance from the base x/h. One notes that there exists a wide range of base pressures for the various models and that the distance to reattachment is considerably different for each case. While the pressure profiles appear to be quite uncorrelatable in the form C_p vs. x/h, Roshko and Lau found that they could reduce the measured pressure distribution to nearly a single curve (Fig. 29) provided that a pressure coefficient $\tilde{C}_p$ defined as

$$\tilde{C}_p = \frac{P - P_{base}}{\frac{1}{2}\rho U_e^2{}_{base}} \qquad (9.3)$$

† ∞ refers to conditions upstream of the body.

is plotted against the distance $\tilde{x}$ defined as the axial distance divided by the distance to the rear stagnation point, i. e.

$$\tilde{x} = x/x_{rsp} \tag{9.4}$$

In finding a correlation in terms of the pressure coefficient C_p (equation 9.3) the base pressure is essentially removed as a parameter which influences the reattachment process, and thus it acts only to alter the level of the pressure field. It will be seen in the following section, by considering the integral interaction equations, that it is the conditions in the far wake (as affected by model and tunnel geometry) that determine the base pressure level and that the dynamics of the near wake reattachment process are influenced basically by the local reattachment mechanism as suggested by Roshko and Lau.

IX.2. Differential Equations for Incompressible Interaction

The integral momentum, mechanical energy, and continuity equations for the single parameter portion of the incompressible wake flow are easily deduced from equations (5.8), (5.13) and (5.9) by taking the limit as $M_e \to 0$, hence

$$\mathcal{H} \frac{d\delta^*}{dx} + \delta^* \frac{d\mathcal{H}}{dx} + [2\mathcal{H}+1] \frac{\delta^*}{U_e} \frac{dU_e}{dx} = 0 \tag{9.5}$$

$$J \frac{d\delta^*}{dx} + \delta^* \frac{dJ}{dx} \frac{d\mathcal{H}}{dx} + 3J \frac{\delta^*}{U_e} \frac{dU_e}{dx} = K_\theta \mathcal{H} R \tag{9.6}^\dagger$$

$$\frac{d\delta^*}{dx} - Z \frac{\delta^*}{U_e} \frac{dU_e}{dx} = \tan \Theta \tag{9.7}^{\dagger\dagger}$$

---

† Green uses Head's entrainment equation $\frac{1}{U_e} \frac{dm}{dx} = F(a) \neq$ entrainment parameter

†† Green makes the error of equating $\tan \Theta$ and $d\delta^*/dx$

We have a system of three equations for the four unknowns, δ^*, $\mathcal{H}(a)$, U_e, and Θ (the induced angle $\tan^{-1}\frac{v_e}{u_e}$ at the edge of the viscous layer). In addition we require an inviscid flow relation between Θ and U_e. Assuming the external flow is inviscid and irrotational, then we may use potential theory. Thus, if the analytic complex function $F(Z)$ is defined as

$$F(Z) = \Phi + i\psi$$

where Φ is the velocity potential ($\bar{u} = \nabla\Phi$) and ψ the stream function, then differentiation of the above expression yields

$$\frac{dF}{dZ} = u - iv$$

where u and v are the horizontal and tangential components of the 2-d velocity vector $\bar{u}$. Since dF/dZ is also analytic, this indicates that u and -v are harmonic conjugates.

Using the Cauchy integral formula for analytic functions, it is easy to find the following integral relationship between the harmonic conjugates u and -v [see Morse and Feschbach (36) p. 371].

$$u(x, y) = \frac{1}{\pi}\int_{-\infty}^{\infty}\frac{(x-\xi)v(\xi, 0)}{(x-\xi)^2 + y^2}\,d\xi \qquad (9.8)$$

$$v(x, y) = \frac{1}{\pi}\int_{-\infty}^{\infty}\frac{(x-\xi)u(\xi, 0)}{(x-\xi)^2 + y^2}\,d\xi \qquad (9.9)$$

Let us introduce the freestream velocity U_∞ as an additive constant in equations (9.8) and (9.9) and assume that $u(x, y)$ denotes a small perturbation from U_∞, i.e. $U(x, y) = U_\infty + u$ where $\frac{u}{u_\infty} << 1$. Thus

$v/U_e \approx v/U_\infty$ and denoting $\tan \Theta(x, \delta) = \frac{v(x, \delta)}{U_e} \approx v(x, \delta)/U_\infty$ then equation (9.9) becomes

$$\tan \Theta(x, \delta) = \frac{1}{\pi} \int_{-\infty}^{\infty} \frac{(x-\xi)\left[1 - \frac{U}{U_\infty}(\xi, 0)\right]}{(x-\xi)^2 + \delta^2} \, d\xi \qquad (9.10)$$

From the condition for the asymptotic matching of the boundary layer and outer inviscid solutions

$$\lim_{y \to 0} \frac{U}{U_\infty}_{\text{outer}}(x, y) \Bigg| = \lim_{y \to \infty} \frac{U}{U_\infty}_{\substack{\text{boundary} \\ \text{layer}}}(x, y) \Bigg| = \frac{U_e}{U_\infty}$$

Then the required relation between Θ and U_e may be written

$$\tan \Theta = \frac{1}{\pi} \int_{-\infty}^{\infty} \frac{(x-\xi)\left[1 - \frac{U_e}{U_\infty}(\xi, 0)\right]}{(x-\xi)^2 + \delta^2} \, d\xi \qquad (9.11)$$

From Bernoulli's equation we have the following approximate relation for the pressure coefficient C_p

$$C_p = \frac{P_e - p_\infty}{\frac{1}{2} \rho U_e^2} \approx 2\left[1 - \frac{U_e}{U_\infty}\right] \qquad (9.12)$$

for

$$\frac{U_e - U_\infty}{U_\infty} << 1$$

IX.3. Integration of the System of Equations

Due to the extremely complex nature of the non-linear differential equations (9.5), (9.6), (9.7) and (9.11), an iterative procedure appears to be the only practical method of solution. We may consider this as a two-point boundary value problem where the solution must satisfy conditions both upstream of the base ($x \to -\infty$) and in the far wake ($x \to +\infty$). It is necessary that the iteration scheme adopted be

both stable and convergent.

It appears that instabilities in the iteration procedure can be avoided provided that the full set of equations((9.5-9.7) are simultaneously integrated for some assumed distribution of tan Θ. The following iteration scheme is thus suggested: †

(1) Assume a distribution of tan Θ vs. $x/\delta_i^*(0)$ which has the proper asymptotic form as $x \to \infty$. ††

(2) Starting at the r.s.p. ($\bar{\delta}_i^* = 1$ $a = 0$) with an assumed value of the pressure coefficient C_p (which will later be obtained by application of the momentum theorem to a control surface enclosing the body) integrate the full set of equations (9.5)-(9.7), first downstream and then upstream of the r.s.p. to some $u^* = u^*_{join}$, using single parameter Stewartson profiles. Since there is no way of knowing á-priori the correct location $[x(0)/\delta_i^*(0)]$ of the rear stagnation

---

† Green suggested an iteration method in which the wake problem is solved as a straight forward boundary layer calculation with a known pressure distribution, C_p, being determined from the thin airfoil theory equation (9.1). Using the integral momentum and entrainment equation, δ^* and $\mathcal{K}(a)$ are calculated for a given $\frac{dC_p}{dx}$. The continuity equation is used to obtain a new distribution of tan Θ and (9.1) is then used to obtain a new pressure distribution. The calculation procedure is then repeated with the new C_p distribution. This method yields unstable solutions in the reverse flow region because the determinant of the subsystem of equations $\tilde{D} = \mathcal{K}\frac{dZ}{d\mathcal{K}} - Z$ not only passes through a zero just downstream of the r.s.p. but is quite small in the region upstream of the r.s.p. Any discrepancies in the assumed pressure gradient are greatly amplified in this region, thus leading to unstable solutions.

†† The asymptotic form of tan Θ is determined in section IX.4.

point for a given initial boundary layer, δ_1/h, different initial starting locations must be chosen until the wake solution satisfying the conditions $a \to 1$, $C_p \to 0$ as $x/\delta_i^* \to \infty$ is obtained.

(3) At the joining point the profiles are changed over to the 2-parameter cosine profiles (valid near the base) and the integration is continued to the base by adding the extra equation along the centerline

$$u_{\mathfrak{C}} \frac{du_{\mathfrak{C}}}{dx} + \frac{1}{U_e} \frac{dU_e}{dx} = 0$$

as outlined for the supersonic case in Section VI. The value of $u^*_{joining}$ is adjusted so that at the point where $u_{\mathfrak{C}} = 0$ (the base) $\tan \Theta$ is equal to the value assumed for it at the base.

(4) With the distribution of $C_p \left(= 1 - \frac{U_e}{U_\infty}\right)$ and δ obtained in steps (2) and (3) a new distribution of $\tan \Theta$ is determined from the integral equation for the external flow

$$\tan \Theta = \frac{1}{\pi} \int_{-\infty}^{\infty} \frac{(x-\xi)\, C_p/2}{(x-\xi)^2 + \delta^2} \, d\xi \qquad (9.13)$$

Steps (2)-(4) are then repeated with this new distribution of $\tan \Theta$ as an input until a suitable numerical convergence is obtained. An example of a typical integration is shown in figure (30) where δ^*/h, θ/h, u^*, and C_p are plotted as a function of x/h. Note that this is <u>not</u> a final solution but only the result of an integration for a given distribution of $\tan \Theta$. The assumed curve of $\tan \Theta$ vs. x was calculated from one of Tani's experimental pressure distributions by means of equation (9.13).

The integral thicknesses δ^*, and θ shown in figure (30), both approach a constant value at the base corresponding to some initial boundary layer thickness at the corner ($\delta_1/h \approx 0.5$). One notes that δ^* decreases away from the base and tends toward a constant value (equal to the drag of the body) in the far wake. The momentum thickness rises from its minimum value at the base and likewise approaches the same asymptotic drag value as does δ^* in the far wake.

The dividing streamline velocity has the same general appearance as in the supersonic case, increasing from zero at the base to a maximum at the joining point and then dropping to zero again at the rear stagnation point. Beyond the r.s.p., the centerline velocity increases rapidly and approaches unity in the far wake.

The centerline pressure distribution shows some of the features noted of incompressible flows. The length of the constant pressure region is approximately one-half the distance to the rear stagnation point. This was approximately the ratio found by Roshko and Lau in figure (29). Also the characteristic peaking of the pressure curve is evident at a distance $x/x_{r.s.p.} = 1.3$. The maximum pressure rise $\tilde{C}_{p_m} = \frac{C_{p_{max}} - C_{p_{Base}}}{1 - C_{p_{Base}}}$ is only about .21 in this calculation as opposed to a value of .34 cited by Roshko and Lau as the maximum value of $\tilde{C}_{p_m}$ based on the Chapman-Korst theory. They did note, however, that the value of $\tilde{C}_{p_m}$ tends to decrease as the initial boundary layer thickness increases. Values as low as .109 have been measured [see Moore reference (37)].

The numerical integration discussed above was only a sample

of the type of solution possible. It did not properly include all the source and sink disturbances which affect the induced vertical component of velocity v_e. In the next section we discuss the effect of the asymptotic solution in the far wake, and the influence of tunnel and flow geometry on determining the base pressure level and how consideration of these effects is essential to obtaining a properly convergent solution for the base flow problem.

IX.4. The Asymptotic Far Wake Boundary Conditions

In the compressible supersonic wake flow solution, the base pressure is essentially determined by the requirement that the solution curve of the integral equations pass smoothly through the critical point, downstream of the r.s.p. The wake flow downstream of the critical point is "supercritical" and thus, any gross disturbances in this region are not propagated upstream to the base. However, for the case of incompressible flow, the wake is always "sub-critical", and a correct solution for the base pressure must depend upon satisfying the conditions at downstream infinity.

We can use the integral momentum and mechanical energy equations to determine the form of the far wake solution, and then use the continuity equation to ascertain the asymptotic form required for tan Θ. To simplify the calculations and to insure a simple closed form solution, we will assume that the velocity profile for the viscous layer is a simple cosine profile of the form †

† This form was used by Green in his integral analysis.

$$\frac{u}{u_e} = 1 - P\left(1 + \cos\frac{\pi y}{\delta}\right) \tag{9.14}$$

where $1 - 2P = u_{\mathcal{L}}/u_e = a$

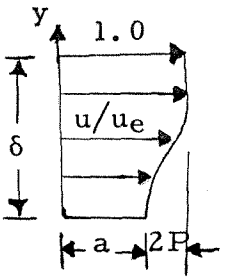

The integral parameters then have the simple form

$$\mathscr{V} = 1 - \frac{3P}{2} \qquad J = 2 - \frac{9}{2}P + \frac{5}{2}P^2$$
$$R = \pi^2 P^3 \qquad Z = \frac{1-P}{P} \tag{9.15}$$

Goldstein (38) has shown that the pressure gradient term $\frac{dP}{dx} \sim \frac{1}{U_e}\frac{dU_e}{dx}$ can be neglected in the first approximation to the far wake solution as being of higher order in x^{-1} than is required.

The momentum and mechanical energy equations (9.5) and (9.6) may then be written as

$$\mathscr{V}\frac{d\delta^*}{dx} + \delta^*\frac{d\mathscr{V}}{dx} = 0$$
$$J\frac{d\delta^*}{dx} + \delta^*\frac{dJ}{dx}\frac{d\mathscr{V}}{dx} = K\mathscr{V}R \tag{9.16}$$

Solving for the derivatives

$$\delta^*\frac{d\mathscr{V}}{dx} = \delta^*\frac{d\mathscr{V}}{dP}\frac{dP}{dx} = \frac{K\mathscr{V}^2 R}{\mathscr{V}\frac{dJ}{d\mathscr{V}} - J}$$
$$\frac{d\delta^*}{dx} = \frac{-K\mathscr{V}R}{\mathscr{V}\frac{dJ}{d\mathscr{V}} - J} \tag{9.17}$$

If we now assume that for x large, $U_{\mathcal{L}} \to U_e$ i.e. $a \to 1$ then we may make the approximation that

$$P = \frac{1-a}{2} \ll 1 \qquad (9.18)$$

therefore,

$$\mathcal{N} \to 1 \quad J \to 2 \quad \frac{dJ}{d\mathcal{N}} = 3 - \frac{10}{3} P \to 3$$

The dissipation integral retains the form $R = \pi^2 P^3$ in this first order approximation.

The application of the momentum theorem to a control surface which encloses the body and extends far enough downstream so that $P_e \approx P_\infty$ gives

$$D = \rho U_\infty^2 \int_0^\infty \frac{u}{U_\infty}\left(1 - \frac{u}{U_\infty}\right) dy \qquad C_D = \frac{D}{\frac{1}{2} U_\infty^2 h \rho} \qquad (9.19)$$

or $$\frac{1}{2} C_D h = \theta_\infty \approx \int_0^\infty \left(1 - \frac{u}{U_\infty}\right) dy \approx \delta_\infty^* = \text{const.}$$

Thus δ^* is to first order constant and is equal to one-half the drag coefficient of the body. But the drag of the body is just equal to the base drag + the initial momentum thickness at the base, hence

$$\boxed{\frac{C_D}{2} = \frac{\theta_\infty}{h} = \frac{-C_{P_{Base}}}{2} + \frac{\theta_{Base}}{h}} \qquad (9.20)$$

Thus the base pressure may be determined by subtracting the momentum defect in the far wake $\frac{\theta_\infty}{h}$ (found from the integral solution) from the base momentum thickness $\frac{\theta_{Base}}{h}$.

Substituting (9.18) and (9.19) into (9.17) produces the following expression for the rate of change of the centerline velocity defect,

$$\frac{dP}{dx} = -\frac{4}{3}\pi^2 \frac{K}{C_D} P^3$$

integration yields

$$\boxed{\begin{aligned} P &= \left(\frac{3}{8\pi^2}\right)^{\frac{1}{2}} \sqrt{\frac{C_D}{Kx}} \\ \frac{\delta^*}{h} &= \frac{C_D}{2}\left[1 + \int \left(\frac{27}{32\pi^2}\right)^{\frac{1}{2}} \sqrt{\frac{C_D}{Kx}}\right] \end{aligned}} \qquad (9.21)$$

To first order, the continuity equation for the far wake has the constant pressure form

$$\tan \Theta = \frac{d\delta^*}{dx}$$

From equation (9.21), we find that the induced normal velocity component is of order $x^{-\frac{3}{2}}$, i.e.

$$\tan \Theta = \frac{-K}{\pi}\left(\frac{3}{8}\right)^{\frac{3}{2}}\left(\frac{C_D}{Kx}\right)^{\frac{3}{2}} \qquad (9.22)$$

Therefore in performing the wake iteration scheme it is necessary that the assumed distribution of tan Θ have the asymptotic form given by equation (9.22), for a given initial guess of the drag coefficient (C_D), in order to produce a convergent wake solution.

In addition to the self induced pressure field of the wake itself, additional pressure contributions can be linearly added to the wake solution to account for the effects of the body.

Since the velocity defect P is of order $x^{-\frac{1}{2}}$ and the wake thickness $\delta = \delta^*(1+Z) \sim x^{\frac{1}{2}}$, then aside from the freestream velocity U_∞, there is a finite inflow along the wake toward the body. But this

inflow must be balanced by an outflow of fluid from the body of equal strength, as shown in the sketch below †

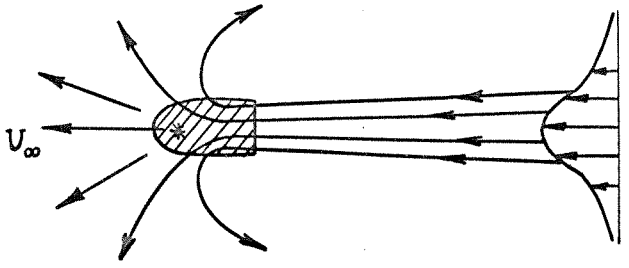

Thus the external potential flow may be thought of as resulting from a source of strength $Q = D/\rho\, U_\infty$ at the nose of the body, and a distribution of sinks produced by the wake interaction. The velocity along the axis due to a source of strength Q is

$$u_{source} = \frac{Q}{2\pi x} = \frac{C_D U_\infty}{4\pi x} \qquad (9.23)$$

The added pressure term due to the body is therefore

$$C_{P_{Body}} = \frac{C_D}{2\pi x} \qquad x/h >> 1 \qquad (9.24)$$

If for a given test setup, the induced velocity at some point in the far wake is altered due to the surrounding tunnel geometry, this will effect the level of the base pressure. These tunnel and model effects are not negligible and can produce a considerable variation in the base pressure as the experimental results of Roshko and Lau (figure 28) have shown. It may be possible to include these geometry effects by using additional image sinks beyond the tunnel walls in order to balance the sinks produced by the free wake.

---

† see Prandtl-Tietjens Hydro and Aeromechanics, p. 124.

In conclusion, we have indicated the direction in which an integral analysis of the incompressible base flow region should proceed. An outline of what appears to be a convergent iteration scheme has been set forth based on the techniques developed for supersonic flow, along with some relevant discussion of the appropriate boundary conditions necessary to establish the level of the base pressure.

X. CONCLUSIONS AND RECOMMENDATIONS FOR FUTURE WORK

In reviewing the theory as presented in this paper, we note that the following broad assumptions were required in order to obtain a solution to the turbulent base flow problem: (1) an eddy viscosity law and compressible transformation [$\rho^2 \epsilon = f(x)$] can be used to describe the scaling effects of the turbulent shear stresses; (2) single parameter Stewartson profiles are adequate to describe the velocity profiles in the turbulent near wake, not too close to the base; (3) the boundary layer assumption $\partial p/\partial y \approx 0$ can be used throughout the near wake flow field within the viscous sublayer region; (4) the outer flow can be considered fully isentropic; and (5) flow perturbations in the vicinity of the corner do not affect the downstream solution.

While the assumptions above are clearly open to question and/or improvement, it is felt that any turbulent base flow solution must incorporate the essential feature of viscous-inviscid interaction. For the case of supersonic flow, any solution must acknowledge the existence of the Crocco-Lees critical point. Theories which are based on matching conditions far downstream of reattachment can be considered only as sophisticated correlation procedures without the proper physical foundation.

As to the five assumptions listed above we can make some important conclusions based on the results obtained so far.

First, it appears that for the free shear layer the use of the eddy viscosity model of equation (4.26) with the reference density equal to the density in the quiescent region, gives good agreement with

experiment for overall growth rates, such as the momentum thickness. While the eddy viscosity model was verified for the asymptotic or similar shear layer (and far wake), it has not been fully established that this model is completely valid in the non-similar mixing regime. A thorough experimental and theoretical investigation of the mean flow quantities and turbulent fluctuations in the non-similar shear layer is considered important. Further, there is essentially no direct verification of the eddy viscosity model used for the compressible reattaching ($\rho_r = \rho_{\mathbb{C}}$). No present experimental fluctuation data exist against which a compressible near wake eddy viscosity model can be compared, as has been done for the data of Tani and Mueller (21, 22) for the incompressible case. This would be a difficult, but most necessary, experimental task to be undertaken if we are to learn more of the essential features of separating and reattaching turbulent flows.

Such an experimental investigation of the details of the wake profiles would also aid in determining the validity of the Stewartson profiles near the rear stagnation point and the two parameter cosine profiles near the base. Even with the relatively simple eddy viscosity model and velocity profiles presented in this study, the results of the integral solution indicate that the basic length scales and pressure gradients in the near wake are well described by this analysis (at least for those cases where non-isentropic outer flow field effects are unimportant).

The last three assumptions, (3)-(5), can actually be considered as one problem, which is directly attributable to events occurring in the immediate vicinity of the corner. As pointed by Golik et. al. (8)

(for the case of supersonic expansion), within the distance (x_e) required for expansion of the boundary layer (δ_1), both vertical and horizontal pressure gradients are of the same order within the rotational layer. This distance can be estimated from the sketch below, which denotes a simple Prandtl-Meyer expansion of the initial boundary layer.

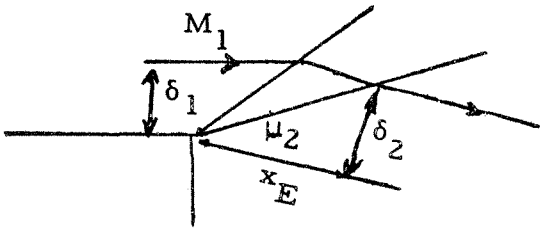

$$\tan \mu_2 = \frac{\delta_2}{x_e} \qquad (10.1)$$

$$\rho_1 u_1 \delta_1 \approx \rho_2 u_2 \delta_2 \qquad (10.2)$$

Therefore

$$\frac{x_E}{h} = \frac{\delta_1}{h} M_1 \left[\frac{1 + \frac{\gamma-1}{2} M_1^2}{1 + \frac{\gamma-1}{2} M_1^2}\right]^{\frac{\gamma+1}{2(\gamma-1)}} \frac{\sqrt{M_2^2 - 1}}{M_2} \qquad (10.3)^{\dagger}$$

One notes that the expansion distance will be small only if the upstream boundary layer thickness and initial edge Mach number are also small. As the results of section VIII indicate, the isentropic boundary layer solution diverges from the data for approach Mach number of the order of 3 or more, for initial values of δ_1 of the order of the step height. But when the approach Mach number was sufficiently low ($M_\infty \leq 2$) good agreement between theory and experiment was obtained.

Thus we conclude that at high Mach numbers ($M_1 \geq 3$) the effect of the corner expansion process becomes very important. Therefore, in order to adequately handle the near wake flow field analysis, an

† For laminar flow, equation (10.3) implies that the expansion length is proportional to the hypersonic interaction parameter $\bar{\chi} = M^3/\sqrt{R_{E_L}}$

outer rotational characteristic calculation procedure must be used to properly account for the entropy gradients and lip shock formation in the outer flow field. Such a calculation procedure is beyond the scope of the present analysis.

X. 1. Summation of the Major Conclusions

1. Assuming that the turbulent shear stress is of the Boussinesq form it was shown, for incompressible flow, that the proportionality constant (K) for the eddy viscosity model $\epsilon = \frac{\tau}{\rho} \frac{\partial u}{\partial y}$ is essentially identical for both similar free shear layers and self preserving wakes (based on the experimental data) provided that ϵ scales only with the momentum thickness θ, and edge velocity u_e, i.e.

$$\epsilon_i = K_\theta u_e \theta$$

2. Employing the compressibility transformation $\rho^2 \epsilon = \rho_r^2 K u_e \theta$ and a modified Stewartson transformation of the coordinates, it was found that the spreading rate of the compressible similar free shear layer momentum thickness is inversely proportional to the square of the reference density. The value of ρ_r which scales the compressible experiments is the density in the quiescent region bounding the shear layer, $\rho_r = \rho_o \approx \rho_{\mathfrak{C}}$.

3. The length of the constant pressure mixing region x_o/h was found to be nearly constant for base flows with initial thicknesses $\delta_1/h < 1$, but x_o/h decreases rapidly as δ_1/h increases above 1. This result was confirmed for both a free shear layer model and a 2 parameter set of wake profiles which were used to join integral wake solution to the base.

4. Using a simple conservation model to relate the viscous sublayer, after the corner expansion, to the initial boundary layer approaching the step, it was shown that the thickness of the sublayer Δ_2 is approximately 10-20% of δ_1. The initial edge Mach number of the sublayer ahead of the turn is always near one, no matter how high the freestream Mach number. This leads to a maximum base pressure ratio $P_b/P_\infty \approx .78$, for all initial Mach numbers, for the case of very thick initial boundary layers ($\delta_1/h >> 1$).

5. For free stream Mach numbers $M_1 \leq 2.3$, the combined supersonic theory gave good estimates for the length of the constant pressure region, the distance to the rear stagnation point, the distribution of centerline pressure during reattachment, and the trend of increasing base pressure with increasing θ_1/h, for the cases of both wake and splitter plate reattachment.

6. An outline of what appears to be a convergent iteration scheme for the incompressible case was presented in section IX. It was shown that the techniques developed for the supersonic integral analysis could be adopted for the low-speed problem, provided that the normal velocity field in the far wake is of order $x^{-\frac{3}{2}}$. It was also pointed out that the low-speed base pressure coefficient is simply the difference between the momentum thickness in the far wake and the value of θ approaching the base.

REFERENCES

1. Korst, H. H., Page, R. H. and Childs, M. W.: "A Theory for Base Pressures in Transonic and Supersonic Flow," University of Illinois ME-TN-392-2, December 1959.

2. Nash, J. F.: "An Analysis of Two Dimensional Turbulent Base Flow Including the Effect of the Approaching Boundary Layer," National Physical Laboratory Aero Report 1036, July 1962.

3. McDonald, H.: "Turbulent Shear Layer Reattachment With Special Emphasis on the Base Pressure Problem," Aeronautical Quarterly, Vol. XV, August 1964.

4. Chapman, D. R., Kuehn, D. M. and Larson, H. K.: "Investigation of Separated Flows in Supersonic and Subsonic Streams With Emphasis on the Effect of Transition," NACA Report 1356, 1958.

5. Crocco, L. and Lees, L.: "A Mixing Theory for the Interaction Between Dissipative Flows and Nearly Isentropic Streams," Journal of the Aerospace Sciences, 19, 649-676 (1952).

6. Carriére, P.: "Recherches Récentes Effectuées A L'O.N.E.R.A. Sur les Problémes de Recollment," Communication Presented at the Seventh Fluid Dynamics Symposium, Jurata (September 1965).

7. Reeves, B. L. and Lees, L.: "Theory of the Laminar Near Wake of Blunt Bodies in Hypersonic Flow," AIAA J., 3, 2061-2074 (1965).

8. Golik, R. J., Webb, W. H. and Lees, L.: "Further Results of Viscous Interaction Theory for the Laminar Supersonic Near Wake," AIAA Paper No. 67-61, Presented at the AIAA 5th Aerospace Sciences Meeting, New York, N. Y. (January 23-26, 1967).

9. Green, J. E.: "Two-Dimensional Turbulent Reattachment as a Boundary Layer Problem," R.A.E. Technical Report No. 66059, Feb. 1966, (AGARD Specialists' Meeting on Separated Flows, VKI, Rhode-Saint Genése, Belgium, 10-13 May, 1966).

10. Larson, R. E., Scott, C. J., Elgin, D. R. and Seiver, R. E.: "Turbulent Base Flow Investigations at Mach Number 3," University of Minnesota, Research Report No. 183, July 1962.

11. Hama, F.: "Experimental Investigations of Wedge Base Pressure and the Lip Shock," Jet Propulsion Laboratory, California Institute of Technology, Technical Report No. 32-1033 (Dec. 1, 1966).

REFERENCES

12. Hastings, R. C.: "Turbulent Flow Past Two-Dimensional Bases in Supersonic Streams," R.A.E. Tech. Note, Aero. 2931, December 1963.

13. Roshko, A. and Thomke, G. J.: "Flow Separation and Reattachment Behind a Downstream Facing Step," Douglas Aircraft Co. Report SM-43056-1, January 1964.

14. Badrinarayan, M. A.: "An Experimental Investigation of Base Flows at Supersonic Speeds," Journal of the Royal Aeronautical Society, Vol. 65, p. 475, July 1961.

15. Scherberg, M. G. and Smith, H. E.: "An Experimental Study of Supersonic Flow Over a Rearward Facing Step," AIAA Journal, Vol. 5, No. 1, p. 51, January 1967.

16. Grange, J. M., Klineberg, J. M. and Lees, L.: "Laminar Boundary Layer Separation and Near-Wake Flow for a Smooth Blunt Body at Supersonic and Hypersonic Speeds," AIAA 5th Aerospace Sciences Meeting, Jan. 23-26, 1967, New York, N. Y., Paper No. 67-62.

17. Townsend, A. A.: "The Structure of Turbulent Shear Flow," (Cambridge University Press, Cambridge, 1956), Chapter 7.

18. Lees, L. and Hromas, L.: "Turbulent Diffusion in the Wake of a Blunt-Nosed Body at Hypersonic Speeds," J. Aerospace Sci. 29, 976-993 (1962).

19. Clauser, F.: "The Turbulent Boundary Layer," Adv. Appl. Mech. 4, 1-51, 1956.

20. Göertler, H.: "Berechnung von Aufgaben der freien Turbulenz aus Grund eines neven Näherungsansatzes," ZAMM 22, 244-254 (1942).

21. Tani, I., Iuchi, M., Komoda,: "Experimental Investigation of Flow Separation Associated with a Step or a Groove," Rep. Aero Res. Inst., Univ. Tokyo, 364, April 1961.

22. Mueller, T. J. and Robertson, J. M.: "A Study of the Mean Motion and Turbulence Downstream of a Roughness Element," Modern Developments in Theoretical and Applied Mechanics, Vol. I, Plenum Press, New York, 1963.

23. Chapman, D. R.: "Laminar Mixing of a Compressible Fluid," NACA Report 958, 1950.

REFERENCES

24. Tollmien, W.: "Berechnung der Turbulenten Ausbreitungsvorgaenge," ZAMM, 6, pp. 468-479, 1926, (Also NACA TM 1085, 1945).

25. Reichardt, H.: "Gesetzmassigkeiten der Freien Turbulenz," VDI-Forshungsheft 414, 1st Ed. (Berlin) 1942; 2nd Ed. (Berlin) 1951.

26. Liepmann, H. W. and Laufer, J.: "Investigations of Free Turbulent Mixing," NACA TN 1257, (1947).

27. Gooderum, P. B., Wood, G. P. and Brevoort, M. J.: "Investigation with an Interferometer of the Turbulent Mixing of a Free Supersonic Jet," NACA Report 963, 1959, (Also NACA TN 1857, April, 1949)

28. Maydew, R. C. and Reed, J. F.: "Turbulent Mixing of Axisymmetric Compressible Jets (In the Half-Jet Region) with Quiescent Air," Sandia Corp. Rep. SC-4764 (RR), Aero-Thermodynamics, (March 1963).

29. Sirieix, M. and Solegnac, J.: "Contribution a l'Etude Experimentale de la Couche de Melange Turbulent Isobare d'un Ecoulement Supersonique," Presented at AGARD Specialists' Meeting on Separated Flows, VKI, Rhode-Saint Genése, Belgium, 10-13 May 1966).

30. Sirieix, M.: "Pression de Culot et Processus de Mélange Turbulent en Écoulement Supersonique Plan," La Recherche Aeronautique, Vol. 13, No. 78, pp. 13-20, September 1960.

31. Bailey, H. E. and Kuethe, A. M.: "Supersonic Mixing of Jets and Turbulent Boundary Layers," WADC TR 54-402 (1957)

32. King, H. H. and Denison, M. R.: "Turbulent Mixing in the Base Flow Region," Electro-Optical Systems, Inc., RN-24, May 1965.

33. Coles, D. E.: "The Law of the Wake in the Turbulent Boundary Layer," Jour. Fluid Mech. 1, Part 2, 191, July 1956.

34. Ai, D. K.: "On the Hypersonic Laminar Near Wake Critical Point of the Crocco-Lees Mixing Theory," AIAA 5th Aerospace Sciences Meeting, Jan. 23-26, 1967, New York, N. Y., Paper No. 67-60.

35. Roshko, A. and Lau, J. C.: "Some Observations on Transition and Reattachment of a Free Shear Layer in Incompressible Flow," Proceedings of the 1965 Heat Transfer and Fluid Mechanics Institute, pp. 157-167, Stanford University Press.

REFERENCES

36. Morse, P. M. and Feschbach, H.: "Methods of Theoretical Physics," McGraw-Hill, 1953.

37. Moore, T. W. F.: "Some Experiments on the Reattachment of a Laminar Boundary Layer Separating From a Rearward Facing Step on a Flat Plate Airfoil," Journal Roy. Aero. Soc., Vol. 64 (1960), pp. 668-672.

38. Goldstein, S.: "On the Two-Dimensional Steady Flow of a Viscous Fluid Behind a Solid Body - I," Proc. Roy Soc. A, 142 (1933), pp. 545-560.

39. Gadd, C. E., Holder, D. W. and Regan, J. D.: "Base Pressures in Supersonic Flow," ARC 17, 490 (March 1955).

40. Beastall, D. and Eggink, H.: "Some Experiments on Breakaway in Supersonic Flow, Part II," R.A.E. Tech. Note Aero. 2061 (November 1951).

41. Wimbrow, W. R.: "Effects of Base Bleed on the Base Pressure of Blunt Trailing Edge Airfoils at Supersonic Speeds," NACA A 4 A07 (1954) (British TIL 4148).

42. Morrow, J. D. and Katz, E.: "Flight Investigation at Mach Numbers from 0.6 to 1.7 to Determine Drag and Base Pressures on a Blunt Trailing Edge Airfoil and Drag of Diamond and Circular Aro Airfoils at Zero Lift," NACA TN 3548 (1955).

43. Goin, K. L.: "Effects of Plan Form, Airfoil Section and Angle of Attack on the Pressures Along the Base of Blunt Trailing Edge Wings of Mach Numbers of 1.41, 1.62 and 1.96," NACA R.M. L52D21 (M.O.A. TIB 3324) (1952).

44. Saltzman, E. J.: "Preliminary Base Pressures Obtained from the X-15 Airplane at Mach Numbers from 1.1 to 3.2," NACA TN D-1056 (August 1961).

45. Rebuffet, R." "Effects de Supports sur l'Ecoulement a l'Arrierre d'un Corps," AGARD Rapport 302 (Mars 1959).

46. White, R. A.: "Turbulent Boundary Layer Separation from Smooth Convex Surfaces in Supersonic Two-Dimensional Flow," Ph. D. Thesis, University of Illinois (1963).

47. Kubota, T. and Dewey, C. F. Jr.: "Momentum Integral Methods for the Laminar Free Shear Layer," AIAA J. 2, 625-629 (1964).

REFERENCES

48. Denison, M. R. and Baum, E.: "Compressible Free Shear Layer with Finite Initial Thickness," AIAA J. 1, 342, Feb. 1963.

49. Nash, J. F.: "The Effect of the Initial Boundary Layer on the Development of a Turbulent Free Shear Layer," N. P. L. Aero. Report 1019, June 1962.

50. Mellor, G. L. and Gibson, D. M.: "Equilibrium Turbulent Boundary Layers," J. Fluid Mech., Vol. 24, Part 2, pp. 225-253 (1966).

51. Thomann, H.: "Measurements of Heat Transfer and Recovery Temperature in Regions of Separated Flow at a Mach Number of 1.8," F. F. A. (Stockholm) Report 82 (November 1958).

52. Fuller, L. and Reid, J.: "Experiments on Two-Dimensional Base Flow at M = 2.4," R. A. E. Aero. Report 2569 (Feb. 1956).

53. Rom, J., Seginer, A. and Kronzon, J.: "The Flow Field in the Turbulent Supersonic Near Wake Behind a Two-Dimensional Wedge-Flat Plate Model," Interim Scientific Report No. 6, TAE Report No. 54, Technion-Israel Institute of Technology (August 1966).

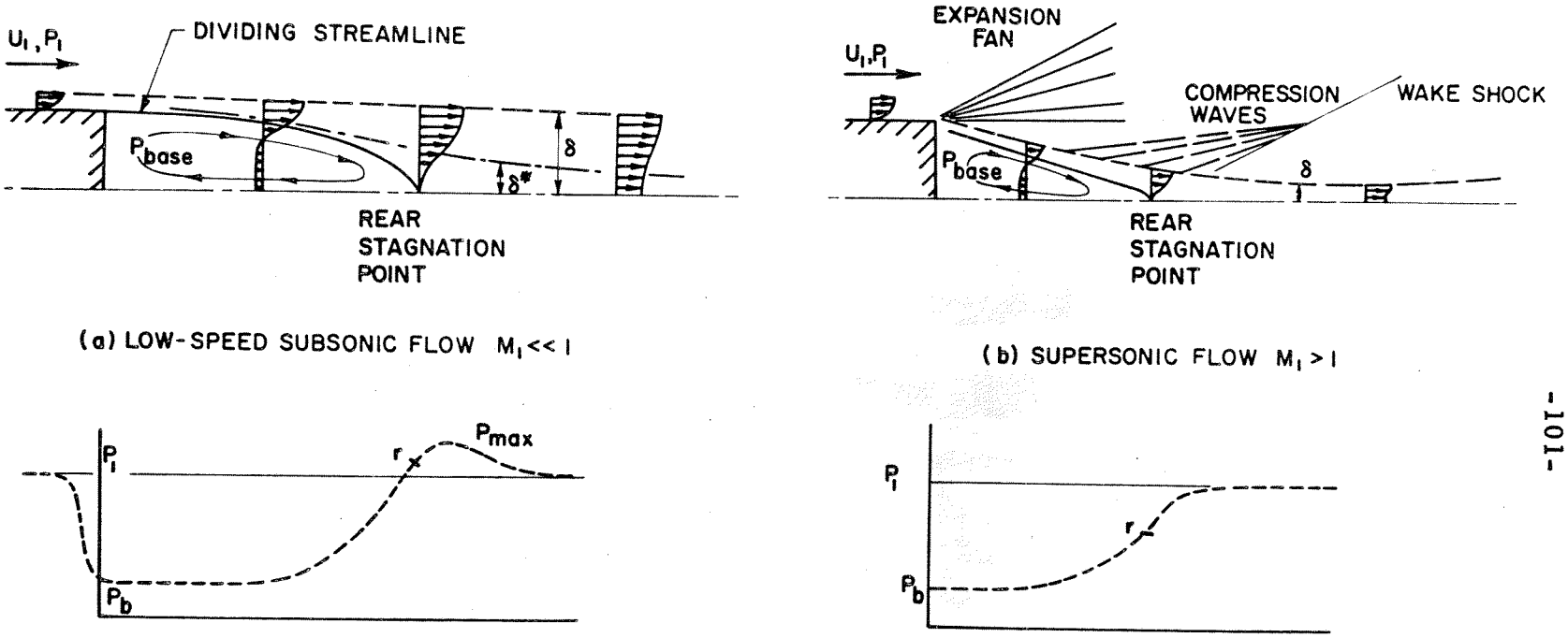

FIG. 1 SCHEMATIC OF THE FLOW FIELD AND ℄ PRESSURE DISTRIBUTION BEHIND A REARWARD FACING STEP

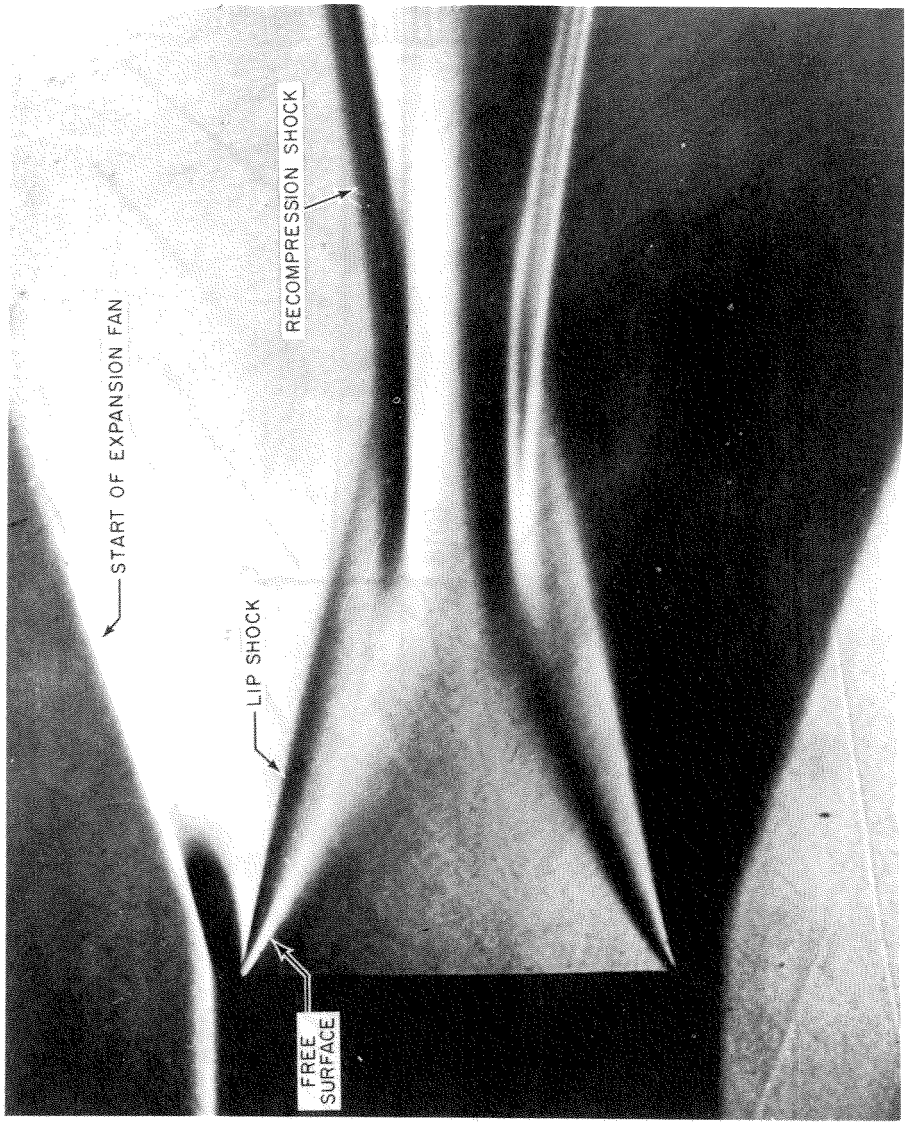

FIG. 2 SCHLIEREN PHOTOGRAPH OF THE TURBULENT NEAR WAKE FOR A TANGENT OGIVE $M_\infty = 3.0$, $R_{e_\infty} = 7 \times 10^6$

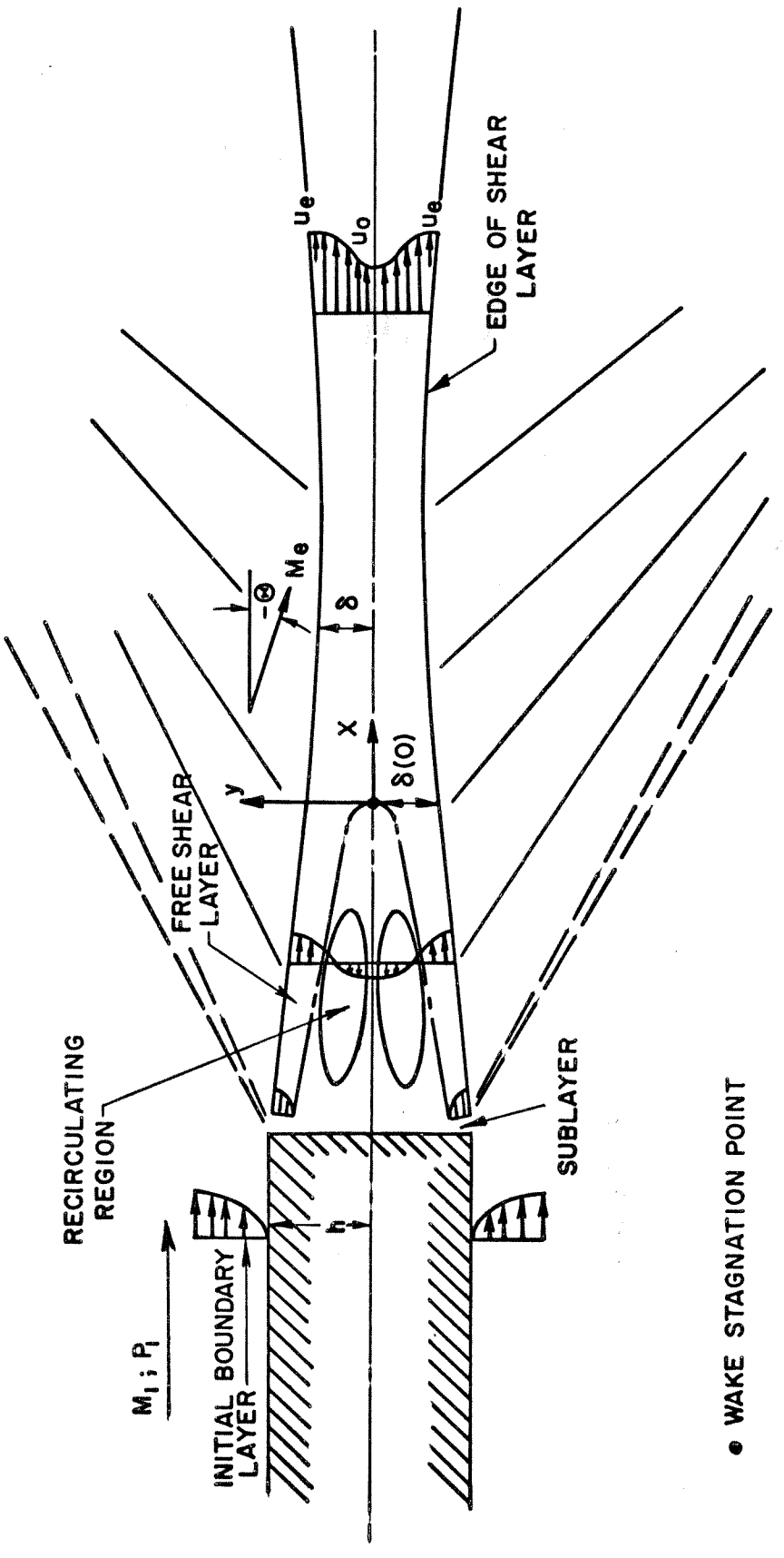

FIG. 3 SCHEMATIC OF TWO-DIMENSIONAL SUPERSONIC BASE FLOW FIELD

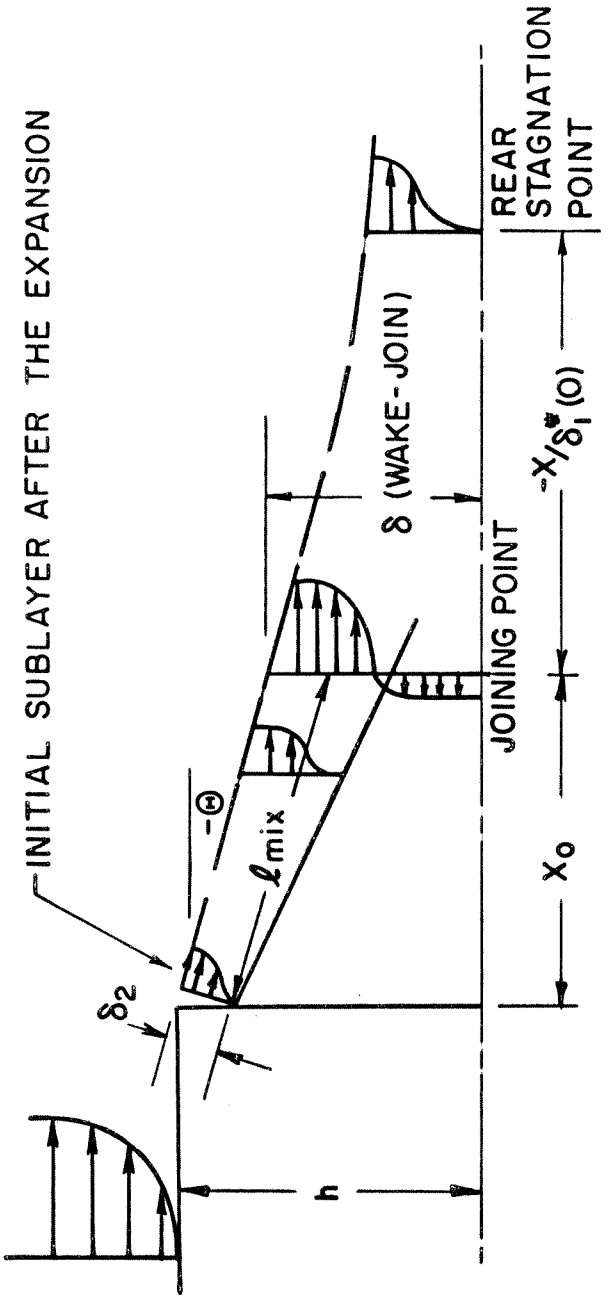

GEOMETRICAL JOINING RELATIONS

$$\left\{ \begin{array}{l} \sin(-\Theta) \approx \dfrac{h-\delta\,(\text{WAKE-JOIN})}{\ell_{mix}} \\ \dfrac{X_0}{h} \approx \dfrac{\ell_{mix}}{h}\cos(-\Theta) \end{array} \right.$$

FIG. 4 SKETCH OF JOINING CONDITIONS

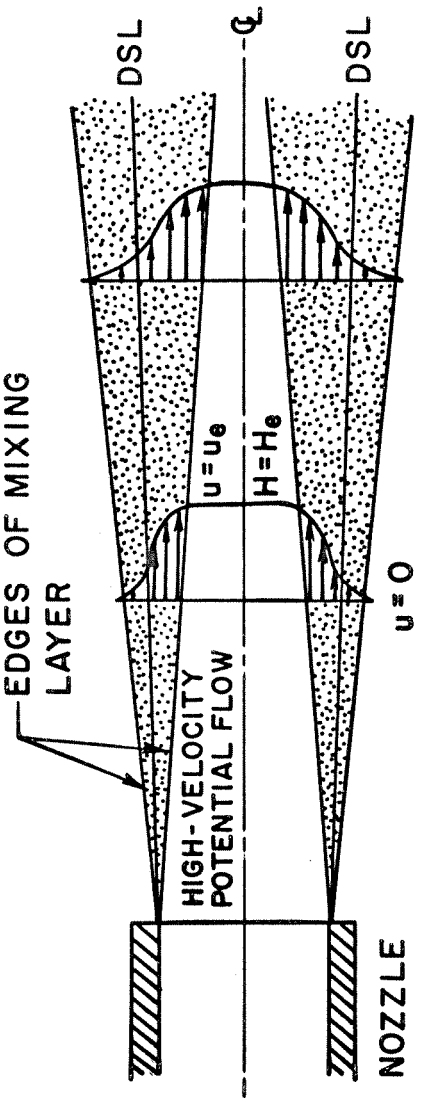

FIG. 5 GEOMETRY OF THE JET MIXING EXPERIMENT TO DETERMINE FREE SHEAR LAYER SPREADING RATES

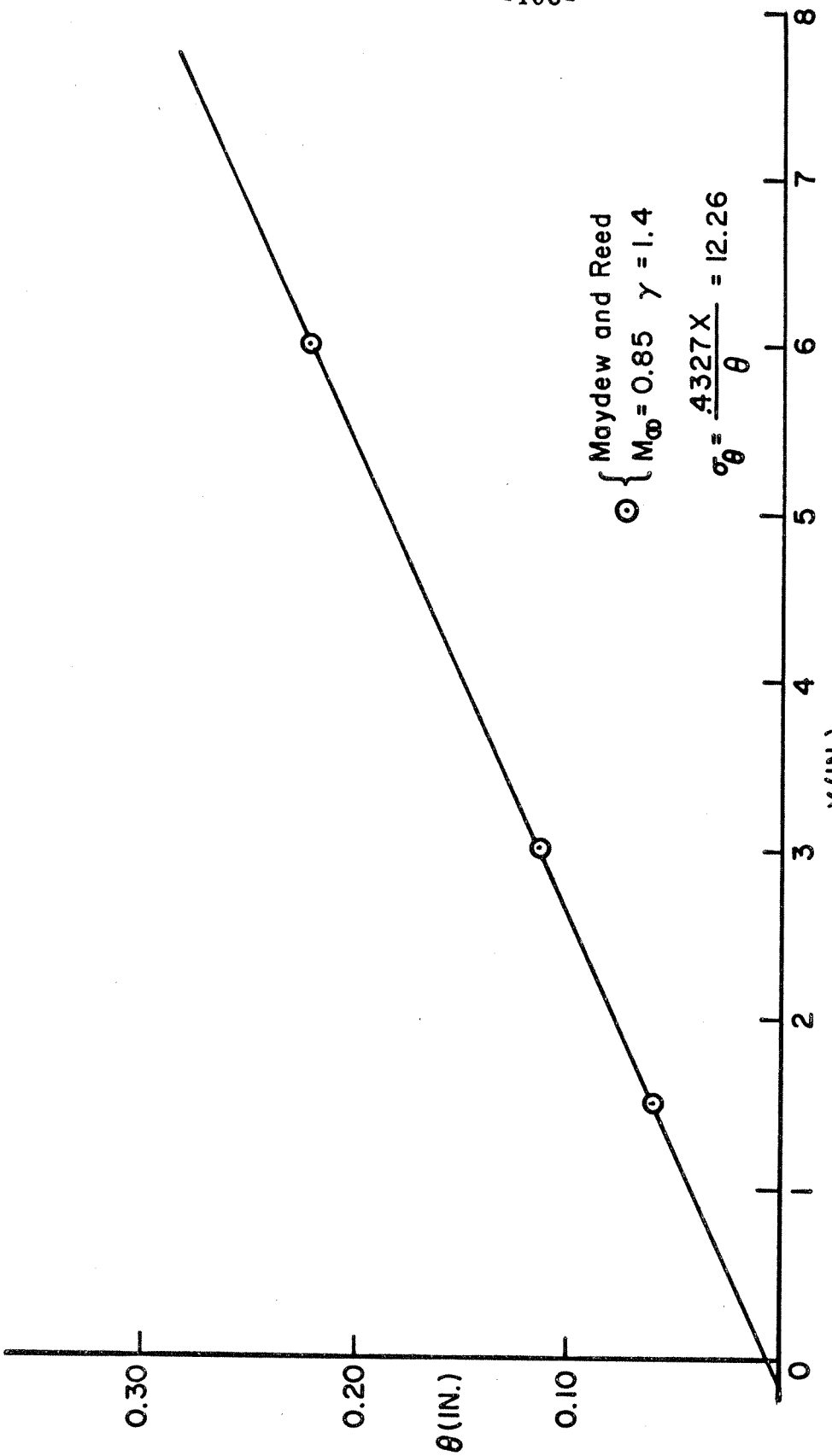

FIG. 6 FREE SHEAR LAYER MOMENTUM THICKNESS VS. X

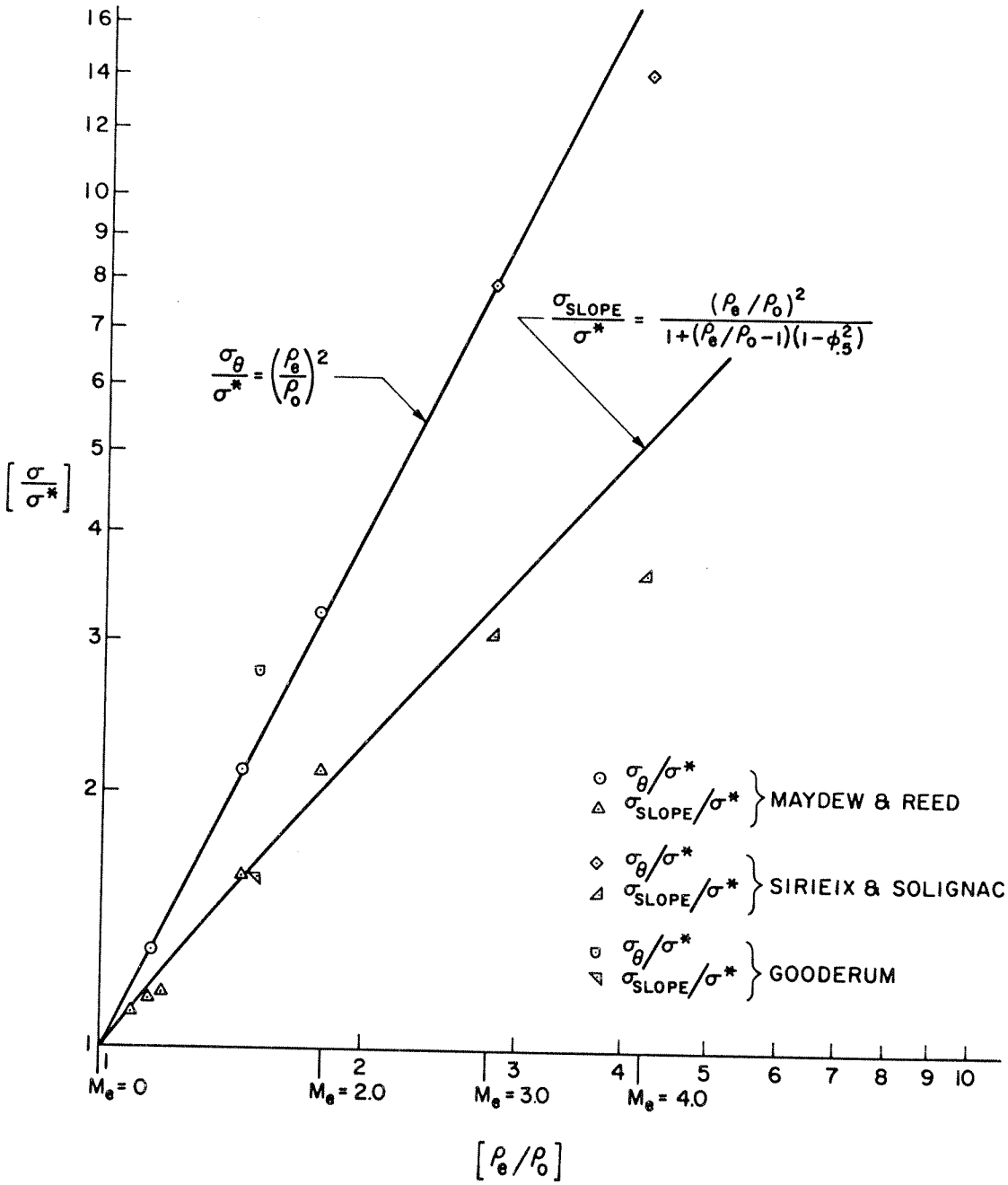

FIG. 7 TURBULENT JET SPREADING PARAMETER σ/σ^* VARIATION WITH DENSITY RATIO ACROSS JET (ρ_e ρ_0) $\sigma^* = 9.42$

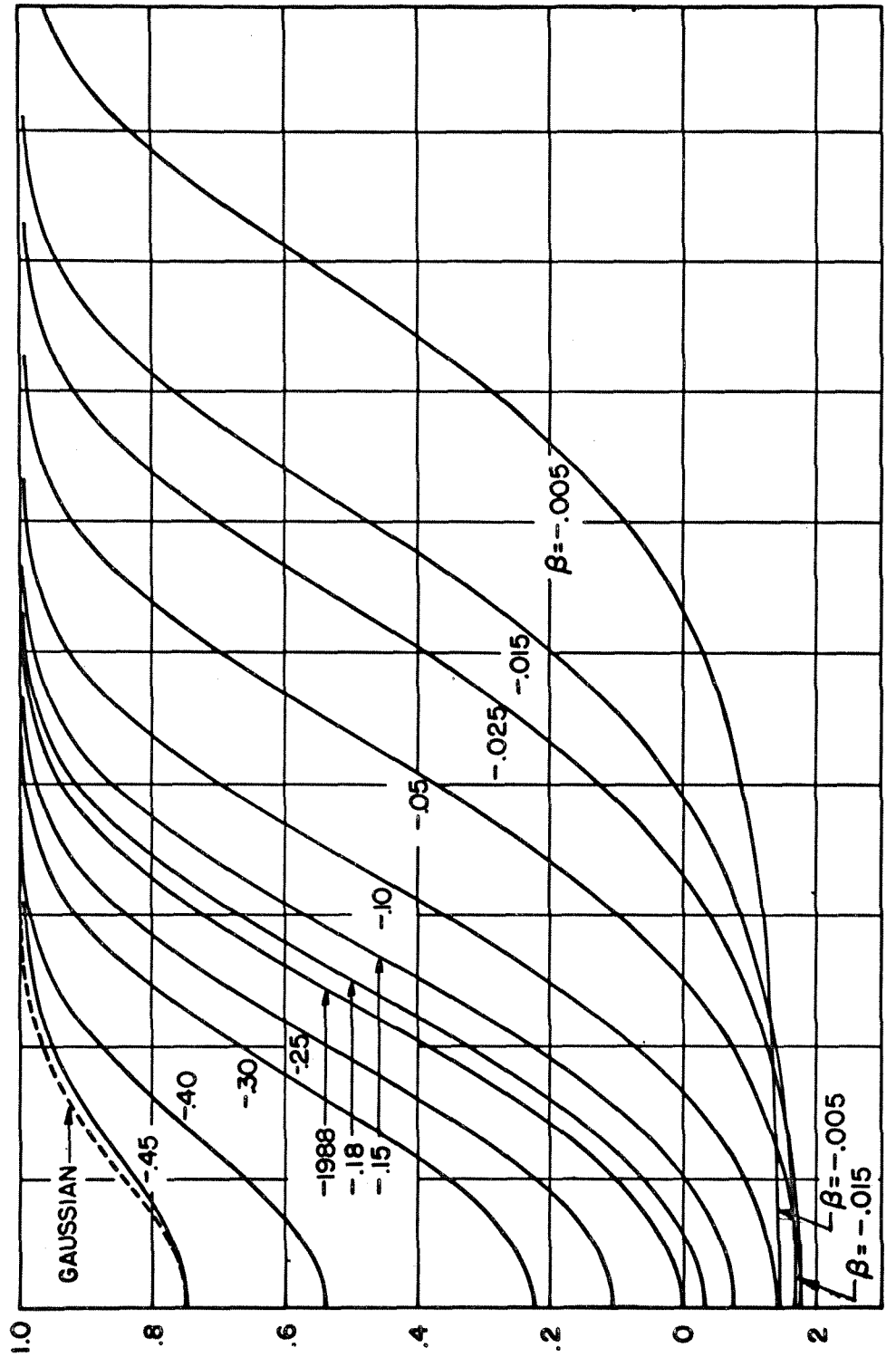

FIG.8 SIMILAR SOLUTION VELOCITY PROFILES FOR ADIABATIC WAKES

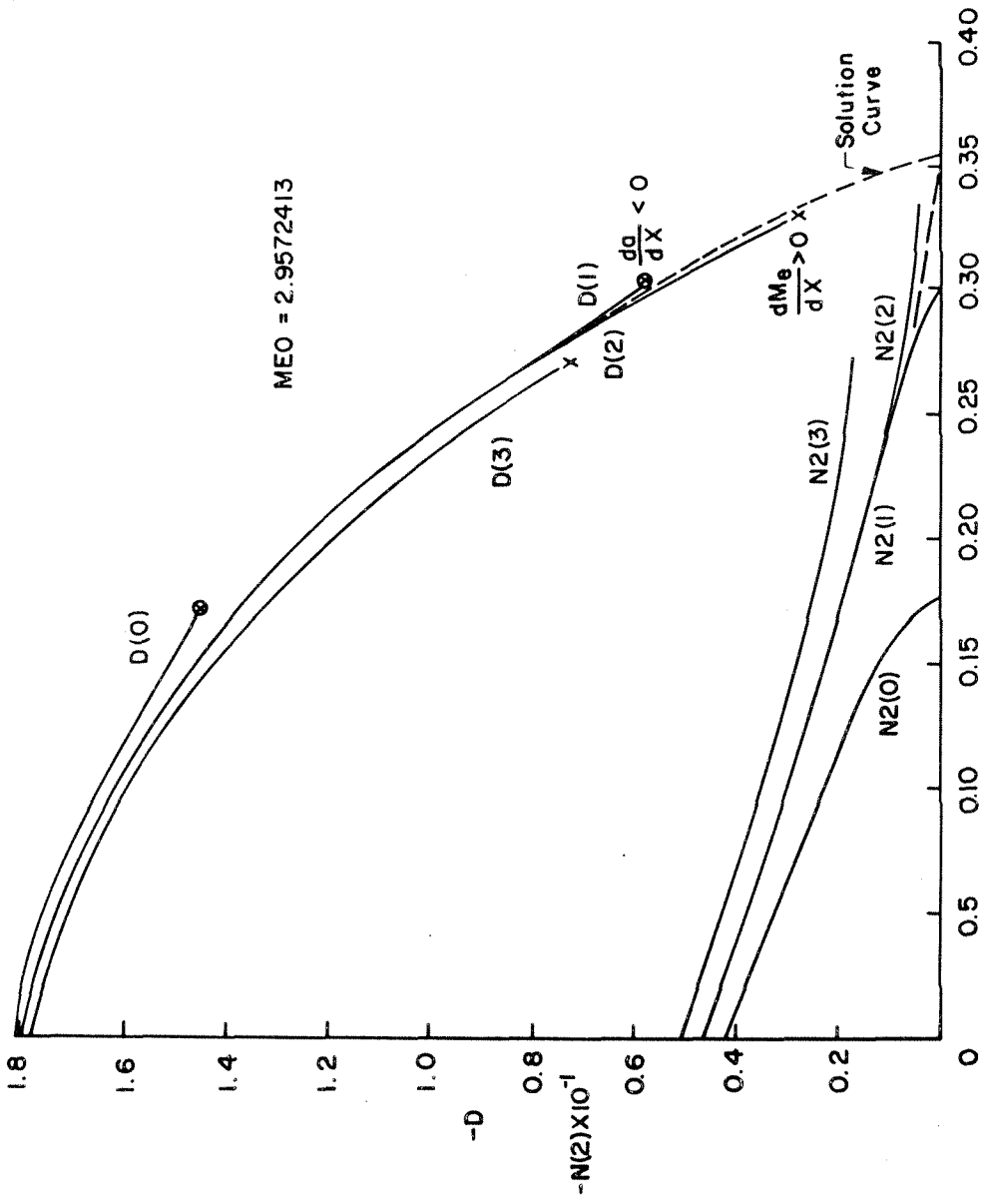

FIG. 9 INTEGRAL CURVES FOR WAKE FLOW SOLUTION

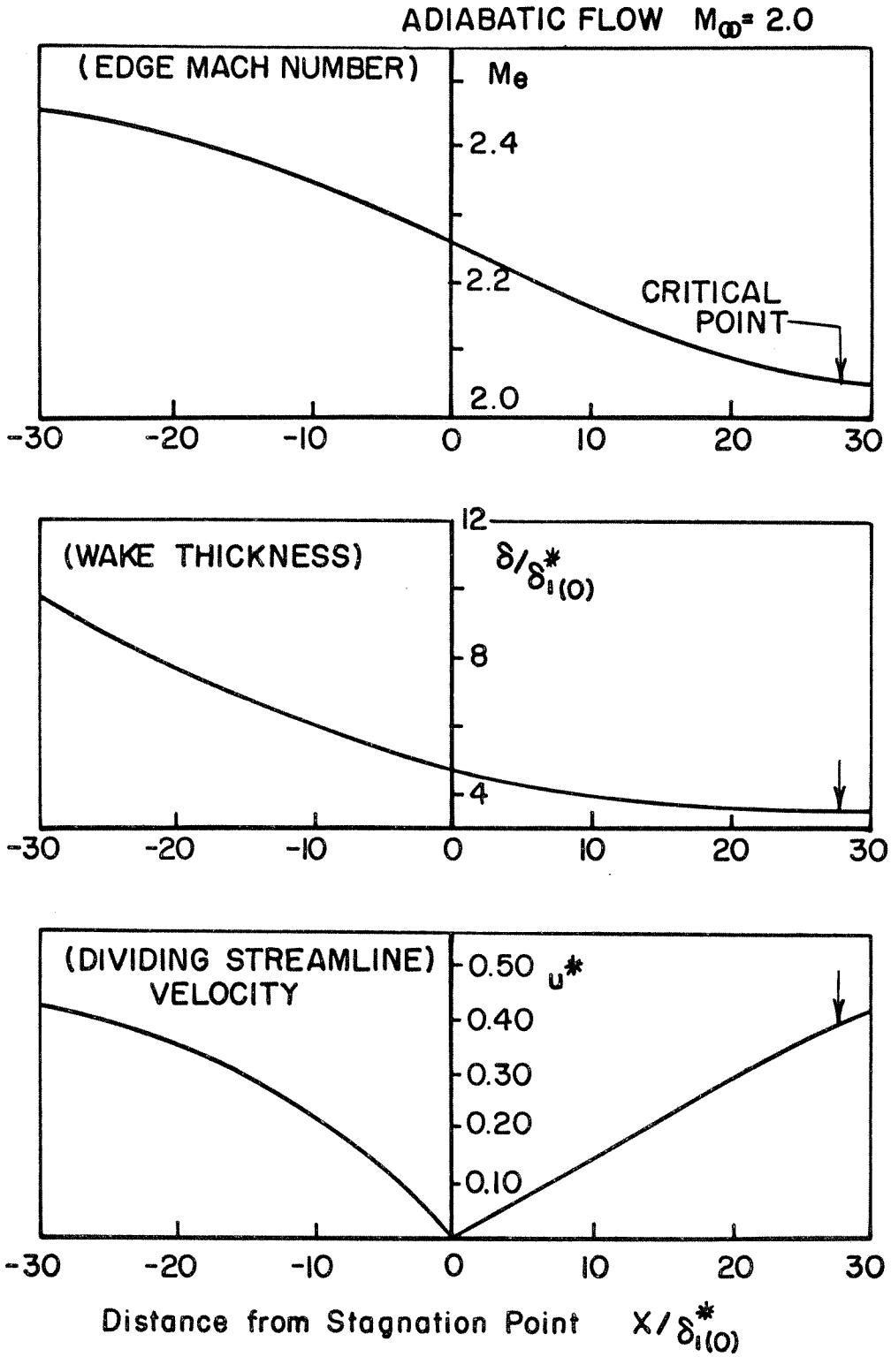

FIG.10 SINGLE PARAMETER WAKE SOLUTION

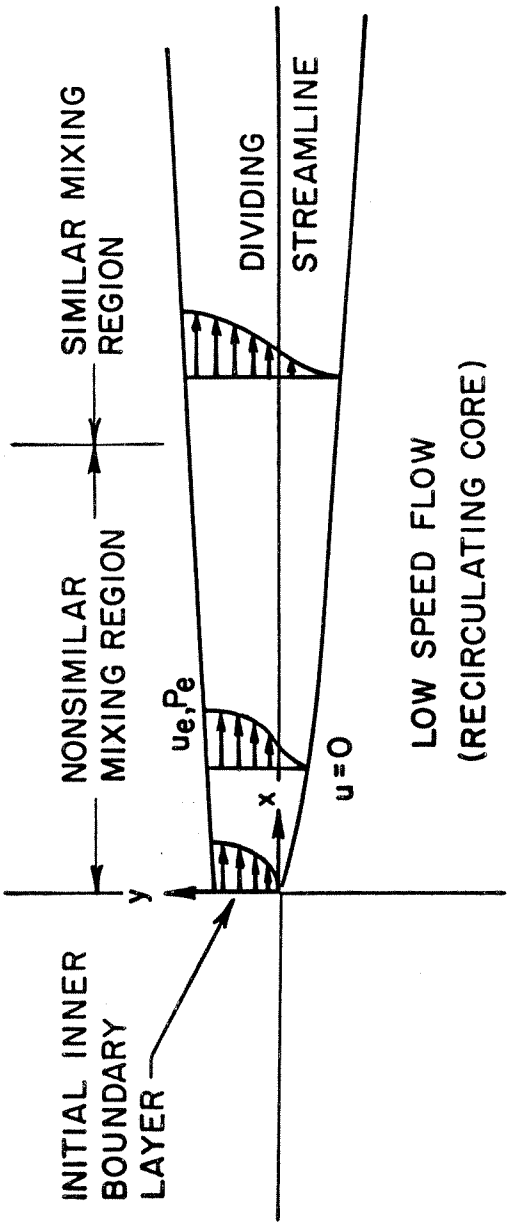

FIG. II MIXING LAYER REGIONS

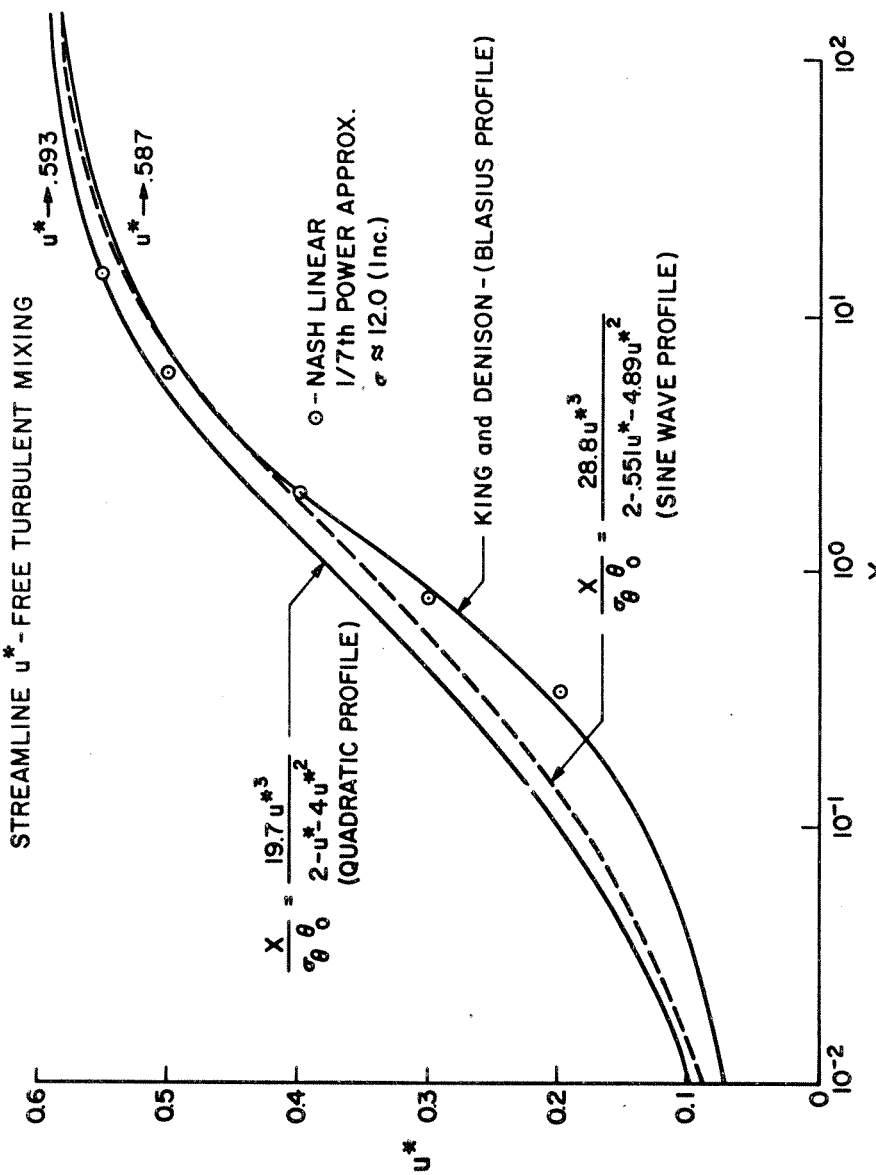

FIG.12 DEVELOPMENT OF VELOCITY ON DIVIDING STREAMLINE u^* - FREE TURBULENT MIXING

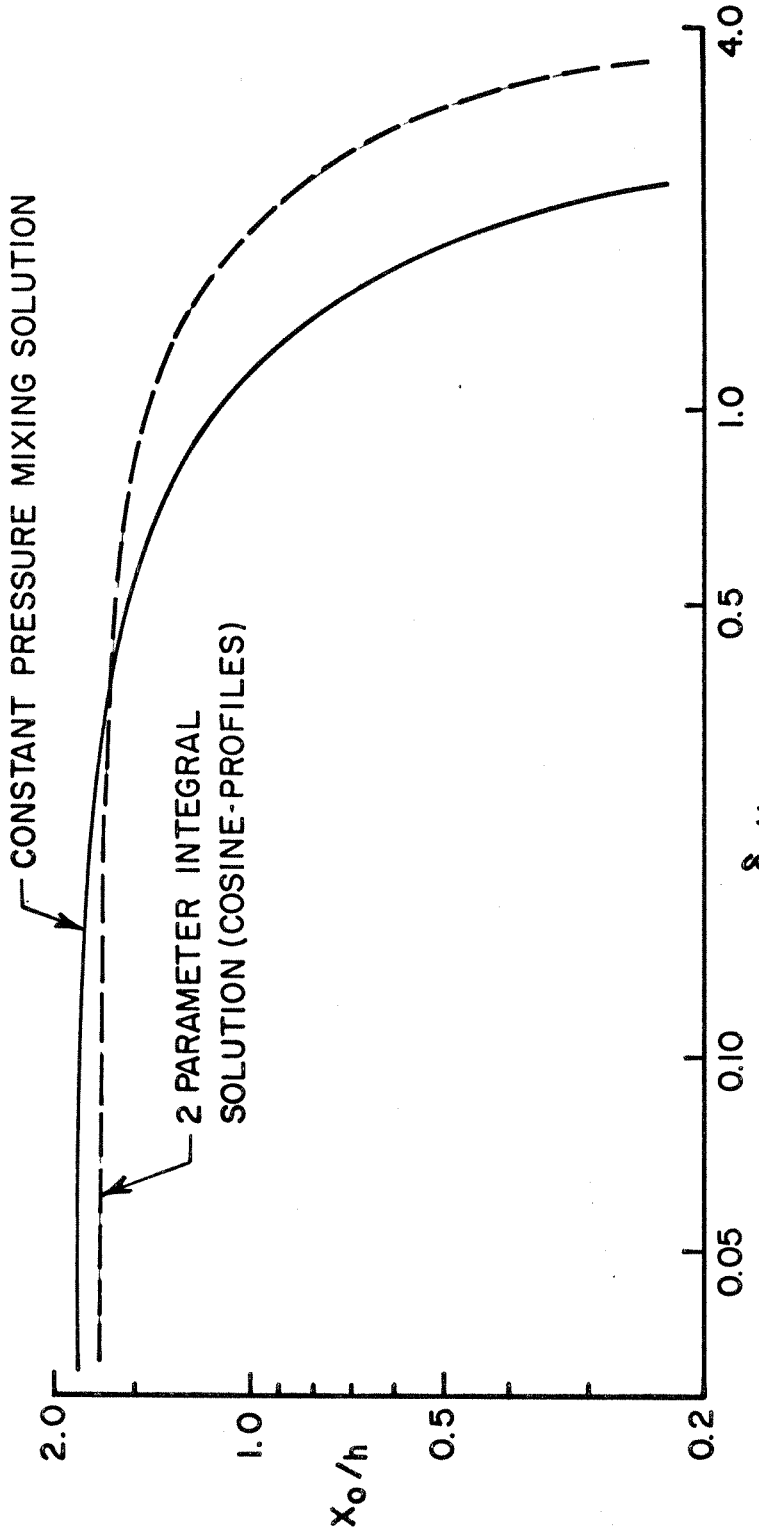

FIG.13 EFFECT OF UPSTREAM BOUNDARY LAYER THICKNESS ON LENGTH OF CONSTANT PRESSURE REGION ($M_\infty = 2.0$)

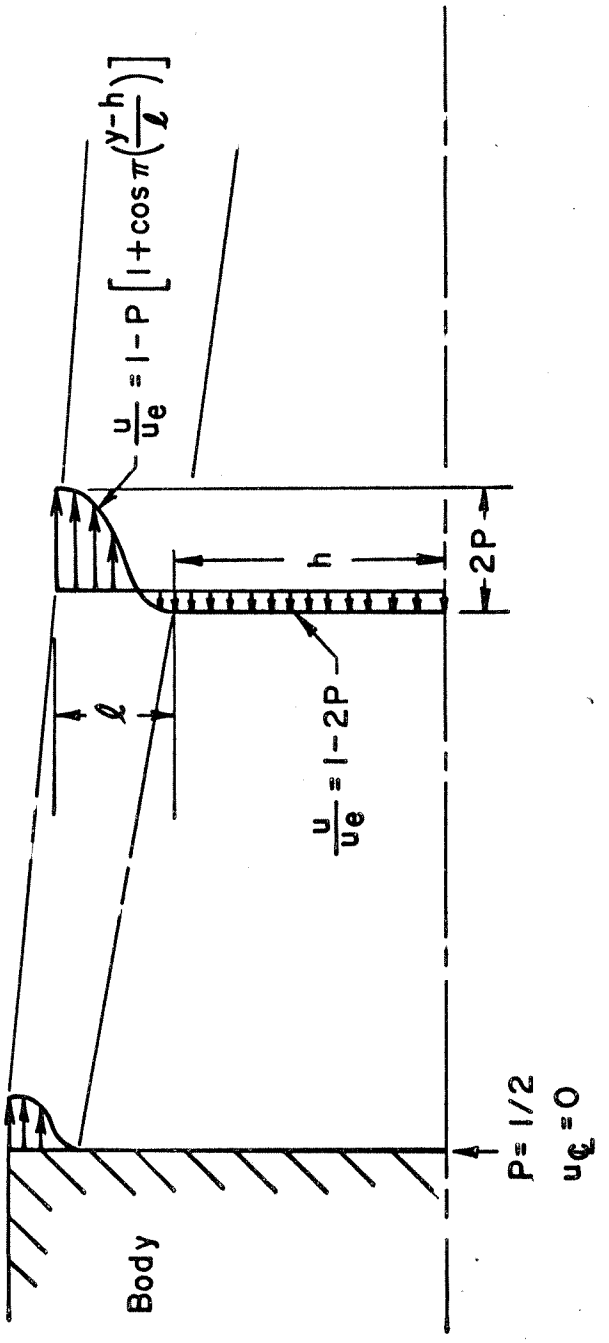

FIG.14 TWO PARAMETER REVERSED FLOW
COSINE - PROFILES (GREEN)

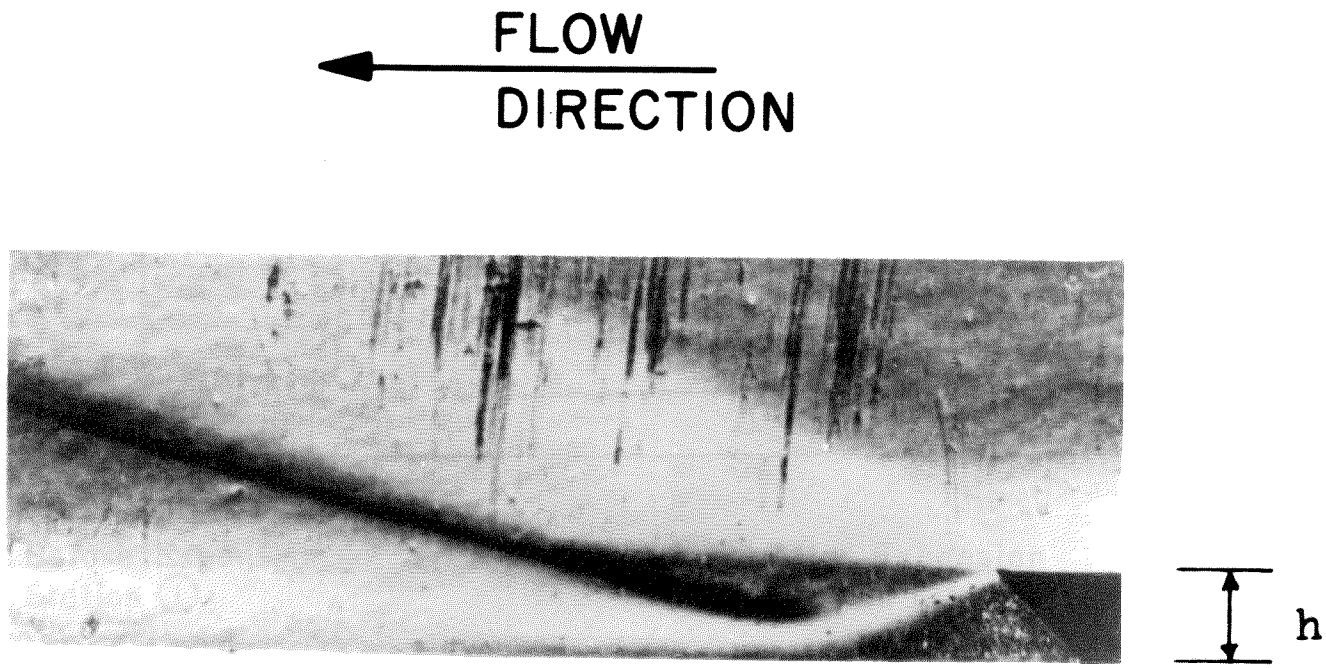

FIG. 15 SCHLIEREN PHOTOGRAPH OF SUPERSONIC TURBULENT BASE FLOW WITH THICK INITIAL BOUNDARY LAYER

PHOTO: HASTINGS $M_\infty = 2.41$

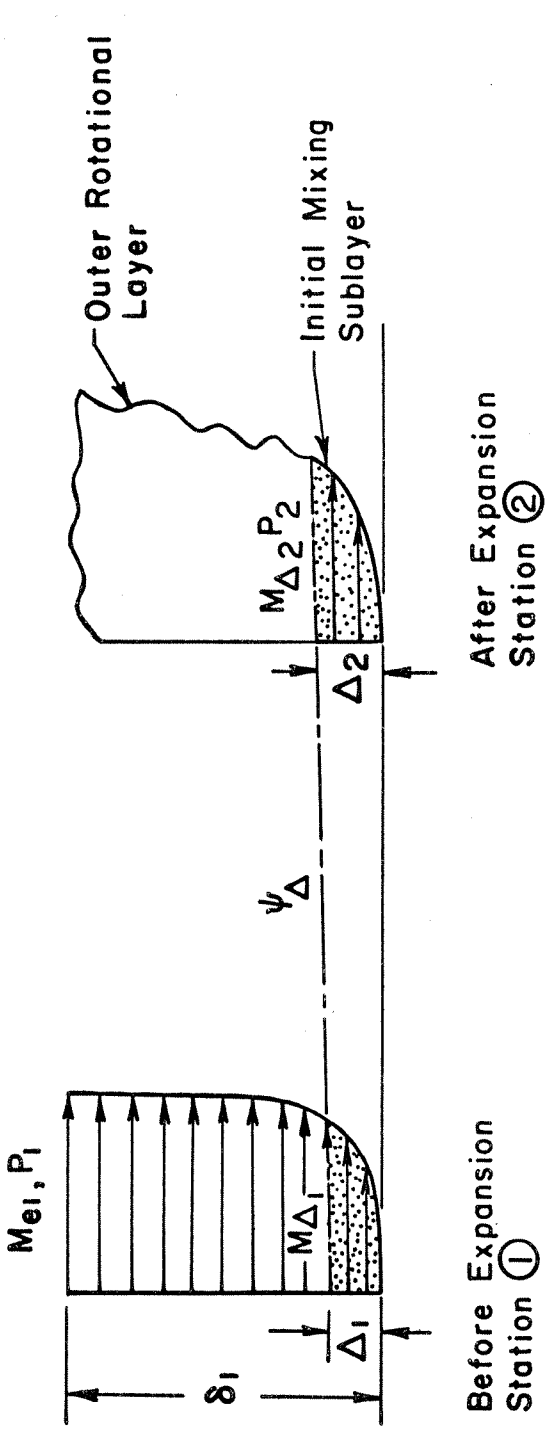

FIG. 16 MODEL FOR CORNER EXPANSION PROCESS

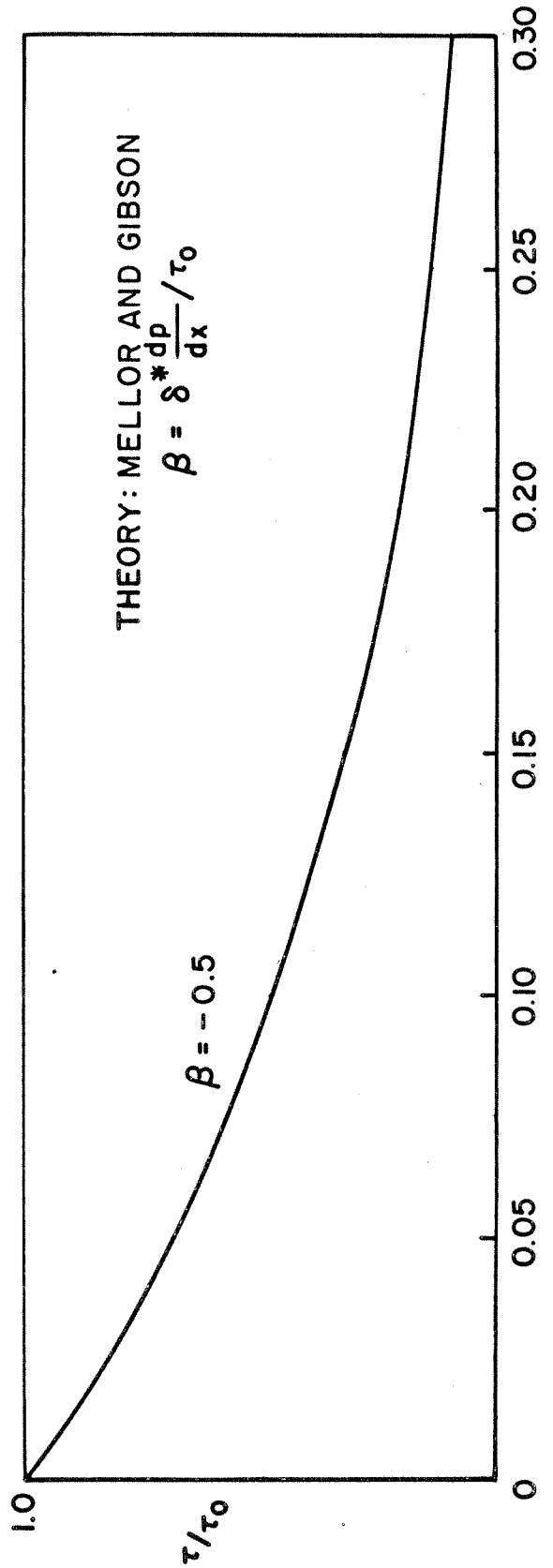

FIG. 17 SHEAR STRESS DISTRIBUTION MAXIMUM ACCELERATING EQUILIBRIUM TURBULENT BOUNDARY LAYER

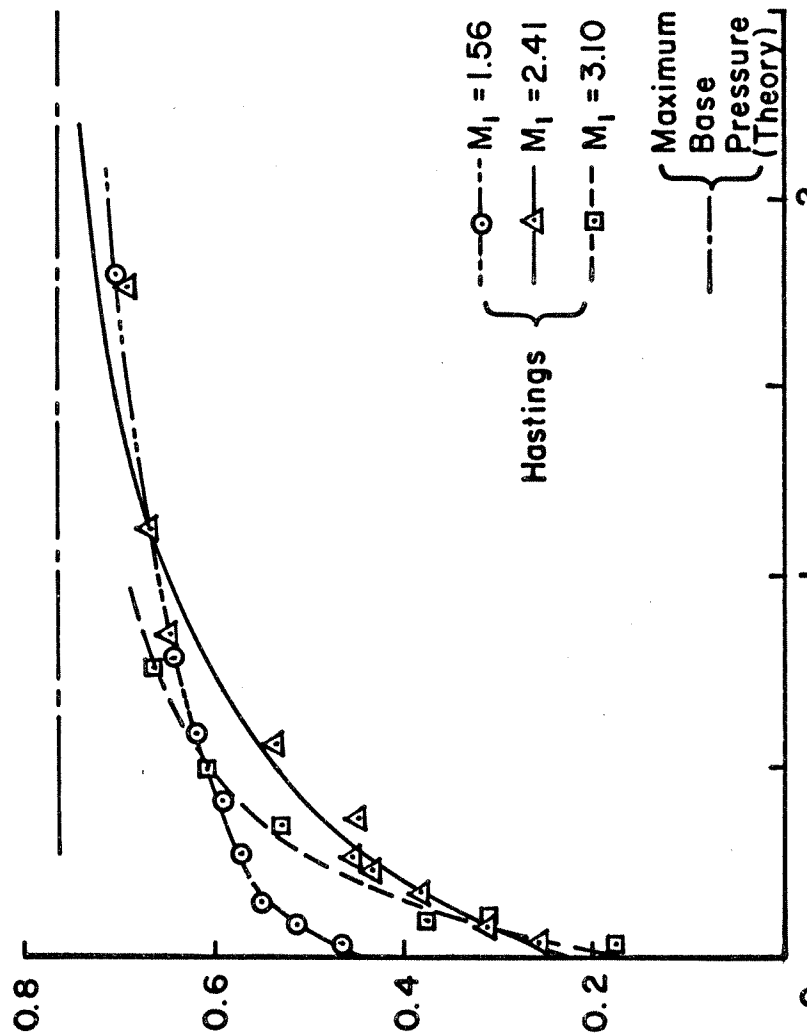

FIG.18 TWO-DIMENSIONAL BASE PRESSURE RATIO VS. INITIAL MOMENTUM THICKNESS

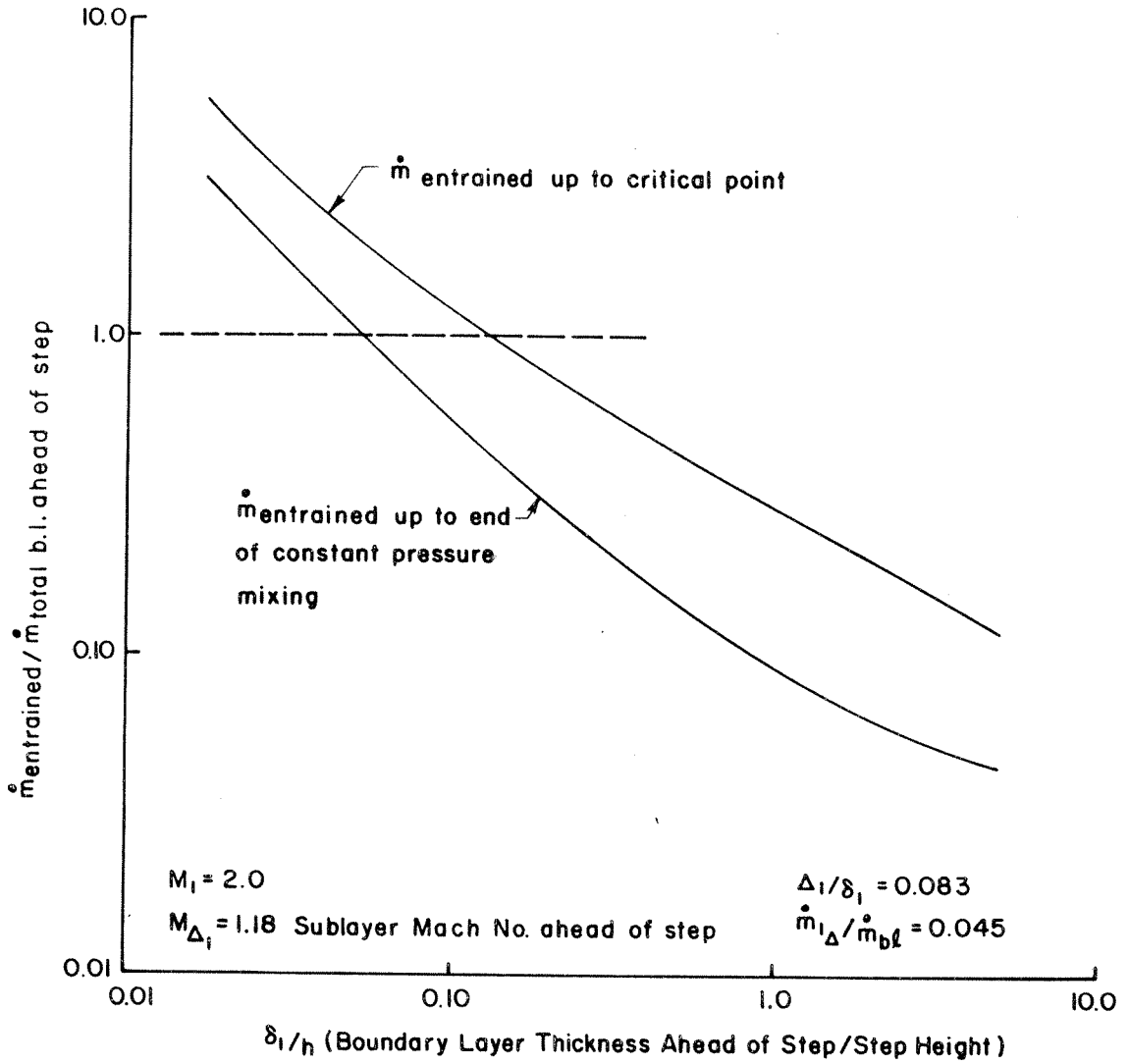

FIG.19 MASS FLOW ENTRAINED BY MIXING AND WAKE

FIG.20 DISTRIBUTION OF WAKE THICKNESS (δ)
℄ STATIC PRESSURE (P_e)
DIVIDING STREAMLINE VELOCITY (u*)

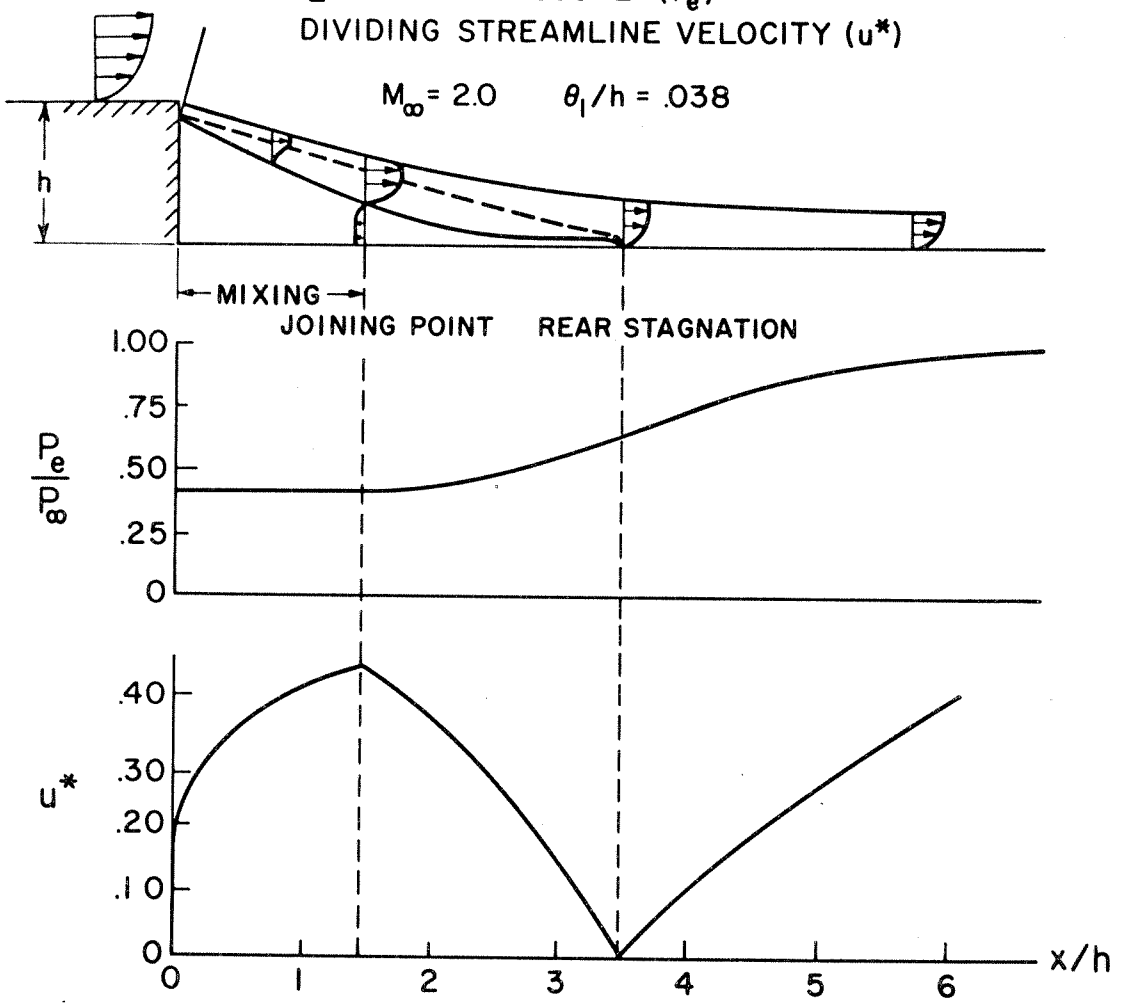

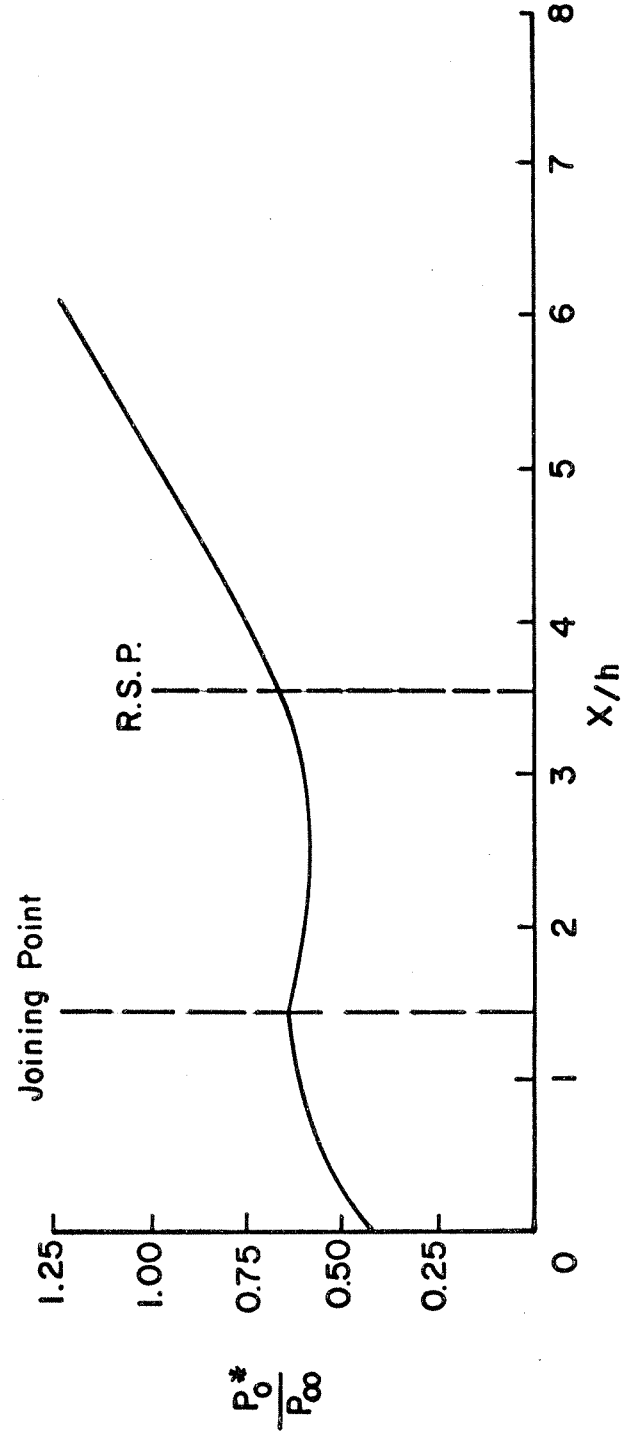

FIG.21 TOTAL PRESSURE ALONG THE DIVIDING STREAMLINE $M_\infty = 2.0$

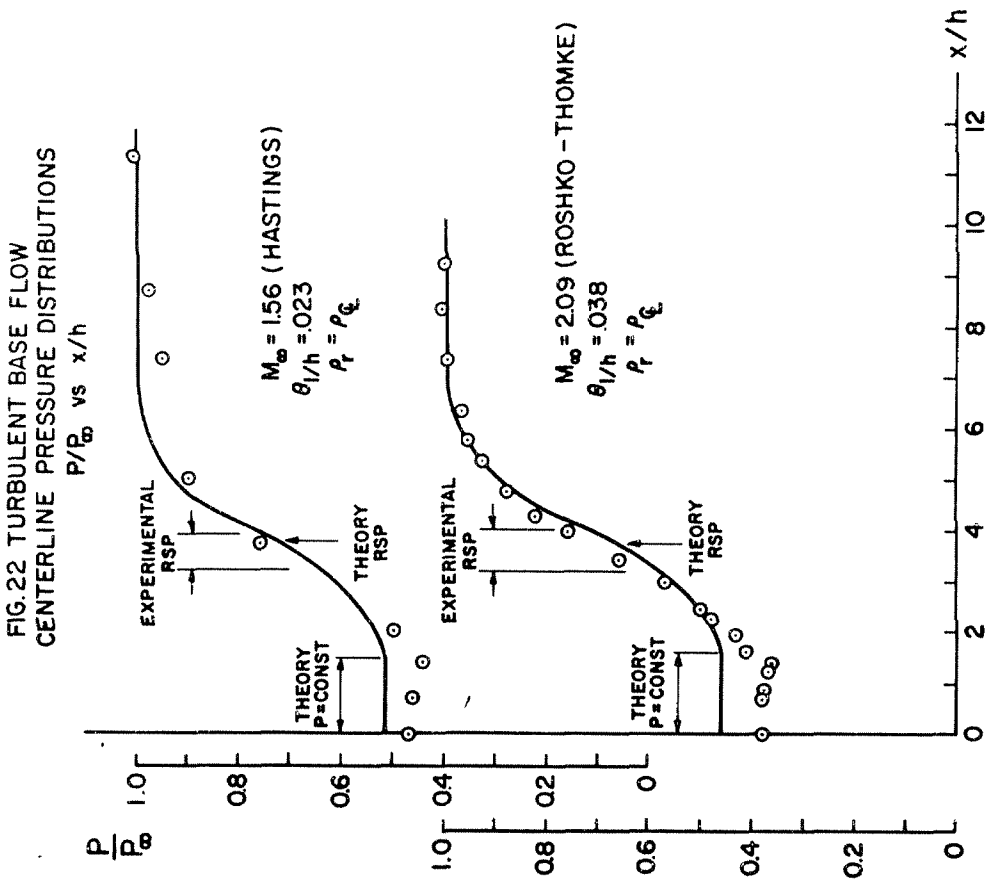
FIG. 22 TURBULENT BASE FLOW
CENTERLINE PRESSURE DISTRIBUTIONS
P/P∞ vs x/h
P/P∞
M∞ = 1.56 (HASTINGS)
θ1/h = .023
Pr = P∞
EXPERIMENTAL RSP
THEORY RSP
THEORY P=CONST
M∞ = 2.09 (ROSHKO-THOMKE)
θ1/h = .038
Pr = P∞
EXPERIMENTAL RSP
THEORY RSP
THEORY P=CONST
x/h

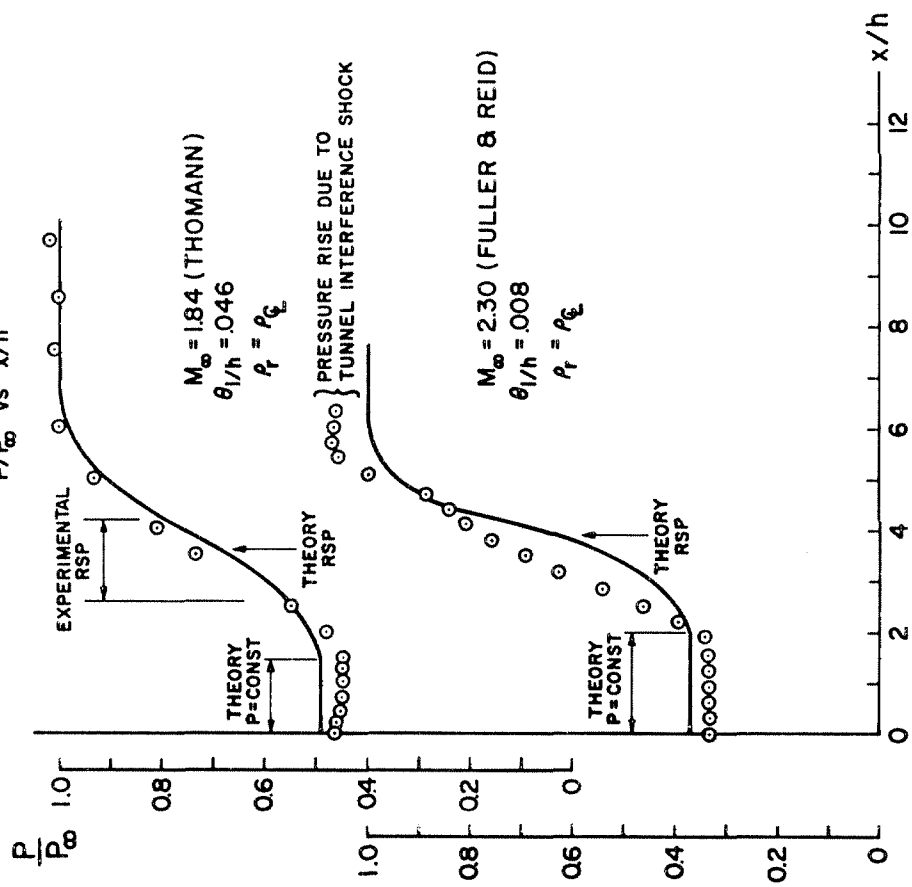

FIG.23 TURBULENT BASE FLOW
CENTERLINE PRESSURE DISTRIBUTIONS
P/P_∞ vs x/h

FIG.24 TURBULENT BASE FLOW
CENTERLINE PRESSURE DISTRIBUTIONS
P/P_∞ vs x/h

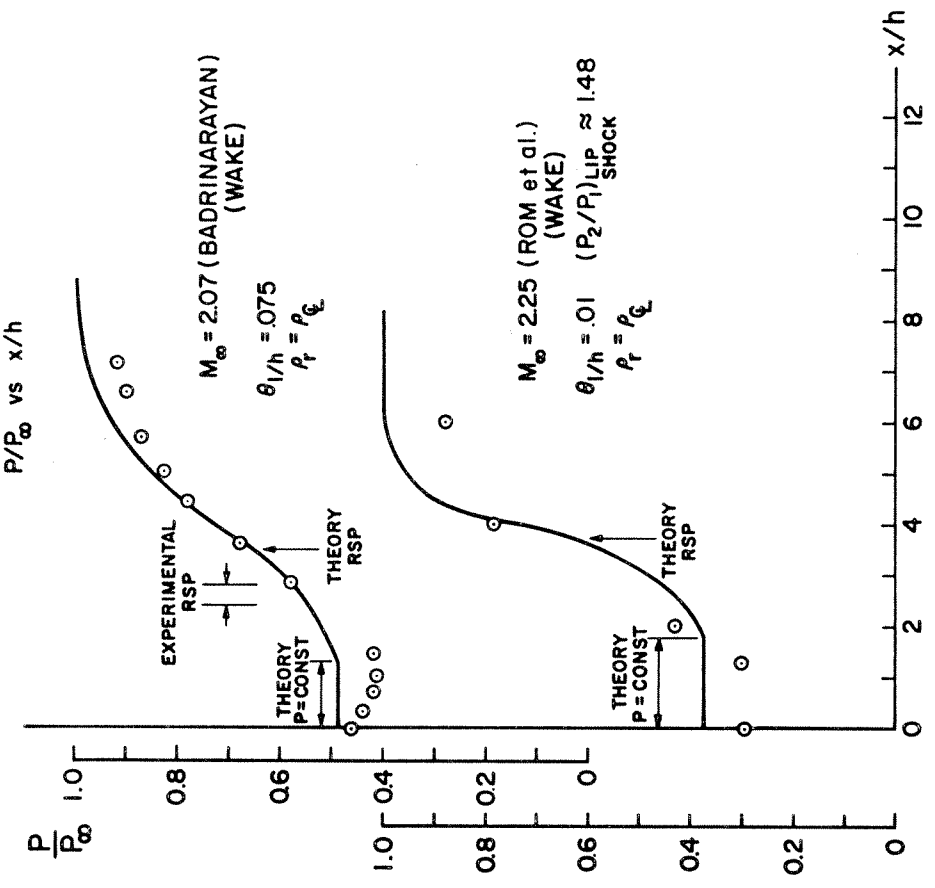

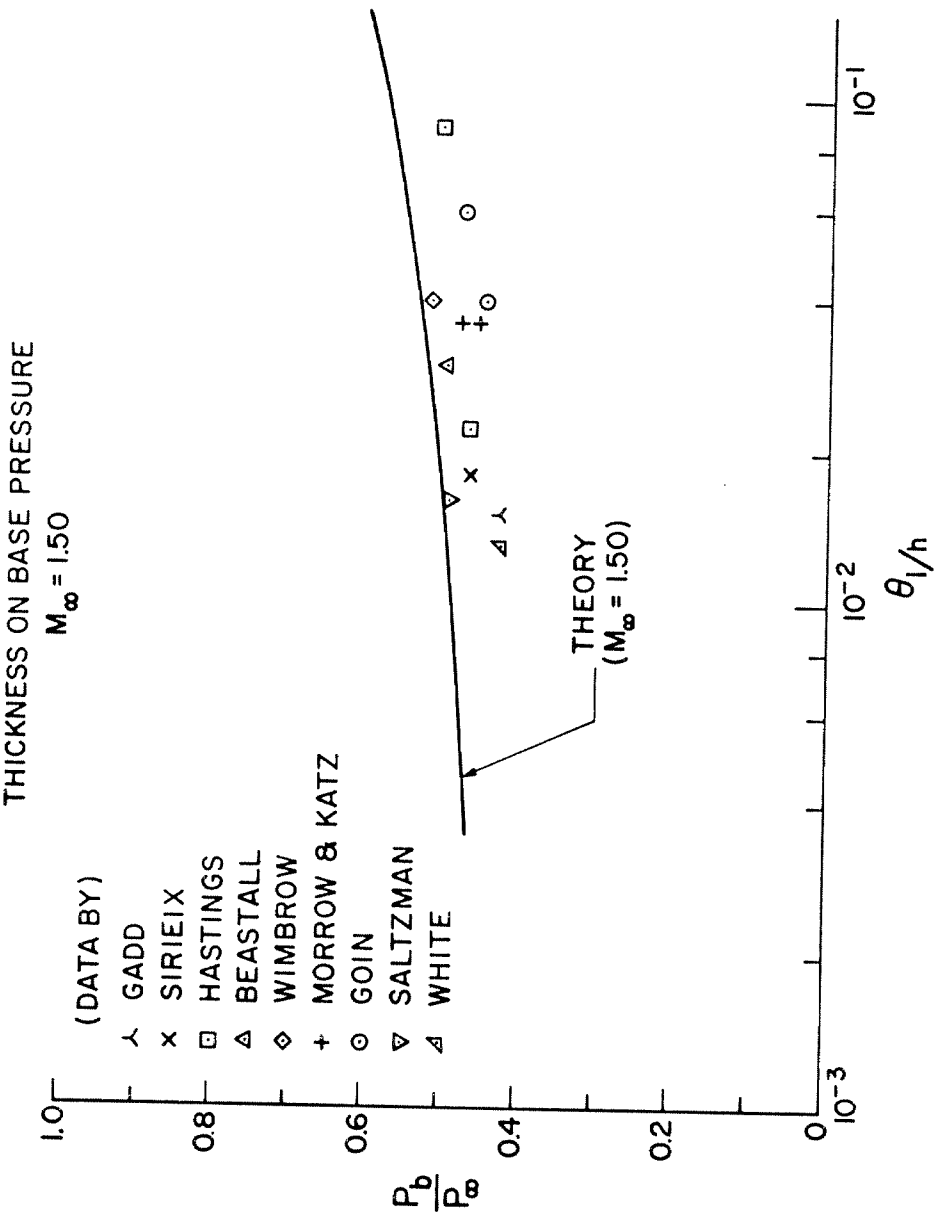

FIG.25 TURBULENT BASE FLOW
EFFECT OF THE UPSTREAM MOMENTUM
THICKNESS ON BASE PRESSURE

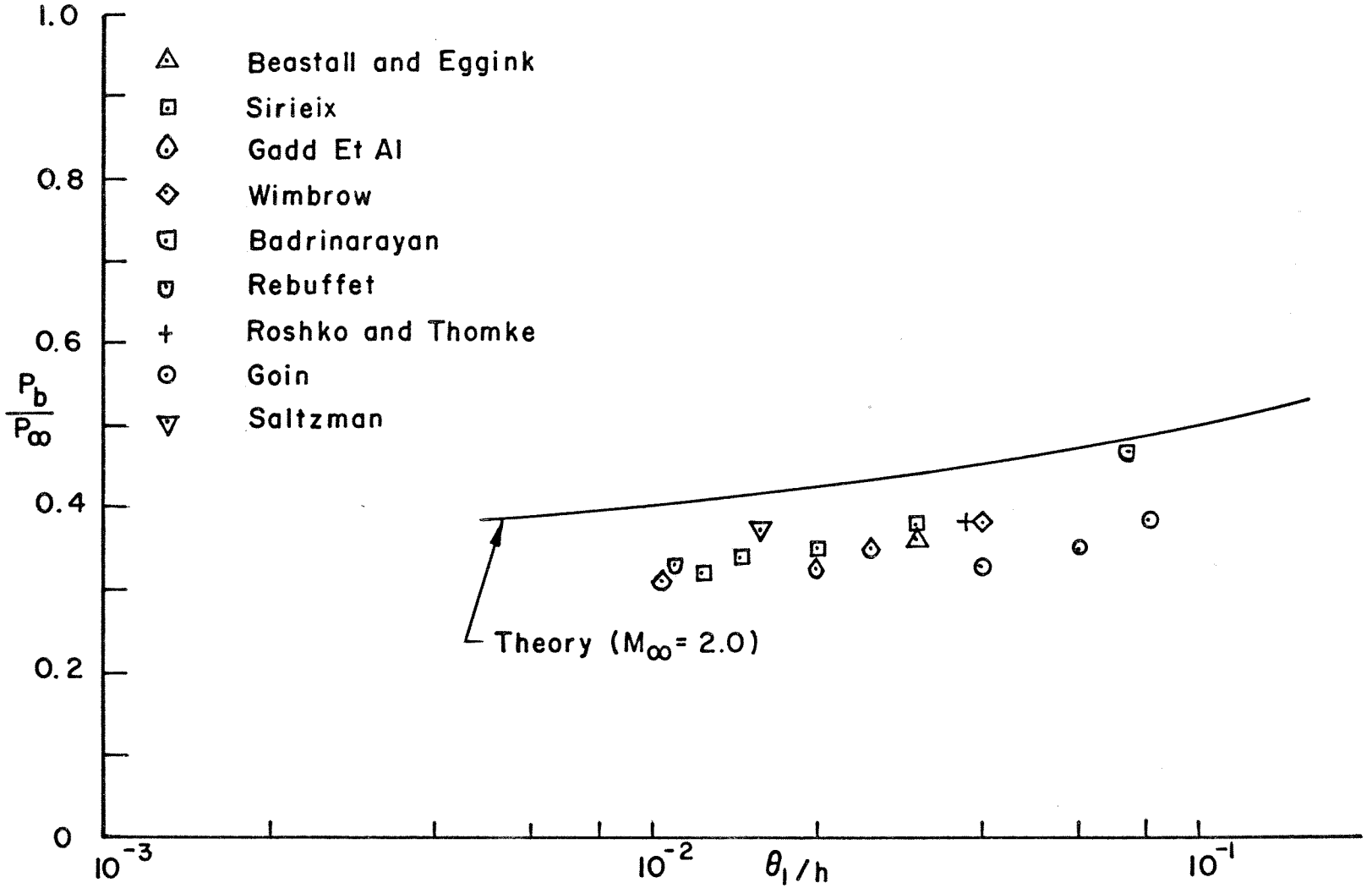

FIG. 26 TURBULENT BASE FLOW EFFECT OF THE UPSTREAM MOMENTUM THICKNESS ON BASE PRESSURE $M_\infty = 2.0$

FIG. 27 INCOMPRESSIBLE TURBULENT STEP FLOW
EXPERIMENTAL DATA OF
TANI, IUCHI, KOMODA $U_0 = 28$ meters/sec

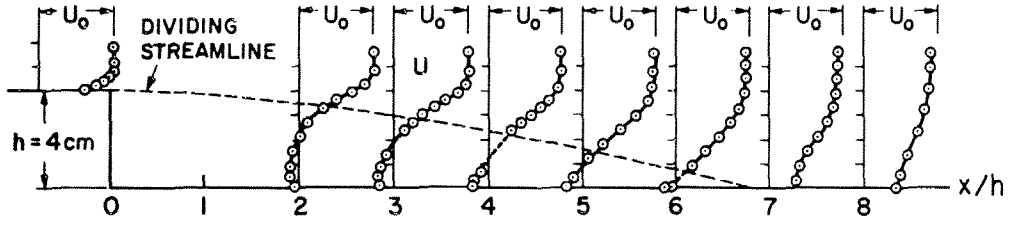

a. MEAN LONGITUDINAL VELOCITY

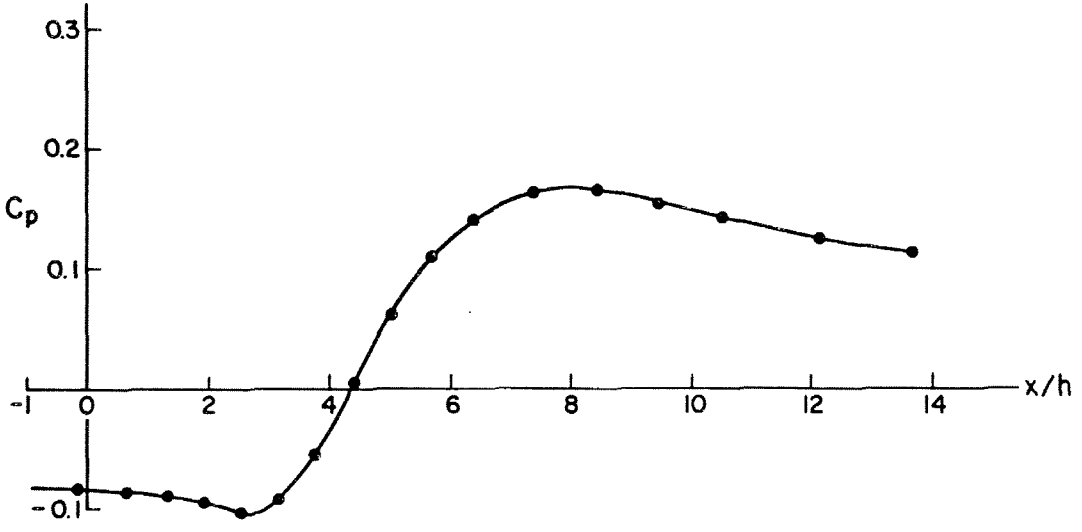

b. PRESSURE DISTRIBUTION ON STEP FACE

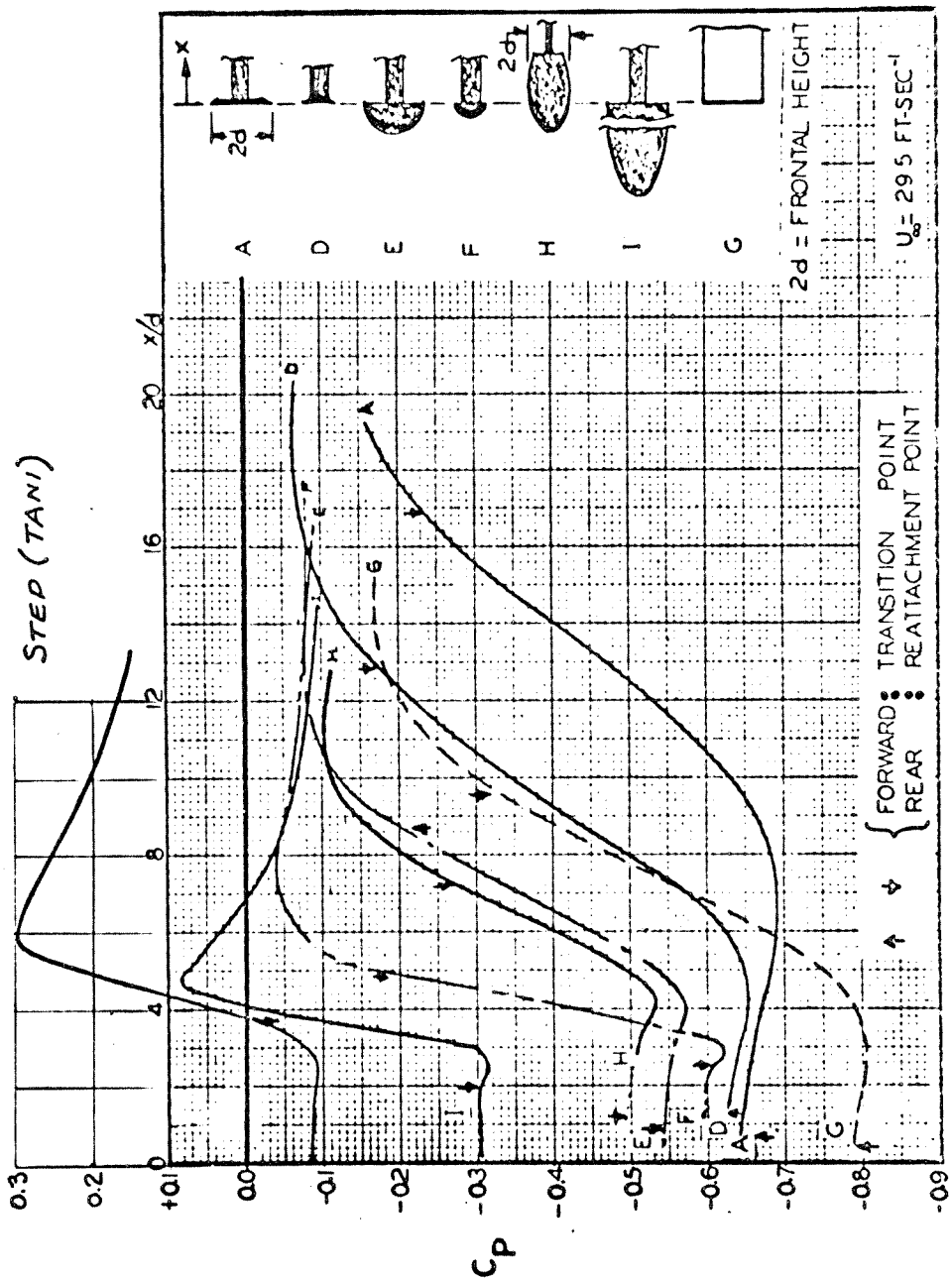

FIG. 28 COMPARISON OF RESULTS FOR VARIOUS SHAPES
(DATA : ROSHKO AND LAU)

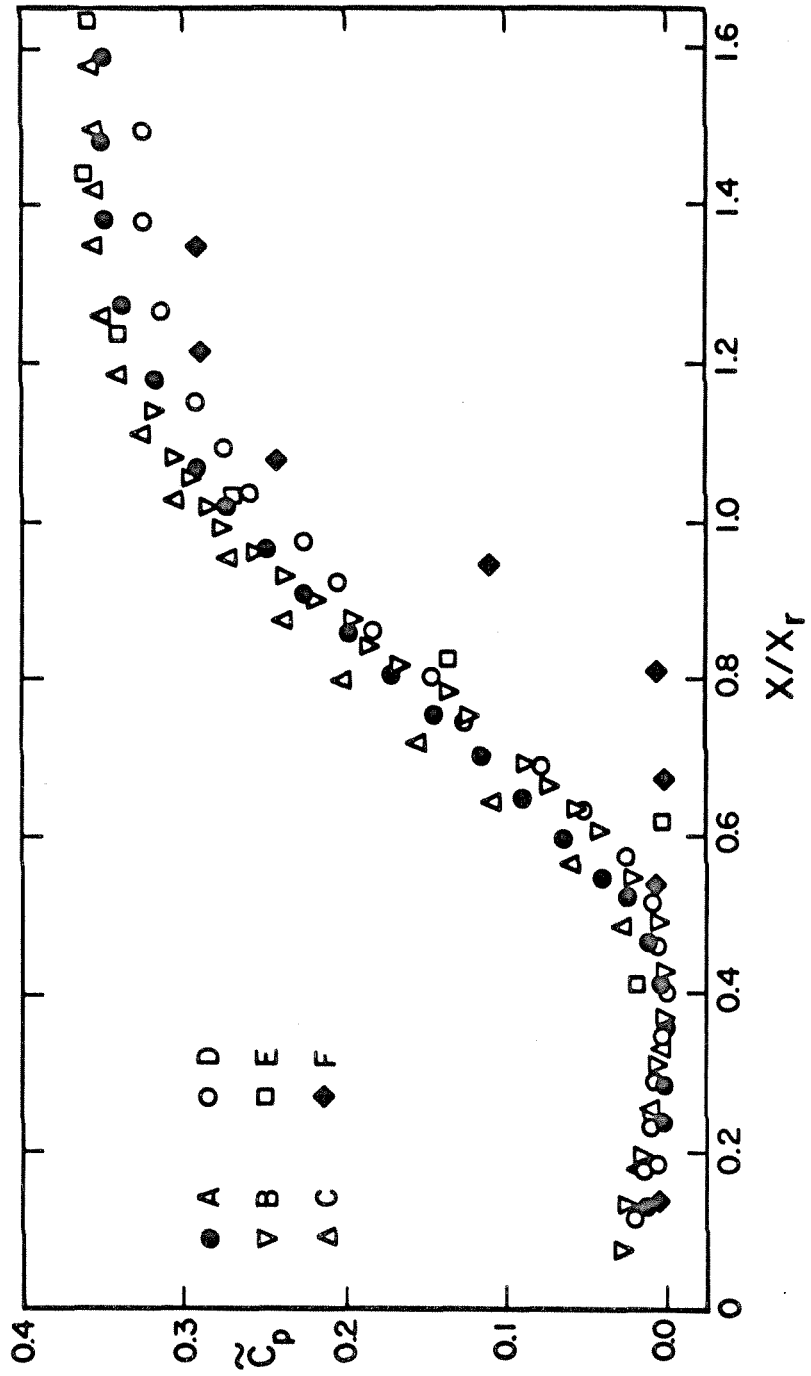

FIG. 29 REATTACHMENT PRESSURE DISTRIBUTION IN REDUCED COORDINATES
(DATA : ROSHKO AND LAU)

U_∞ = 29.5 FT. SEC.$^{-1}$

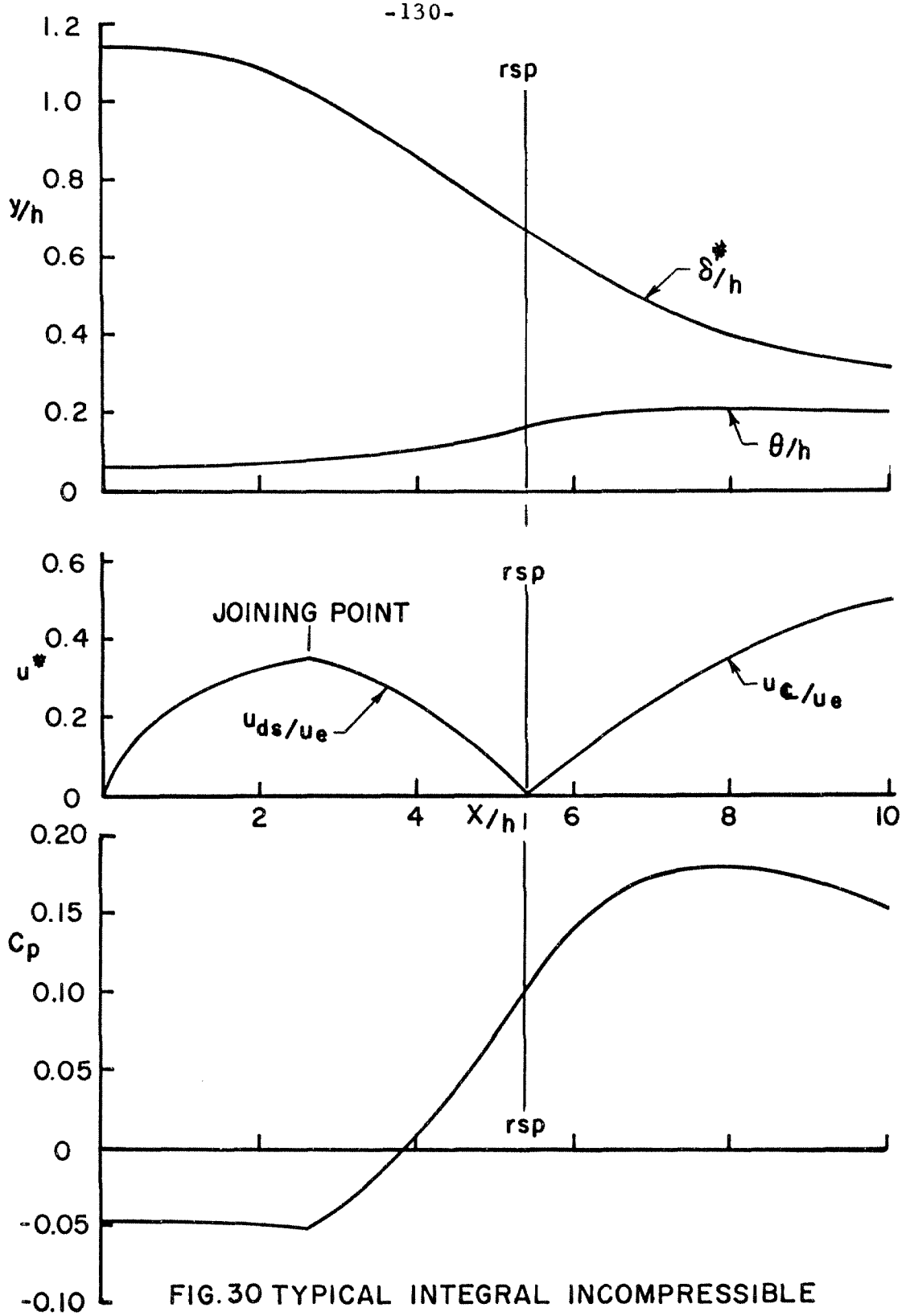

FIG. 30 TYPICAL INTEGRAL INCOMPRESSIBLE TURBULENT WAKE FLOW SOLUTION ($\delta_1/h \approx 0.5$)